

Power and Voltage Regulation of a Quad Active Bridge

by

Mohammed A. Hatatah

B.S in Electrical and Computer Engineering, King Abdulaziz University, 2006

Master of Business Administration (MBA), King Abdulaziz University, 2010

M.S in Electrical and Computer Engineering, Pennsylvania State University, 2015

Submitted to the Graduate Faculty of the
Swanson School of Engineering in partial fulfillment
of the requirements for the degree of
Doctor of Philosophy

University of Pittsburgh

2020

UNIVERSITY OF PITTSBURGH

SWANSON SCHOOL OF ENGINEERING

This dissertation was presented

by

Mohammed A. Hatatah

It was defended on

August 5, 2020

and approved by

Alexis Kwasinski, Ph.D., Associate Professor, Department of Electrical and Computer Engineering

Robert Kerestes, Ph.D., Assistant Professor, Department of Electrical and Computer Engineering

Ahmed Dallal, Ph.D., Assistant Professor, Department of Electrical and Computer Engineering

Luke Solomon, Ph.D., Senior Engineering Manager, Advanced Concepts, ABB

Dissertation Advisor: Brandon Grainger, Ph.D., Assistant Professor, Department of Electrical and
Computer Engineering

Copyright © by Mohammed A. Hatatah

2020

Power and Voltage Regulation of a Quad Active Bridge

Mohammed A. Hatatah, Ph.D.

University of Pittsburgh, 2020

The solid-state transformer (SST) has received substantial attention because of its potential in helping to achieve more intelligent grid systems. The SST is a combination of power electronic (PE) converters and a high-frequency transformer (HFT), thus, reducing volumetric footprint resulting in space savings. The SST provides several functions such as controllable voltage and disturbance isolation. It also provides a dc-link voltage that helps advancements towards complete DC distribution systems.

A challenge identified from within the literature is balancing the voltages for each of the ports on the MV side of the QAB. Renewable energy supply to these ports will be stochastic in nature resulting in voltage variations at the output of the MV bridges feeding the transformer. If this is not managed appropriately, unequal power flow will be drawn by each of the ports leading to undesired voltage ripples that impact the DC-link voltage. In addition, the voltage unbalance problem makes it difficult to feed a common load without violating its voltage limits. Therefore, voltage regulation has to be investigated to target this voltage unbalance and maintain constant output voltage.

The proposed approach is based upon linear–quadratic regulator (LQR) control for the DC-DC stage of the SST to alleviate the issues mentioned for improved renewable energy regulation for SST applications. Despite the effort reported, nonlinearity and uncertainty are still a challenge in some applications. So, other combined techniques have been investigated to mitigate the

phenomena mentioned earlier. This motivates the use of adaptive linear–quadratic regulator (ALQR) and nonlinear model predictive control (NMPC) to track the nonlinear change of the QAB converter due to the renewable energy. Although regulation purpose has been maintained in, stability is still a challenging point in the NMPC design. Thus, a control strategy is proposed to improve the regulation of the SST based QAB considering a practical NMPC scheme with guaranteed stability.

Table of Contents

Acknowledgements	xii
Nomenclature	xiii
1.0 Introduction.....	1
1.1 Background Information.....	1
1.2 Objective.....	3
1.3 Thesis Organization	3
2.0 Review of The Previous Work	5
2.1 Review of Solid-State Transformer	5
2.1.1 Architecture	5
2.1.2 Control for Different Applications	7
2.2 Review of DC-DC Converters	8
2.2.1 Modeling of Power Converters	9
2.2.2 Control of Power Converters	10
2.3 Conclusion.....	11
3.0 LQR Approach for Regulating Voltage and Power Flow Through the Ports of a Medium Voltage QAB	12
3.1 System Description and Modeling	14
3.2 Controller Design for Regulating QAB Port Power and DC Output Voltage.....	15
3.2.1 Basic Primer of State Feedback Control Using LQR	18
3.2.2 Proposed Power Balance Control	19
3.2.3 Proposed Power Distribution Control.....	25

3.2.4 Mathematical Relation Between Power and Voltage in The Power Distributed Control	26
3.3 Power and Voltage Regulation Verification	31
3.4 Conclusion.....	36
4.0 Power Regulation of a Solid-State Transformer Based Quad-Active Bridge DC-DC Converter Using Adaptive Linear Quadratic Regulator and Nonlinear Model Predictive Control.....	37
4.1 System Description and Converter Model	39
4.2 Controller Design for Regulating QAB Port Power and DC Output Voltage	41
4.2.1 Proposed Output Voltage Control.....	41
4.2.2 Proposed Power Balance Control	42
4.2.3 Proposed Power Distribution Control.....	45
4.3 Power and Voltage Regulation Verification	51
4.4 Conclusion.....	55
5.0 Power and Voltage Regulation of Quad Active Bridge DC-DC Converter Considering Stability	56
5.1 Background of Model Predictive Control	58
5.2 System Description and Mathematical Model	59
5.2.1 Converter Modeling.....	59
5.2.2 The Mathematical Model and Error Modeling.....	61
5.3 Controller Design for Regulating QAB Port Power and Dc Output Voltage	65
5.3.1 Proposed Output Voltage Control.....	66
5.3.2 Proposed Power Balance Control	67

5.3.3 Proposed Power Distribution Control.....	70
5.4 Principle of Operation in NMPC Controller for Power Distribution Control	70
5.4.1 The Design of Finite Time LQ Control System.....	74
5.4.2 Suboptimal Control When Out of Equilibrium State.....	77
5.5 Power and Voltage Regulation Verification	77
5.6 Conclusion.....	81
6.0 Summary of Research.....	82
Appendix A Supplementary materials used in Chapter 3	84
Appendix A.1 Output voltage loop	84
Appendix A.2 Power balance loop	84
Appendix A.3 Power distribution loop	85
Appendix B Supplementary materials used in Chapter 4.....	86
Appendix B.1 Power distribution loop (NMPC).....	86
Appendix C Supplementary materials used in chapter 5.....	101
Appendix C.1 Power distribution loop (NMPC: Stability).....	101
Appendix C.2 The State space representation of the system.....	111
Appendix C.3 Simulink file.....	118
Bibliography	119

List of Tables

Table 1 Parameters of the Simulation Model.....	32
Table 2 Power Alterations at Each MV Port.....	33
Table 3 The Resilient Backpropagation (RPROP) algorithm	50
Table 4 Parameters of the Simulation Model.....	52
Table 5 Power Alterations at Each MV Port.....	52
Table 6 Suboptimal verison of Dual mode NMPC.....	73
Table 7 Parameters of the Simulation Model.....	78
Table 8 Power Alterations at Each MV Port.....	79

List of Figures

Figure 1 Comparison between LFT and HFT [2]	2
Figure 2 Topology classification of SST	5
Figure 3 Potential application of SST	6
Figure 4 A future MV power system based solid-state transformer configuration.....	7
Figure 5 SST Architecture using the QAB module.....	12
Figure 6 Modulation of the QAB.....	14
Figure 7 Current waveform according to the change of $\Delta D2i$.....	19
Figure 8 Structure of Control for the QAB	24
Figure 9 Measured voltages on the MV and LV side	33
Figure 10 Power measurements throughout the QAB	34
Figure 11 Power references and measurements on MV side	34
Figure 12 Duty cycles at MV side and LV side	35
Figure 13 Voltages and currents using TCM	36
Figure 14 SST based QAB module	37
Figure 15 Modulation of the QAB.....	40
Figure 16 Control Structure for the SST based QAB	43
Figure 17 The design structure of the balanced control loop	44
Figure 18 Basic NMPC control loop	46
Figure 19 Measured voltages on the MV and LV side	53
Figure 20 Power measurements throughout the QAB	53

Figure 21 Power references and measurements on MV side	54
Figure 22 Duty cycles at MV side and LV side	54
Figure 23 Voltages and currents using TCM	55
Figure 24 SST based QAB module	56
Figure 25 Modulation of the QAB	60
Figure 26 Unbalance power flow through the QAB	61
Figure 27 Control Structure for the SST based QAB	68
Figure 28 The design structure of the balanced control loop	69
Figure 29 The suboptimal dual mode NMPC algorithm.....	72
Figure 31 Measured voltages on the MV and LV side	79
Figure 32 Power measurements throughout the QAB	80
Figure 33 Duty cycles at MV side and LV side	80
Figure 34 Eigenvalue of the control system	81

Acknowledgements

Firstly, I thank my God for giving me the strength I have needed throughout my Ph.D. journey.

I want to thank my advisor Dr. Brandon Grainger. I appreciate his contributions of time and comments to make my work productive and stimulating. I would also like to thank my committee members, Dr. Kwasinski, Dr. Kerestes, Dr. Dallal, and Dr. Solomon, for their invaluable insights and suggestions. I would also like to take this opportunity to thank the Saudi Arabia Government for financial support.

Special thanks to my mother and sisters for all of their support during the last five years. I extend my gratitude to my beloved wife for her constant love and support. Finally, I would like to thank my kids for making me feel so special.

This dissertation is dedicated to the memory of my father, Abdullah Hatatah. You are my inspiration.

Nomenclature

HV	High voltage
MV	Medium voltage
LV	Low voltage
PE	Power electronics
LFT	Low-frequency transformer
HFT	High-frequency transformer
DER	Distributed energy resources
AC-DC	Conversion from AC voltage to DC voltage
DC-DC	Conversion from DC voltage to DC voltage
DC-AC	Conversion from DC voltage to AC voltage
SST	Solid-state transformer
QAB	Quadruple-active bridge
TCM	Triangular current mode
ZCS	Zero current switching
LQR	Linear quadratic regulator
ALQR	Adaptive linear quadratic regulator
NMPC	Nonlinear model predictive control
V_L	Voltage at the LV side
a	Module at the LV side
D_1	Duty cycle for the LV module

P_{a1}	Total power supplied to the LV
$b, c, \text{ and } d$	Modules at the MV side
V_M	Voltage at the MV side
V_i	Voltage at the MV modules, where i reflects MV bridges $b, c, \text{ and } d$
D_{2i}	Duty cycles of the MV modules, where i reflects MV bridges $b, c, \text{ and } d$
ΔD_{2i}	Dynamic component of the duty cycle at the MV modules
P_i	Average power at the MV modules, where i reflects MV bridges $b, c, \text{ and } d$
n	Transformer turns ratio
f_s	Switching frequency
T_s	Switching period
V_{ref}	Voltage reference set-point
$G_v(s)$	Voltage regulator
τ	Control delay
C_a	Capacitor
R	Load on the LV side
$A \text{ and } B$	Discrete state space model of the balanced plant
V_{iref}	Voltage reference
V_0	Voltage set point at no load condition
I_{iref}	Current reference
v_x	Central point voltage
K_p	State feedback matrix

1.0 Introduction

Nowadays, the electrical power grid has grown due to the increased use of distributed energy sources. This expansion will make the grid more complex. Thus, new technologies are required for better performance of the grid.

1.1 Background Information

The traditional power system network is characterized through different voltage levels, e.g., a high-voltage (HV) level for transmission lines, medium-voltage (MV) level for long power distribution network, and a low-voltage (LV) level for a loads side. The isolation between the different voltage levels is realized by passive transformers operated at line frequency (50Hz/60Hz). The location of the transformer is subject to different issues, such as losses. In the case of the HV level, these transformers are placed closed to the load to minimize the losses in the transmission line. The main drawback of the line frequency transformers (LFTs) is their size and weight. A large amount of metal is used for the transformer core itself. It makes the transportation, installation, and maintenance of these transformers complicated and expensive.

The increasing awareness of environmental issues and gas emissions have enhanced the research towards a modern power system: the smart grid. In order to make the smart grid realized, several technologies have to be developed. Power electronics (PE) is the primary key to advance the smart grid. Also, the HFTs are more compatible with the requirements of these new technologies, such as distributed energy recourses (DER), which are increasingly being employed

in the modern power system. For example, Germany has a goal to use renewable sources to generate 80% of its electricity, which likely is fed into LV and MV level. The new era of power system needs multi-objective performance levels such as low supply chain and small floor space requirement [1]. Besides, as the integration of power electronics increased, different performance issue needs more attention.

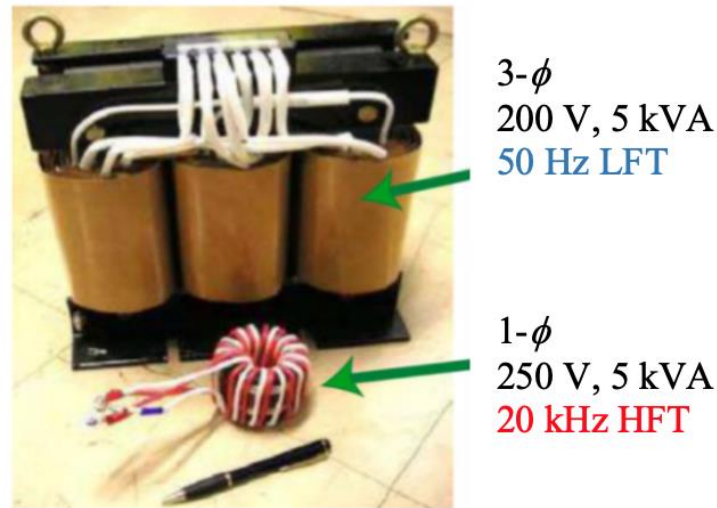


Figure 1 Comparison between LFT and HFT [2]

PE converters, such as solid-state transformers (SST), are becoming essential for the smart grid concept. The SST is a combination of PE converters and high-frequency transformer (HFT) that offers a proper solution to the LFT shortages. Considerable reduction in the volumetric of the SST is achieved, as shown in Fig. 1, since the HF transformer holds galvanic isolation.

The SST provides a dc-link voltage that enriches the concept of the DC distribution system. Moreover, an advanced protection scheme can be applied, considering the switching nature of power electronic devices. Some authors define the SST as a power electronic transformer (PET) or an intelligent universal transformer (IUT).

1.2 Objective

This work aims to provide a generic framework for the solid-state transformer based quad active bridge. The objective of this thesis is to propose control strategies for dc-dc conversion to regulate power and voltage. Although this work is done with the specified values, the equations are kept flexible enough for applications at any value.

This work is dual-purpose in the objective, 1) to enlighten electric power engineers with more advanced technologies such as SST based power electronic converter that not only convert voltage but also provide several functions to the grid. 2) to provide a controller for the DC-DC conversion that enhances its dynamic behavior under unbalance condition.

1.3 Thesis Organization

This thesis is organized into three main parts: literature review, control design work, and conclusion. First, Section 2 focuses on the literature review on the SST and DC-DC converters. This section presents the power converters architectures and control.

Secondly, Section 3 concentrates on the power and voltage regulation of SST. A linear quadratic regulator (LQR) controller is implemented for the DC-DC stage of the SST to regulate voltage and power of the SST. In Section 4, the objective is to develop a control strategy to improve the voltage and power regulation of the SST, maintain the output voltage, and mitigate the effects of nonlinearity and uncertainty on reference tracking. An adaptive Linear quadratic regulator (ALQR) control and nonlinear model predictive control (NMPC) are proposed for the DC-DC stage of the SST. The last part, Section 5, focuses on stability as it is an interesting point to discuss

in the NMPC design. This section aims to develop a control strategy to improve the regulation of the SST based QAB considering a practical NMPC scheme with guaranteed stability. The stability based suboptimal fixed horizon versions of NMPC for discrete-time systems is presented.

Lastly, Section 6 presents a research conclusion and provides a summary of the thesis work.

2.0 Review of The Previous Work

Several researchers have been investigating the SST for different applications. This has led to different SST architectures and control strategies. This chapter provides an overview of the existing architectures and control methods.

2.1 Review of Solid-State Transformer

2.1.1 Architecture

Several SST configurations have been proposed and classified in literature [1][3][4]. SST configurations can be classified into single-stage, two-stage, and three-stage that provide more functions than the other configurations, see Fig 2.

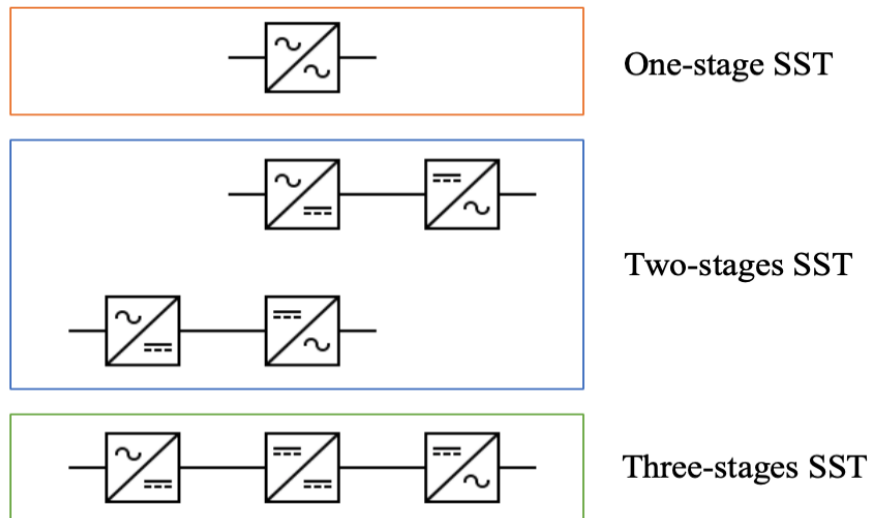


Figure 2 Topology classification of SST

A three-stage configuration can be a suitable choice to implement different PE topologies. It provides several functionalities such as DER, bidirectional power flow, and voltage compensation that enhance the electric power system's performance. The DER and energy storage sources can be integrated into the SST through the dc-link [5][6]. Unlike the LFT, the SST offers fault isolation property, which is extremely valuable. Potential applications of SST are summarized in Fig. 3.

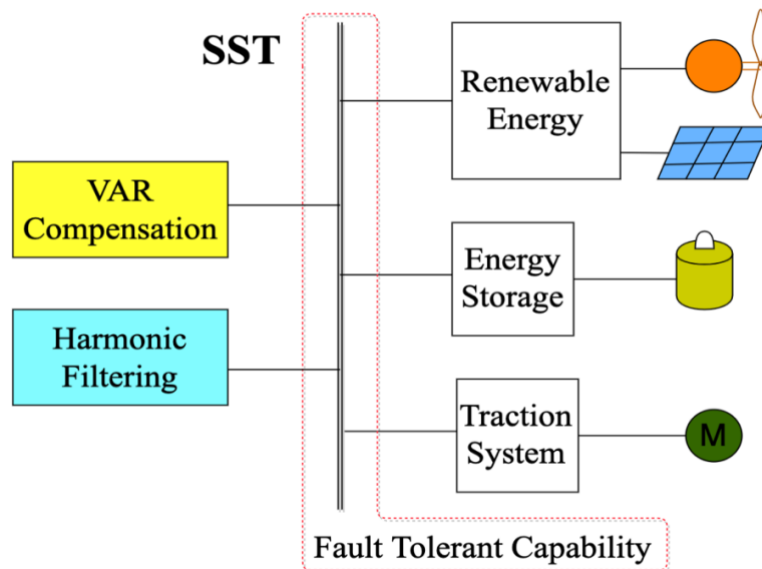


Figure 3 Potential application of SST

The availability of the dc-link is suitable for the connection of different sources, as shown in Fig. 4. The MV dc-link can feed new loads and sources such as a fast-charging electric vehicle, renewable energy, and energy storage. Also, the LV dc-link allows connecting the LV dc loads or sources directly. The DC/DC stage separates the AC power flow between the MV and LV grids, so the two grids can be controlled individually.

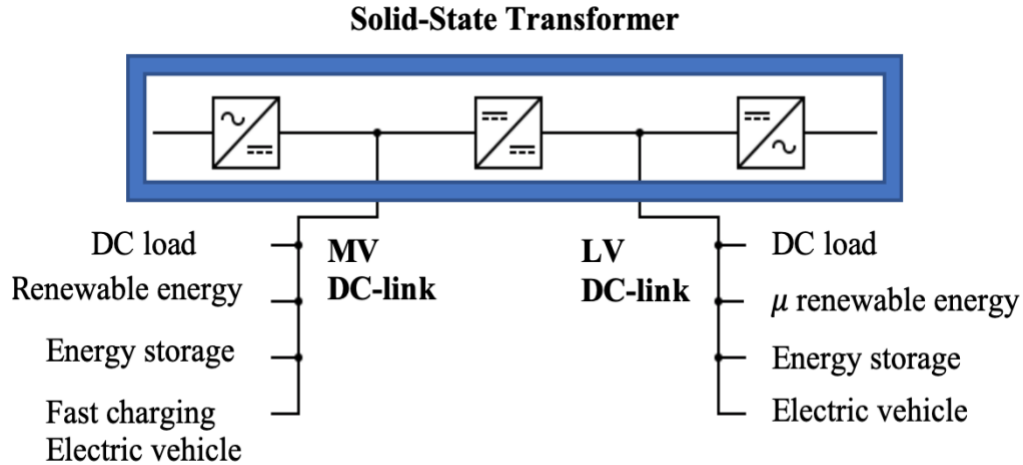


Figure 4 A future MV power system based solid-state transformer configuration

The SST consists of several PE converters, which increase the converter size and cost. This can be solved by combining the PE converters in multi-winding HF transformers such as multi-port solid-state transformer (MPSST), which helps to connect different elements in the system [7]. This way, the functionality of the several PE converters is combined in one converter, while the number of the PE components is minimized; thus, the power density is increased.

2.1.2 Control for Different Applications

Several control strategies have been proposed in the literature for controlling the SST. This section focuses on the control methods developed for different applications regardless of the SST configuration.

Soft switching techniques are often required in MV and HF applications, such as SST, to perform high efficiency [8]. The soft switching techniques are strongly related to the stored energy in the semiconductor devices. Phase shift modulation provides simple and effective control, as implemented in [9] for FB converter. Trapezoidal current mode presents an attraction solution as

implemented in [10] for DAB converter two-stage SST. Triangular current mode (TCM) applied to the series resonant DAB in [8] to achieve soft switching and then extended to the QAB in [11].

The dynamic performance of an isolated dc-dc converter was proposed in [12]. The proposed control strategy enhances the availability of the converter in case of multiple device failures. Another fault-tolerant topology was proposed in [13] that the FB based SRC can be reconfigured in a half-bridge topology using the idea of a voltage-doubler rectifier to maintain the operation.

A power and voltage balance control scheme of a cascaded H-bridge modular inverter is presented in [14]. The control method was designed for applications in microgrid under unbalanced conditions. Power and voltage balance control based on the single-phase dq model was implemented for a cascaded H-Bridge converter-based SST [15]. A novel controller for balancing the power of cascaded multilevel converter-based SST without sensing any current in the dc/dc stage presented in [16]. A control strategy in [17] was proposed for a three-stage H-bridge based SST to regulate the DC link voltage and therefore maintain the output voltage. A power and voltage balance control using comprehensive control-based master-slave control was proposed in [18]. The controller was applied for the cascaded H-bridge multilevel and for the DAB based SST.

2.2 Review of DC-DC Converters

The multi-active bridge (MAB) converters have been receiving more attention for several reasons [19][20]. The MAB converters have multi FB modules, which are coupled through a multi winding HF transformer. The MAB converters provide several advantages: integration of DER,

soft switching capability, and high-power density. However, the control design has to be handled wisely as the control complexity significantly increases as the number of ports increases.

The dual-active bridge (DAB) converter can be considered as the most straightforward module of the MAB converter. The triple-active bridge (TAB) converter was proposed as a first form of the MAB converter [19]. The nonlinearity of the TAB converter is a common thing for the other MAB converters. The QAB converter, with the integration of PV and storage integration, was proposed in [11]. The power was injected into SST directly through the HF transformer. Another modeling and control design of QAB was proposed in [21] for integrating distributed generation and storage.

2.2.1 Modeling of Power Converters

Control design needs a suitable system model. HF converter is a nonlinear time-varying system due to the switching characteristic. To avoid complexity, more control designers prefer to deal with a linear and time-invariant system. Thus, several modeling methods have been developed to provide a linear and time-invariant model as an approximation of the converter model. This can be done either in the continuous-time domain or discrete-time domain.

State-space averaging is one of the modeling techniques that generally used [22]. This technique assumes the ripples in the state variables are very small. It approximates the state equations, which results in a time-invariant model. A small-signal model technique can be used for linearization [23]. Another method is called generalized state-space averaging [24]. This method considers the ripples resulting in more terms to the state equation. Sampled-date models can be used in the discrete-time domain [25].

2.2.2 Control of Power Converters

A closed-loop controller is used to regulate the output voltage and compensate disturbances. The idea of this control is to minimize the error between actual output and the desired output. The conventional control design method is to apply a small signal approximation, obtain a transfer function, then design the control loop [23]. A Proportional-Integral (PI) is a commonly used controller in power electronics applications. Another controller is a lead compensator that increases the phase margin of the loop. PI controller and lead compensator can only attain infinite gain at the DC signal. Whereas, a Proportional-Resonant (PR) controller can reach infinite gain at a given frequency [26]. LQR is suitable for a multi input – a multi output system like SST. It was used to improve the steady-state and dynamic performances of SST, as presented in [27]. Also, it has an excellent robustness property, and its stability is insensitive to small variations.

The control techniques mentioned above are normally used for one operating point. However, dynamic operation cannot be guaranteed when there is a large deviation. Gain-scheduling control is one of the methods that can be used to enhance performance over a range of operating points [28]. Adaptive control can be used for gain-scheduling control where controller parameters are adjusted on-line according to a pre-defined schedule [29]. Besides, Adaptive control is a useful tool in modern optimal control, such as adaptive LQR [30].

There are several nonlinear control techniques that have been used for more precious control design. Lyapunov-based control is one of these control designs [31]. Another nonlinear control technique is sliding mode control (SMC), a variable structure control method. SMC has been used for dc-dc converters [32].

Model predictive control (MPC) is another effective technique that useful under parameter uncertainties, as shown [33]. The MPC has had an excellent history in both the academic and

industrial literature. It was adopted by the process industries, which proved to be a very effective method of multivariable control. It can handle complex systems with hard constraints and many inputs and outputs. The nonlinear model predictive control (NMPC) is an extension of well-established linear MPC to the nonlinear system.

Reference [34] used a predictive control technique for the DC-DC converter. This control evaluates the optimized delay-angle between the primary and secondary voltages using a predictive algorithm. A proposed MPC for SST formed by matrix converters was evaluated in [35]. The state variables and the present circuit variables are predicted, then an optimal switching state for the next sampling time is selected.

The MPC stability was investigated in early academic literature but did not receive attention in the industrial literature. Stability has been intensively investigated, resulting in different strategies: a locally stabilizing terminal feedback controller, a terminal constraint, and a terminal cost [36].

2.3 Conclusion

SST is becoming one of the most crucial technologies for the electric power system. As the electric power grid moving toward new concepts, more work needs to be done. One of the challenges is the voltage and power balance control in the DC-DC converters. In the next section, the analysis will be presented, which is applied to the QAB converter. The dynamic performance is verified analytically and validated extensively in the MATLAB/Simulink environment.

3.0 LQR Approach for Regulating Voltage and Power Flow Through the Ports of a Medium Voltage QAB

The SST is one of many smart grid solutions that has been receiving substantial attention for several reasons [37][38]. The SST uses a high-frequency (HF) transformer, thus, reducing volumetric footprint resulting in space savings. The SST version utilized in this work is the three-stage SST composed of a medium voltage (MV) ac-dc stage, HF isolated dc-dc stage, and low-voltage (LV) dc-ac stage as shown in Fig. 5. Although several converters have been used as a module of the SST, the dual active bridge (DAB) and the series-resonant converter (SRC) have been used more regularly as described in [1][8]. The multiple active bridge (MAB) is a good alternative which was first investigated in [39], then applied in [21] to connect different renewable sources and storage.

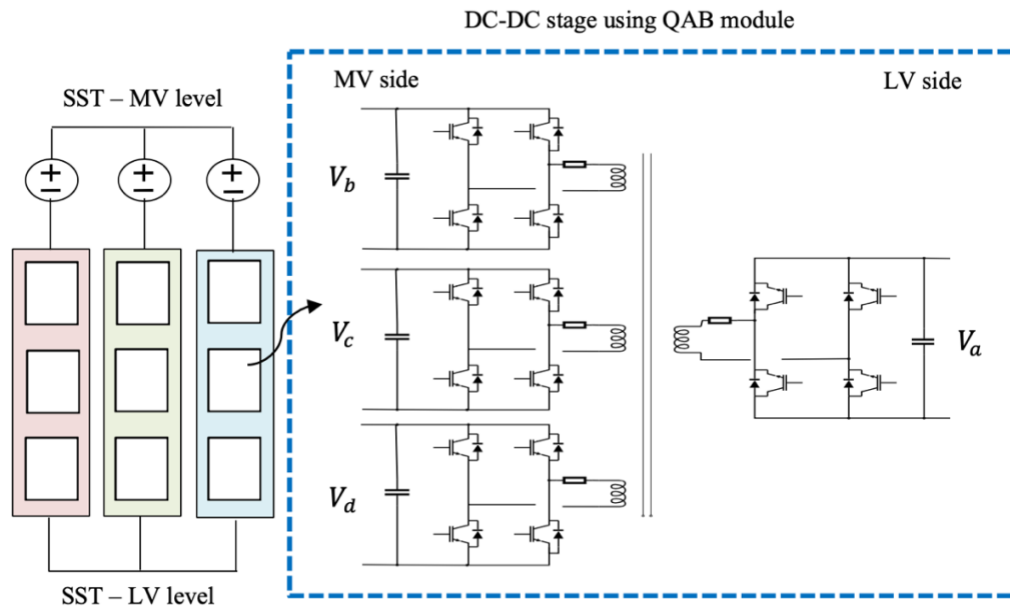


Figure 5 SST Architecture using the QAB module

The use of the MAB as a module of the SST helps to reduce the number of transformers and modules compared to the SST based on the DAB while providing the same advantages such as high efficiency and soft switching. The QAB is an extension of the MAB and can exchange power among the modules of the MV bridges across the HF transformer. Compared to the DAB, the QAB offers a cost reduction of 14.8%. The efficiency of both solutions is very similar, a slightly improvement of 5% is obtained in the QAB [40].

A challenge identified from within the literature is balancing the voltages for each of the ports on the MV side of the power electronic unit, labeled b , c , and d in Fig. 6. Renewable energy supply to these ports will be stochastic in nature resulting in voltage variations at the output of the bridges feeding the transformer. If this is not managed appropriately, unequal power flow will be drawn by each of the ports leading to undesired voltage ripples that impact the DC-link voltage [9][15].

Control strategies have been presented in the literature, like droop regulation in [41], but most have been applied to H-bridge topologies [42]. Another notable reference on the control subject is provided in [15]. State feedback control is well known for multi variable systems. The LQR is one of the most common optimal control techniques that is suitable for a multi-input–multi- output system. It has a nice robustness property and its stability is insensitive to small variations. In addition, it has been widely used in many applications [27][30][43][44]. The LQR can be used in a tracking problem; where the output is compared to a reference to drive the error between the reference and the output to zero.

In this work, we implement a LQR controller for the DC-DC stage of the SST to alleviate the issues mentioned for improved renewable energy regulation for SST applications. This work, in this section, has three control objectives: (1) to maintain the output voltage of the QAB at the

LV side at a constant value, namely, output voltage loop. (2) to balance the output power of the QAB at the MV side, namely, power balance control loop. (3) to balance the dc-link voltage of the QAB at the MV side, namely, power distribution loop.

3.1 System Description and Modeling

In this study, triangular current modulation (TCM) is used for the QAB converter to expand the soft switching range in case of variation in the output voltage [11] as shown in Fig. 6. The duty cycle for the LV module, a , is given by D_1 whereas the duty cycles of the MV modules are given by D_{2b} , D_{2c} and D_{2d} .

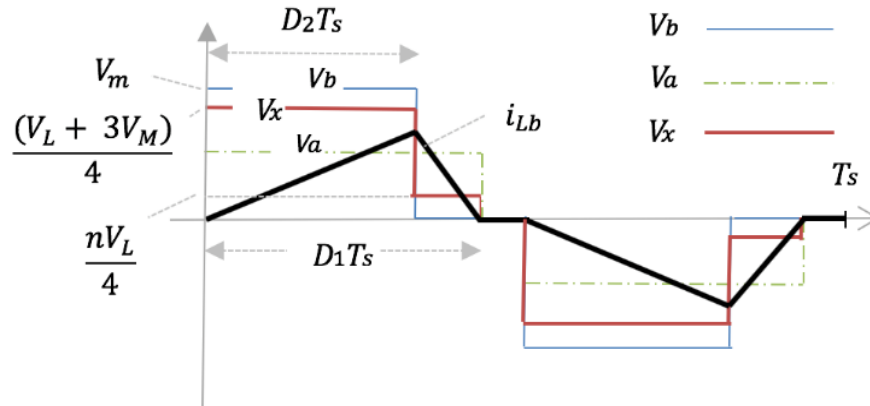


Figure 6 Modulation of the QAB

To achieve ZCS operation, $\Delta i_{Lb} (0 < t < D_2 T_s)$ must equal $\Delta i_{Lb} (D_2 T_s < t < T_s/2)$, [11], where D_1 and D_2 are calculated with (3.1). By knowing the system duty cycles, the inductance value, L , to transfer nominal power, P , can be calculated with (3.2). In this work, it is assumed that the QAB ports operate in an unbalanced power condition, that is, $P_b \neq P_c \neq P_d$. Therefore, the duty cycle

of each MV bridge will have a nominal value and dynamic component defined by (3.3) where, $\Delta D_{2i} = P_{ref} - P_i$. Under nominal operating conditions, P_{ref} will be set to 1/3 of the total power supplied, P_{a1} , to the low voltage end. The average power, P_i , is the product of voltage, V_i , and the average current, I_i , where i reflects MV bridges b , c , and d . The voltage at the MV side and the LV side is represented as V_M and V_L , respectively. Note that n is the transformer turns ratio and f_s is the power electronic device switching frequency.

$$D_2 = \frac{n V_L}{V_M} D_1 ; \text{ where } D_1 \leq 0.5 \quad (3.1)$$

$$L = \frac{3D_1^2 (V_L n)^2 (V_M - nV_L)}{4 P f_s V_M} \quad (3.2)$$

$$D_{2i} = D_2 - \Delta D_{2i} \quad (3.3)$$

3.2 Controller Design for Regulating QAB Port Power and DC Output Voltage

The control design for the SST DC-DC stage is performed using the conventional PI controller [21]. Although, many modern control algorithms, including the LQR approach, have been proposed by researchers as control approaches to improve their performance [27]. In [44], the authors used a hybrid control algorithm using PI and LQR to improve the performance for wind turbine. In this work, we are assuming that the system can be linearized around an operating point. To maintain the output voltage, we are going to design a PI controller.

Herein, the voltage regulator $G_v(s)$ ensures that the output voltage V_L tracks the voltage reference set-point, V_{ref} . To obtain the transfer function, (3.8a), showing the relationship between the output voltage and duty cycle, the averaged, state-space relationships were obtained for the time period between $0 < t < \frac{1}{2}T_s$, where T_s is the switch period.

The control delay, τ , is set to $1/20e^3$ for 1, PWM period, [11], C_a represents the capacitor, and R represents the load on the LV side of the converter. $G_v(s)$ will be analytically developed here.

First, it is assumed that the MV side voltage is equal to V_M , that is the value in the nominal state. At this time, the LV side current increases from zero to its next maximum current and then decreases again as described by (3.4a). $\frac{dv_L}{dt}$ can be calculated with (3.5a) – (3.5c).

$$i_{La}^{\max} = 3\Delta i_{Lb} = \frac{3(V_M - nV_L)}{4Lf} \cdot \frac{nV_L D_1}{V_M} = \frac{3nV_L D_1}{4LfV_M} (V_M - nV_L) \quad (3.4a)$$

$$I_L = \frac{3nV_L(V_M - nV_L)}{8LfV_M} \quad (3.4b)$$

$$\begin{cases} C_a \frac{dv_L}{dt} + \frac{v_L}{R} = I_L = \frac{3nv_L V_M}{8LfV_M} - \frac{3n^2 v_L^2}{8LfV_M}, & 0 < t < D_1 T_s \\ C_a \frac{dv_L}{dt} + \frac{v_L}{R} = 0, & D_1 T_s < t < 0.5T_s \end{cases} \quad (3.5a)$$

$$\frac{dv_L}{dt} = \left(\frac{3n}{8Lf} - \frac{1}{R} \right) \frac{v_L}{C_a} - \frac{3n^2}{8LfV_M} \frac{v_L^2}{C_a} \quad (3.5b)$$

$$\begin{cases} \frac{dv_L}{dt} = k_1 v_L - k_2 v_L^2, & 0 < t < D_1 T_s \\ \frac{dv_L}{dt} = -\frac{v_L}{C_a R}, & D_1 T_s < t < 0.5T_s \end{cases} \quad (3.5c)$$

Where, $k_1 = \left(\frac{3n}{8Lf} - \frac{1}{R}\right) \frac{1}{C_a}$, $k_2 = \frac{3n^2}{8Lfc_a v_M}$, $k_3 = \frac{3n}{8Lfc_a}$

Therefore, the averaged state-space relationships can be described by (3.6).

$$\begin{aligned} \frac{1}{2} \frac{dv_L}{dt} &= (k_1 v_L - k_2 v_L^2) d_1 - \frac{1}{C_a R} (1 - d_1) v_L \\ &= k_3 v_L d_1 - k_2 v_L^2 d_1 - \frac{1}{C_a R} v_L \end{aligned} \quad (3.6)$$

To linearize (3.6), we apply a small signal approximation as follows: $v_L = V_L + \tilde{v}_L$, and $d_1 = D_1 + \tilde{d}_1$. Therefore, $\frac{d\tilde{v}_L}{dt}$ can be obtained and is listed as (3.7a) and (3.7b). Note that the linearization will be around the operating point.

$$\frac{1}{2} \frac{d\tilde{v}_L}{dt} = k_3 (V_L + \tilde{v}_L) (D_1 + \tilde{d}_1) - k_2 (V_L + \tilde{v}_L)^2 (D_1 + \tilde{d}_1) - \frac{1}{C_a R} (V_L + \tilde{v}_L) \quad (3.7a)$$

$$\frac{d\tilde{v}_L}{dt} = 2 \left[(k_3 - 2k_2 V_L) D_1 - \frac{1}{C_a R} \right] \tilde{v}_L + 2(k_3 - k_2 V_L) V_L \tilde{d}_1 \quad (3.7b)$$

Then, $G_v(s) = \frac{\tilde{v}_L(s)}{\tilde{d}_1(s)} = \frac{b}{s+a} e^{-\tau s}$

Where,

$$a = 2 \left[(k_3 - 2k_2 V_L) D_1 - \frac{1}{C_a R} \right]$$

$$b = 2(k_3 - k_2 V_L) V_L \quad \text{when } R = \infty, \frac{1}{C_a R} = 0.$$

Finally, we obtain $G_v(s)$ listed as (3.8). So, we can design the output voltage control loop using PI controller.

$$G_v(s) = \frac{\tilde{v}_L(s)}{\tilde{d}_1(s)} = \frac{b}{s+a} e^{-\tau s} \quad (3.8a)$$

$$a = \left(\frac{6n}{8LfC_a} - \frac{12n^2V_L}{8LfC_aV_M} \right) D_1 \quad (3.8b)$$

$$b = \left(\frac{6n}{8LfC_a} - \frac{6n^2V_L}{8LfC_aV_M} \right) V_L \quad (3.8c)$$

3.2.1 Basic Primer of State Feedback Control Using LQR

Consider a linear, discrete-time, dynamic system in the state-space form described by (3.9) and (3.10). The cost function is presented as (3.11) and (3.12). The optimal control design here is to find a control input u to minimize the cost function. Since the linearization is around the operating point and the deviation is assumed not large, LQR will be considered for the other two controllers.

After taking the derivative with respect to the control inputs, we can represent the control signal u as a linear state feedback at time $N-1$ as shown in (3.13), where K is called the state feedback matrix. The dynamic system can be represented by (3.14). Note that H is the final state cost, Q is the state cost, and R is the input cost with $H = H^T \geq 0$, $Q = Q^T \geq 0$ and $R = R^T > 0$.

$$x_{k+1} = A_k x_k + B_k u_k \quad (3.9)$$

$$y_{k+1} = C_k x_k \quad (3.10)$$

$$J = \frac{1}{2} x_N^T H x_N + \frac{1}{2} \sum_{k=0}^{N-1} g_d(x_k, u_k) \quad (3.11)$$

$$g_d(x_k, u_k) = \frac{1}{2} (x_k^T Q_k x_k + u_k^T R_k u_k) \quad (3.12)$$

$$u_{N-1}^* \equiv -K_{N-1} x_{N-1} \quad (3.13)$$

$$x_{k+1} = (A_k - B_k K) x_k \quad (3.14)$$

3.2.2 Proposed Power Balance Control

For the power balance loop, the controller is implemented using LQR based state feedback control under the condition that the system is completely controllable. In the balanced condition, P_{b1} , P_{c1} and P_{d1} should be 1/3 of the total power supplied, P_{a1} , whereas in an unbalanced condition, $P_{b1} + P_{c1} + P_{d1} = P_{a1}$. A change in any of the duty cycles in the conversion system will alter the power flow in a given port described later by (3.26). As seen in Fig. 7 in red, a positive change or a negative change in ΔD_{2i} , (3.3), will dynamically alter the peak currents and, hence, port power.

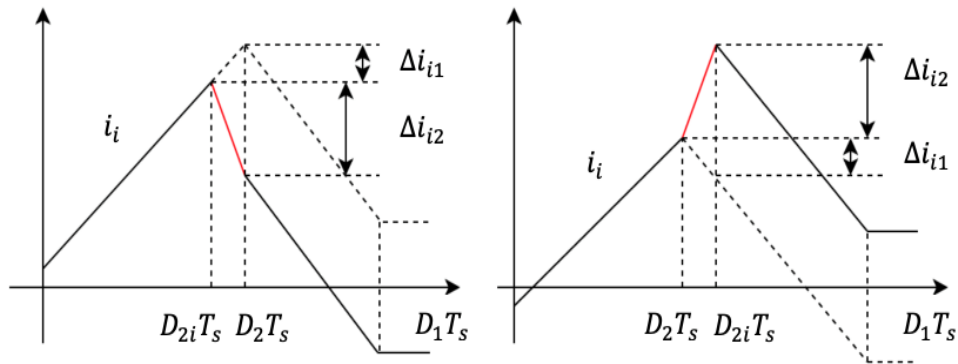


Figure 7 Current waveform according to the change of ΔD_{2i}

Two operation scenarios of i_i were examined analytically to quantify the relationship between ΔD_{2i} and the dynamic power change ΔP_i at the MV bridges. This analysis will be useful in finding matrix B of the state-space form, (3.28c). We will start with the operation action that can be changed due to ΔD_{2b} , then we will only present the final results for ΔD_{2c} and ΔD_{2d} .

Scenario 1: It is assumed that $\Delta D_2 > 0$ occurs on the M_b side: ($\Delta D_2 = \Delta D_{2b}$).

The change of i_b before the operation is $\frac{di_b}{dt} = \frac{V_b - \frac{nV_L + V_b + V_c + V_d}{4}}{L} = \frac{3V_b - nV_L - V_c - V_d}{4L}$, where the change of i_b after the operation is $\frac{di_b}{dt} = \frac{0 - \frac{nV_L + V_b + V_c + V_d}{4}}{L} = -\frac{V_c + V_d + nV_L}{4L}$. Therefore, the change of i_b due to ΔD_{2b} can be found in (3.15a) and (3.15b). So, the current change on M_b due to ΔD_{2b} is presented in (3.15c). Thus, the amount of power change is presented in (3.15d).

$$\Delta i_b^2 = \frac{3V_b - nV_L - V_c - V_d}{4Lf} \Delta D_{2b} \quad (3.15a)$$

$$\Delta i_b^1 = -\frac{V_c + V_d + nV_L}{4Lf} \Delta D_{2b} \quad (3.15b)$$

$$\Delta i_b = \Delta i_b^1 - \Delta i_b^2 = -\frac{3V_b}{4Lf} \Delta D_{2b} \quad (3.15c)$$

$$\Delta P_b = \frac{3V_b^2}{2Lf} D_{2b} \Delta D_{2b} \quad (3.15d)$$

Next, the change that ΔD_{2b} can make on the M_c side is formulated as follows. The current change of i_c before the operation is $\frac{di_c}{dt} = \frac{V_c - \frac{nV_L + V_b + V_c + V_d}{4}}{L} = \frac{3V_c - nV_L - V_b - V_d}{4L}$, where the change of i_c after the operation is $\frac{di_c}{dt} = \frac{V_c - \frac{nV_L + V_b + V_c + V_d}{4}}{L} = \frac{3V_c - V_d - nV_L}{4L}$. Therefore, the change of i_c and then ΔP_c due to ΔD_{2b} can be found in (3.16a) - (3.16d).

$$\Delta i_c^2 = \frac{3V_c - nV_L - V_b - V_d}{4Lf} \Delta D_{2b} \quad (3.16a)$$

$$\Delta i_c^1 = \frac{3V_c - V_d - nV_L}{4Lf} \Delta D_{2b} \quad (3.16b)$$

$$\Delta i_c = \Delta i_c^1 - \Delta i_c^2 = \frac{V_b}{4Lf} \Delta D_{2b} \quad (3.16c)$$

$$\Delta P_c = -\frac{V_b V_c}{4Lf} D_{2c} \Delta D_{2b} \quad (3.16d)$$

Similarly, the current change and the amount of power change on the M_d side due to the change operation of ΔD_{2b} is presented in (3.17a) and (3.17b).

$$\Delta i_d = \Delta i_d^1 - \Delta i_d^2 = \frac{V_b}{4Lf} \Delta D_{2b} \quad (3.17a)$$

$$\Delta P_d = -\frac{V_b V_d}{4Lf} D_{2d} \Delta D_{2b} \quad (3.17b)$$

Scenario 2: It is assumed that $\Delta D_2 < 0$ occurs on the M_b side ($\Delta D_2 = \Delta D_{2b}$).

The change of i_b before the operation is $\frac{di_b}{dt} = \frac{nV_L}{L}$, where the change of i_b after the operation is $\frac{di_b}{dt} = \frac{V_b - \frac{nV_L + V_b}{4}}{L} = -\frac{3V_b - nV_L}{4L}$. Therefore, the change of i_b due to ΔD_{2b} can be found in (3.18a) - (3.18c).

$$\Delta i_b^2 = \frac{nV_L}{4Lf} \Delta D_{2b} \quad (3.18a)$$

$$\Delta i_b^1 = \frac{nV_L - 3V_b}{4Lf} \Delta D_{2b} \quad (3.18b)$$

$$\Delta i_b = \Delta i_b^1 - \Delta i_b^2 = -\frac{3V_b}{4Lf} \Delta D_{2b} \quad (3.18c)$$

Then, the change of ΔD_{2b} that can be made on the M_c side is formulated as follows. The current change i_c before the operation is $\frac{di_c}{dt} = \frac{-nV_L}{L}$, where the change of i_c after the operation is $\frac{di_c}{dt} = \frac{-nV_L + V_b}{L}$. Therefore, the change of i_c due to ΔD_2 can be found in (3.19a) - (3.19c).

$$\Delta i_c^2 = \frac{nV_L}{4Lf} \Delta D_2 \quad (3.19a)$$

$$\Delta i_c^1 = \frac{nV_L + V_b}{4Lf} \Delta D_{2b} \quad (3.19b)$$

$$\Delta i_c = \Delta i_c^1 - \Delta i_c^2 = \frac{V_b}{4Lf} \Delta D_{2b} \quad (3.19c)$$

Since (3.18c) is found to be equal to (3.15c), and (3.19c) is equal to (3.16c). So, the amount of power change on the M_d side can be evaluated by Equation (3.17b).

The action of ΔD_{2c} on the power change at a given port can be formulated as (3.20) – (3.22), and the action of ΔD_{2d} on the power change at a given port can be formulated as (3.23) – (3.25).

$$\Delta P_c = \frac{3V_c^2}{2Lf} D_{2c} \Delta D_{2c} \quad (3.20)$$

$$\Delta P_b = -\frac{V_b V_c}{2Lf} D_{2b} \Delta D_{2c} \quad (3.21)$$

$$\Delta P_d = -\frac{V_c V_d}{2Lf} D_{2d} \Delta D_{2c} \quad (3.22)$$

$$\Delta P_d = \frac{3V_d^2}{2Lf} D_{2d} \Delta D_{2d} \quad (3.23)$$

$$\Delta P_b = -\frac{V_b V_d}{2Lf} D_{2b} \Delta D_{2d} \quad (3.24)$$

$$\Delta P_c = -\frac{V_c V_d}{2Lf} D_{2c} \Delta D_{2d} \quad (3.25)$$

From Equations (3.15d), (3.16d), (3.17b), and (3.20) - (3.25), the change in power caused by adjustments in ΔD_{2b} , ΔD_{2c} , ΔD_{2d} can be represented as (3.26).

$$\begin{bmatrix} \Delta P_b \\ \Delta P_c \\ \Delta P_d \end{bmatrix} = \begin{bmatrix} \frac{3V_b^2}{4Lf} D_{2b} & -\frac{V_b V_c}{4Lf} & -\frac{V_b V_d}{4Lf} \\ -\frac{V_b V_c}{4Lf} & \frac{3V_c^2}{4Lf} D_{2c} & -\frac{V_c V_d}{4Lf} \\ -\frac{V_b V_d}{4Lf} & -\frac{V_c V_d}{4Lf} & \frac{3V_d^2}{4Lf} D_{2d} \end{bmatrix} \begin{bmatrix} \Delta D_{2b} \\ \Delta D_{2c} \\ \Delta D_{2d} \end{bmatrix} \quad (3.26)$$

$$D_{2d} = \frac{nV_L}{3V_d - V_b - V_c} D_1 \quad (3.27)$$

A design objective is to balance the power at the MV side, yet, also guarantee ZCS of all the semiconductor cells. To do so, D_{2d} is determined with (3.27) and duty cycle D_{2b} and D_{2c} are updated with the LQR algorithm, Fig. 8. The nonlinear change of the converter due to the duty cycle D_2 is not considered to decrease the deviation.

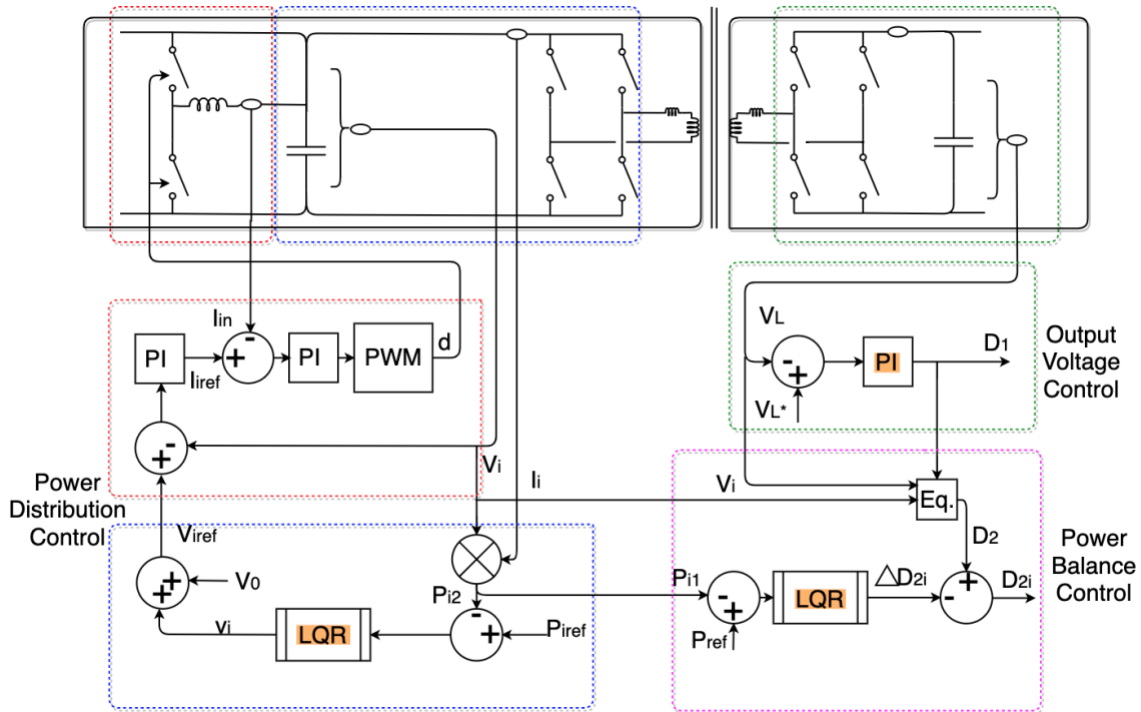


Figure 8 Structure of Control for the QAB

The discrete state space model of the balanced plant, (3.28a), which focuses only on bridge b and c , can be constructed using (3.26). It is assumed that A , (3.28b), is not changed, but matrix B , (3.28c), will alter according to the disturbances in the voltages and duty cycles on the MV side. Therefore, the plant is a nonlinear abnormal system. The uncertainty can be limited by bounding the voltage, or the change of ΔD_2 .

$$\begin{bmatrix} P_{b1}(n+1) \\ P_{c1}(n+1) \end{bmatrix} = A \begin{bmatrix} P_{b1}(n) \\ P_{c1}(n) \end{bmatrix} + B \begin{bmatrix} \Delta D_{2b} \\ \Delta D_{2c} \end{bmatrix} \quad (3.28a)$$

$$A = \begin{bmatrix} 1 & 0 \\ 0 & 1 \end{bmatrix} \quad (3.28b)$$

$$B = \begin{bmatrix} D_{2b} & 0 \\ 0 & D_{2c} \end{bmatrix} \begin{bmatrix} \frac{3V_b^2}{4Lf} & -\frac{V_b V_c}{4Lf} \\ -\frac{V_b V_c}{4Lf} & \frac{3V_c^2}{4Lf} \end{bmatrix} \quad (3.28c)$$

3.2.3 Proposed Power Distribution Control

For our study, a weighted value for x_b , x_c , and x_d is assigned to simulate the change in the power states at the MV port. Thus, $P_{iref} = x_i P_a$, where $i = b, c$, and d for each MV port. This power distribution control uses v_b , v_c , v_d as control signals. Thus, we can obtain the discrete state space model with PWM period as a sampling period. Since the power balance control and the power distribution control can interfere with each other at the MV side, for regulation purposes, we utilize the current of the first switching half period to obtain, P_{i1} , (power balance control) and the current of the second switching half period to obtain, P_{i2} , (power distributed control). Using the state feedback based LQR technique, we can obtain the state feedback matrix, K_P around the operating point.

Refer to Fig. 8 for the remaining discussion on the control. The offset signals, v_i , are used to obtain the voltage reference, V_{iref} , where V_0 is the voltage set point at no load condition. The current reference I_{iref} is generated by regulating the difference between V_{iref} and the output voltage V_i . From here, the duty cycle for the inner DC-DC converter is obtained to balance the voltage as shown in Fig. 8.

3.2.4 Mathematical Relation Between Power and Voltage in The Power Distributed Control

In order to find the control matrix B_p , (42), analytically, some assumptions will be considered. The half period starts at $t = 0$, (v_b, v_c, v_d) are constant, and a switching function, S_{D2i} , described by (3.29) will be utilized. In the forthcoming section, specific relationships will use the following relationship where x and y are specific port letters.

$$\min(D_{2x}, D_{2y}) = \begin{cases} D_{2x}, & \text{if } D_{2x} \geq D_{2y} \\ D_{2y}, & \text{else} \end{cases}$$

The central point voltage, v_x , shown in Fig. 2, can be written as (3.30). The current flowing on the MV side, i_i , is expressed by (3.31); where i_{i0} is the initial value of the current at the start of the half cycle. Therefore, the mean value of the power (P_{b2} , P_{c2} and P_{d2}) in one cycle, which considers only the half period, can be calculated by (3.32).

$$S_{D2i} = \begin{cases} 1, & 0 < t < D_{2i}T_s \\ 0, & D_{2i}T_s < t < \frac{T_s}{2} \end{cases} \quad (3.29)$$

$$v_x = \begin{cases} \frac{nv_L + v_b S_{d2b} + v_c S_{d2c} + v_d S_{d2d}}{4}, & 0 < t < D_1 T_s \\ 0, & D_1 T_s < t < \frac{T_s}{2} \end{cases} \quad (3.30)$$

$$i_i(t) = i_{i0} + \frac{1}{L} \int_0^t (v_i S_{d2i} - v_x) d\tau, \quad 0 < t < \frac{T_s}{2} \quad (3.31)$$

$$P_{i2} = \frac{1}{T_s} \int_0^{D_{2i} T_s} v_i i_i(t) dt \quad (3.32)$$

$$= \frac{v_i}{L T_s} \int_0^{D_{2i} T_s} dt \int_0^t (v_i S_{d2i} - v_x) d\tau + D_{2i} v_i i_{i0}$$

$$P_{b2} = \frac{v_b}{L T_s} \int_0^{D_{2b} T_s} dt \int_0^t \frac{3v_b S_{d2b} - v_c S_{d2c} - v_d S_{d2d} - nv_L}{4} d\tau + D_{2b} v_b i_{b0}$$

$$P_{b2} = \frac{v_b \left((3v_b - nv_L) D_{2b}^2 - v_c (\min(D_{2b}, D_{2c}))^2 - v_d (\min(D_{2b}, D_{2d}))^2 \right)}{8Lf} \quad (3.33)$$

$$+ D_{2b} v_b i_{b0}$$

$$P_{c2} = \frac{v_c \left((3v_c - nv_L) D_{2c}^2 - v_b (\min(D_{2b}, D_{2c}))^2 - v_d (\min(D_{2c}, D_{2d}))^2 \right)}{8Lf} \quad (3.34)$$

$$+ D_{2c} v_c i_{c0}$$

$$P_{d2} = \frac{v_d \left((3v_d - nv_L) D_{2d}^2 - v_b (\min(D_{2b}, D_{2d}))^2 - v_c (\min(D_{2c}, D_{2d}))^2 \right)}{8Lf} \quad (3.35)$$

$$+ D_{2d} v_d i_{d0}$$

The approximate change of the current waveform on the M_i side during one cycle assumes that D_1 and D_{2i} are both constant. Thus, i_{i0} is constant between the neighboring cycles (for samples taken at n and $n + 1$ as an example) and the changes in D_1 , D_{2i} , v_b , v_c , v_d and v_L can be ignored.

We introduce the notation $P_2 = [P_{b2}, P_{c2}, P_{d2}]^T$, $v = [v_b, v_c, v_d]^T$, and rewrite (3.33), (3.34) and (3.35) between n and $n + 1$ states as (3.36) and (3.37).

$$P_2(n) = P_{21}(v(n)) + P_{22}(v(n)) \quad (3.36)$$

$$P_2(n + 1) = P_{21}(v(n + 1)) + P_{22}(v(n + 1)) \quad (3.37)$$

Where,

$$P_{21}(v) = \frac{1}{8Lf} \begin{bmatrix} v_b \left((3v_b - nv_L) D_{2b}^2 - v_c (\min(D_{2b}, D_{2c}))^2 - v_d (\min(D_{2b}, D_{2d}))^2 \right) \\ v_c \left((3v_c - nv_L) D_{2c}^2 - v_b (\min(D_{2b}, D_{2c}))^2 - v_d (\min(D_{2c}, D_{2d}))^2 \right) \\ v_d \left((3v_d - nv_L) D_{2d}^2 - v_b (\min(D_{2b}, D_{2d}))^2 - v_c (\min(D_{2c}, D_{2d}))^2 \right) \end{bmatrix}$$

and

$$P_{22}(v) = D_{2d} i_{d0} \begin{bmatrix} v_b \\ v_c \\ v_d \end{bmatrix}$$

It is assumed that $P_{22}(v(n)) \approx P_{22}(v(n + 1))$, so we can obtain (3.38) by subtracting (3.36) from (3.37). Let the design parameter be $v = [v_b, v_c, v_d]^T$. Considering only a small change in v , $P_{21}(v)$ can be expressed as (3.39). Substitute (3.39) into (3.38) to obtain (3.40), while noting that $\Delta v = v(n + 1) - v(n)$ and a definition provided by (3.41).

$$P_2(n + 1) = P_2(n) + P_{21}(v(n + 1) - v(n)) \quad (3.38)$$

$$P_{21}(v) = P_{21}(V) + \frac{\partial P_{21}(v)}{\partial v} \Big|_V (v - V) + \frac{1}{2!} \frac{\partial^2 P_{21}(v)}{\partial v^2} \Big|_V (v - V)^2 \quad (3.39)$$

$$P_2(n + 1) = P_2(n) + \frac{\partial P_{21}(v)}{\partial v} \Big|_V \Delta v \quad (3.40)$$

$$\frac{\partial P_{21}(v)}{\partial v} \Big|_V = \frac{1}{8Lf} \begin{bmatrix} f_{bb} & f_{bc} & f_{bd} \\ f_{cb} & f_{cc} & f_{cd} \\ f_{db} & f_{dc} & f_{dd} \end{bmatrix} \quad (3.41)$$

Where,

$$f_{bb} = 6V_b D_{2b}^2 - V_c (\min(D_{2b}, D_{2c}))^2 - V_d (\min(D_{2b}, D_{2d}))^2 - nV_L D_{2b}^2$$

$$f_{bc} = -V_b (\min(D_{2b}, D_{2c}))^2$$

$$f_{bd} = -V_b (\min(D_{2b}, D_{2d}))^2$$

$$f_{cb} = -V_c (\min(D_{2b}, D_{2c}))^2$$

$$f_{cc} = 6V_c D_{2c}^2 - V_b (\min(D_{2b}, D_{2c}))^2 - V_d (\min(D_{2c}, D_{2d}))^2 - nV_L D_{2c}^2$$

$$f_{cd} = -V_c (\min(D_{2c}, D_{2d}))^2$$

$$f_{db} = -V_d (\min(D_{2b}, D_{2d}))^2$$

$$f_{dc} = -V_d (\min(D_{2c}, D_{2d}))^2$$

$$f_{dd} = 6V_d D_{2d}^2 - V_b (\min(D_{2b}, D_{2d}))^2 - V_c (\min(D_{2c}, D_{2d}))^2 - nV_L D_{2d}^2$$

Therefore, the discrete-time state space model of the power distribution control plant is found to be (3.42) after using (3.41).

$$P_2(n+1) = A_p P_2(n) + B_p \Delta v \quad (3.42)$$

Where, $A_p = I_{3 \times 3}$, $B_p = \frac{\partial P_{21}(v)}{\partial v} \Big|_V$

The matrix B_p is expressed as B_{p1} , (3.43), when $V_b = V_c = V_d = V_M$, and $D_{2b} = D_{2c} = D_{2d} = D_2$. The final form of B_p is listed as (3.45a).

$$B_{p1} = \frac{1}{8Lf} \begin{bmatrix} 4V_M - nV_L & -V_b & -V_b \\ -V_c & 4V_M - nV_L & -V_c \\ -V_d & -V_d & 4V_M - nV_L \end{bmatrix} D_2^2 \quad (3.43)$$

$$B_{p0} = \frac{1}{8Lf} \begin{bmatrix} 4V_M - nV_L & -V_b & -V_b \\ -V_c & 4V_M - nV_L & -V_c \\ -V_d & -V_d & 4V_M - nV_L \end{bmatrix} \quad (3.44)$$

$$B_p = (I_{3 \times 3} + D_2^{-2} \begin{bmatrix} D_{2b}^2 - D_2^2 & 0 & 0 \\ 0 & D_{2c}^2 - D_2^2 & 0 \\ 0 & 0 & D_{2d}^2 - D_2^2 \end{bmatrix}) \cdot D_2^2 \cdot B_{p0} \cdot (I_{3 \times 3} + B_{p0}^{-1} \dots \quad (3.45a)$$

$$(B_{p01} - B_{p0}))$$

$$B_p = (I_{3 \times 3} + \Delta_{2b}) \cdot D_2^2 \cdot B_{p0} \cdot (I_{3 \times 3} + \Delta_{1b})$$

$$\Delta_{2b} = \begin{bmatrix} \frac{D_{2b}^2}{D_2^2} - 1 & 0 & 0 \\ 0 & \frac{D_{2c}^2}{D_2^2} - 1 & 0 \\ 0 & 0 & \frac{D_{2d}^2}{D_2^2} - 1 \end{bmatrix} \quad (3.45b)$$

$$\Delta_{1b} = B_{p0}^{-1} (B_{p01} - B_{p0}) \quad (3.45c)$$

$$B_{p01} = \begin{bmatrix} B_{p01}(1,1) & B_{p01}(1,2) & B_{p01}(1,3) \\ B_{p01}(2,1) & B_{p01}(2,2) & B_{p01}(2,3) \\ B_{p01}(3,1) & B_{p01}(3,2) & B_{p01}(3,3) \end{bmatrix} \quad (3.45d)$$

Where,

$$B_{p01}(1,1) = 6V_M - V_M \frac{(\min(D_{2b}, D_{2c}))^2 + (\min(D_{2b}, D_{2d}))^2}{D_{2b}^2} - nV_L$$

$$B_{p01}(1,2) = -V_M \frac{(\min(D_{2b}, D_{2c}))^2}{D_{2b}^2}$$

$$\begin{aligned}
B_{p01}(1,3) &= -V_M \frac{(\min(D_{2b}, D_{2d}))^2}{D_{2b}^2} \\
B_{p01}(2,1) &= -V_M \frac{(\min(D_{2b}, D_{2c}))^2}{D_{2c}^2} \\
B_{p01}(2,2) &= 6V_M - V_M \frac{(\min(D_{2b}, D_{2c}))^2 + (\min(D_{2c}, D_{2d}))^2}{D_{2c}^2} - nV_L \\
B_{p01}(2,3) &= -V_M \frac{(\min(D_{2c}, D_{2d}))^2}{D_{2c}^2} \\
B_{p01}(3,1) &= -V_M \frac{(\min(D_{2b}, D_{2d}))^2}{D_{2d}^2} \\
B_{p01}(3,2) &= -V_M \frac{(\min(D_{2c}, D_{2d}))^2}{D_{2d}^2} \\
B_{p01}(3,3) &= 6V_M - V_M \frac{(\min(D_{2b}, D_{2d}))^2 + (\min(D_{2c}, D_{2d}))^2}{D_{2d}^2} - nV_L
\end{aligned}$$

Equation (3.45a) is the multiplicative uncertainty expression of the control matrix B_p separated by the input side, Δ_{2b} , and the output side, Δ_{1b} , with $B_{p0} \cdot D_2^2$ as the nominal plant. Here D_2^2 is chosen so that the norm of the model uncertainty Δ_{2b} may be small.

3.3 Power and Voltage Regulation Verification

The parameters of the QAB converter are shown in Table 1. Assumed weighted values are used to represent the change in the state of power at the MV side for each port as shown in Table 2. The proposed control scheme maintains the LV bus at 700 V and regulates the MV bus to its nominal value as shown in Fig. 9. With the prescribed change in power settings at 0.02 seconds

on the MV side and change at 0.04 seconds on the LV side, Fig. 10 and 11 shows the system regulation to the reference values to ensure power is equally shared by all three ports to the load.

The transition at 0.02 seconds is performed by changing the weighted value (x_b , x_c , and x_d). They are assigned to simulate the change in the power states at the MV side of the converter. A load step change is initiated at 0.4 seconds. In both scenarios, the transition processes are achieved smoothly, which validates the effectiveness of the proposed control scheme. As these system alterations occur, the duty cycle D_1 is updated accordingly resulting in duty cycle updates to D_{2b} , D_{2c} , and D_{2d} , according to (3.1), as shown in Fig. 12.

Table 1 Parameters of the Simulation Model

Symbol	Parameters	Value
V_M	DC input voltage	1120 V
V_L	Output voltage	700 V
n	T.F turns ratio	1.2
$L_{b,c,d}$	MV Inductors	12.7 μH
L_a	LV Inductor	7.5 μH
f_s	Switching frequency	20 kHz

Table 2 Power Alterations at Each MV Port

Time (s)	P_a (W)	P_{bref} (W)	P_{cref} (W)	P_{dref} (W)
0 - 0.02	5.5×10^4	$0.43P_a$	$0.20P_a$	$0.37P_a$
0.02 - 0.04	5.5×10^4	$0.27P_a$	$0.33P_a$	$0.40P_a$
0.04 - 0.06	10.3×10^4	$0.27P_a$	$0.33P_a$	$0.40P_a$

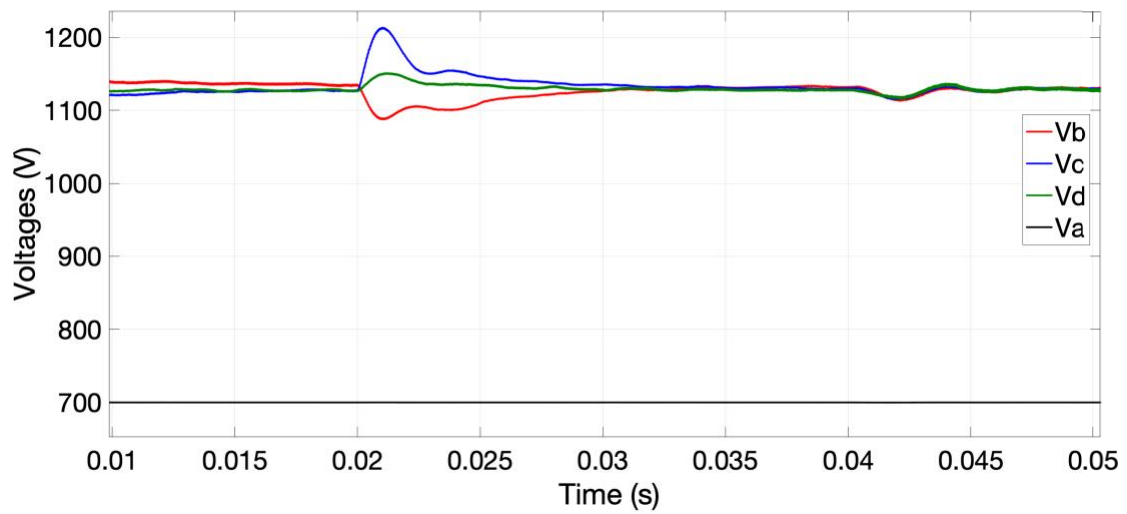


Figure 9 Measured voltages on the MV and LV side

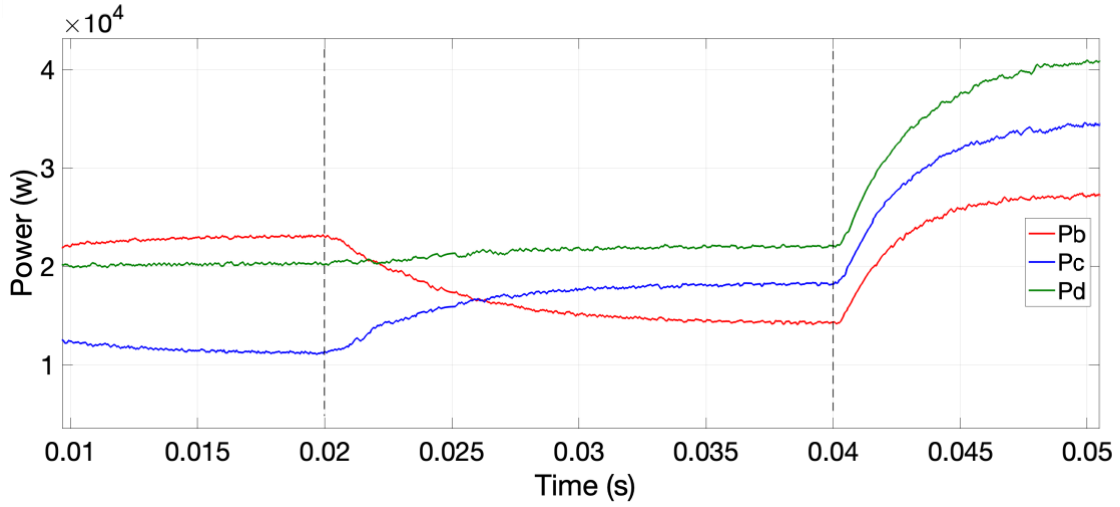


Figure 10 Power measurements throughout the QAB

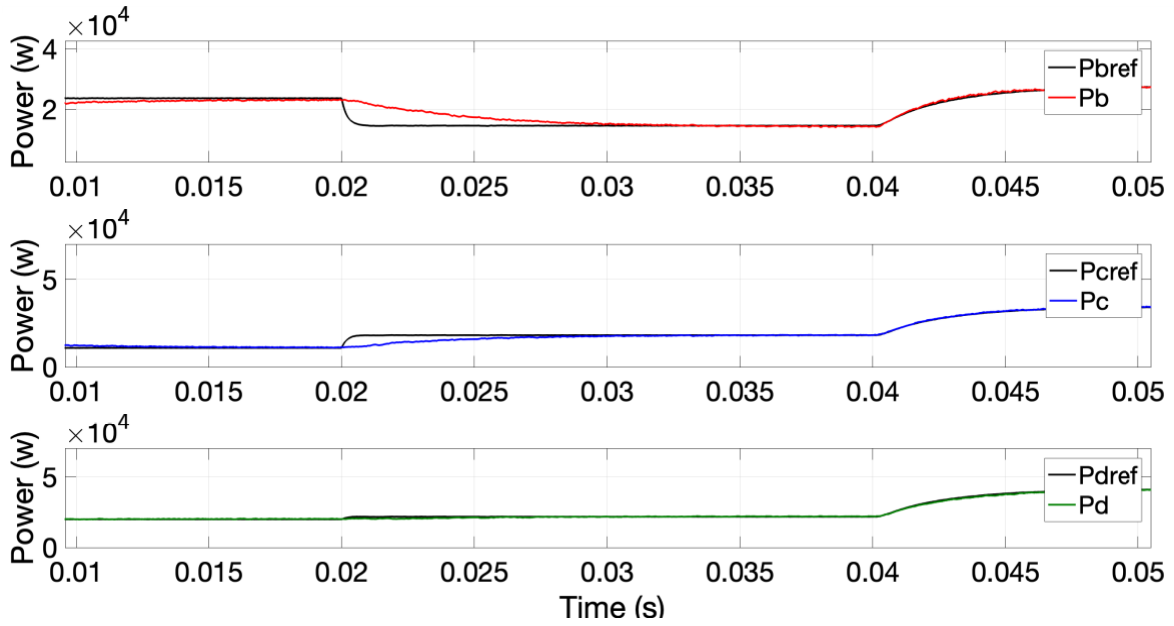


Figure 11 Power references and measurements on MV side

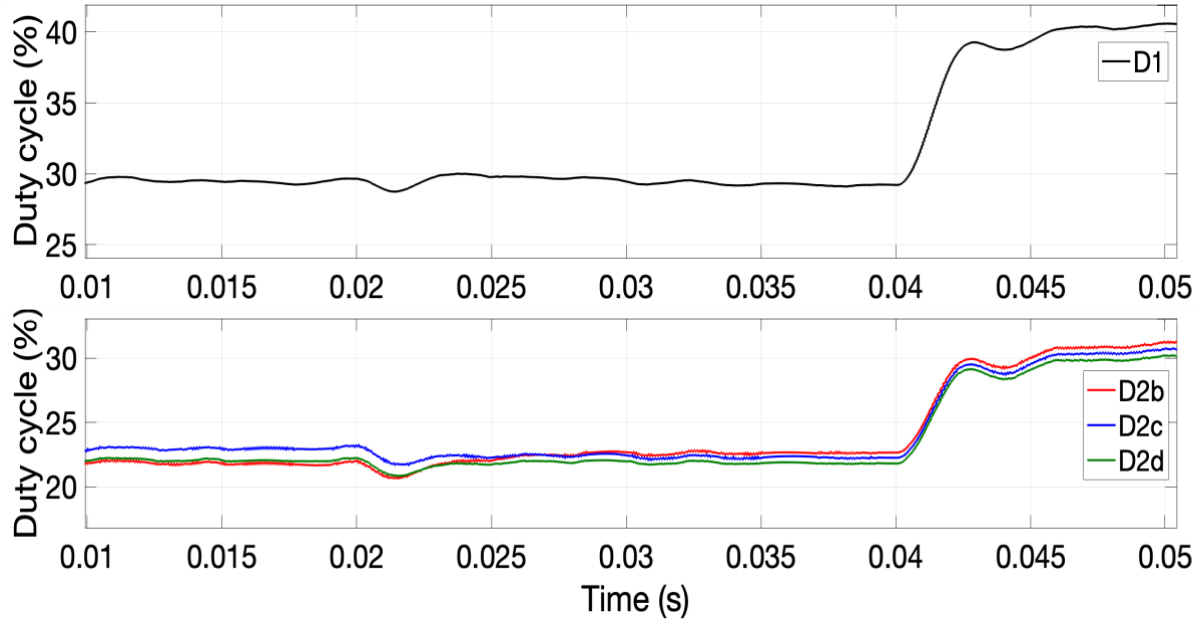


Figure 12 Duty cycles at MV side and LV side

For verification purposes, the voltage (V_a , V_b , and V_x) and current waveforms (i_{La} , i_{Lb} , i_{Lc} , and i_{Ld}) in the unbalance condition are shown in Fig. 13. The current i_{Lb} , i_{Lc} and i_{Ld} have an offset due ΔD_{2b} , ΔD_{2c} , and ΔD_{2d} , respectively. Lastly, the QAB converter maintains ZCS at the LV side.

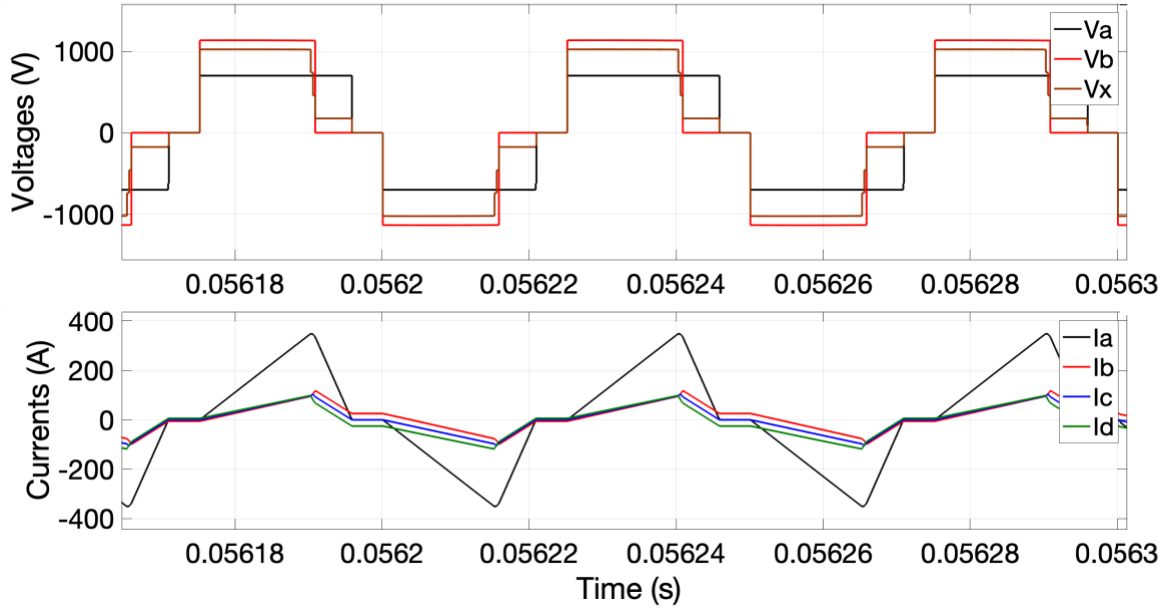


Figure 13 Voltages and currents using TCM

3.4 Conclusion

The power and voltage regulation for the SST based QAB has been performed on the MV side using the LQR based state feedback technique. Two operations were simulated. First, as the state of power was changed at the MV side and then, second, as a step change was applied at the LV side. In both scenarios, it has been shown that the power flow regulation in the converter can be achieved.

4.0 Power Regulation of a Solid-State Transformer Based Quad-Active Bridge DC-DC Converter Using Adaptive Linear Quadratic Regulator and Nonlinear Model Predictive Control

The SST is a combination of power electronic (PE) converters and a high-frequency transformer (HFT) as shown in Fig.14. Distributed energy resources (DER's) increasingly interface the SST. However, the high penetration of the intermittent DER can cause an unequal processed power through the QAB which leads to voltage unbalances on the MV side that impact the DC-link voltage [11]. This voltage unbalance problem makes it difficult to feed a common load without violating its voltage limits.

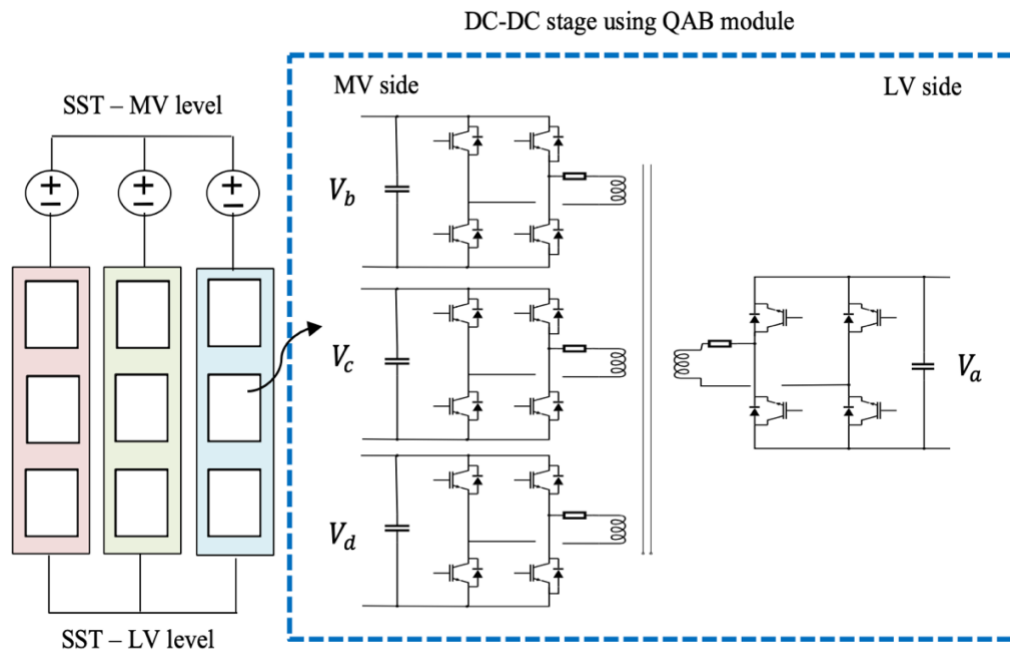


Figure 14 SST based QAB module

Therefore, voltage regulation routines must be investigated to target these voltage unbalances in order to maintain constant output voltage. A challenge identified and solved in this work is balancing the power at each of the ports on the MV side of the QAB module, labeled b , c , and d in Fig. 14. Several control techniques have been presented in the literature [11][16], but most have been applied to H-bridge topologies [14][15][18]. Power and voltage regulation of a SST based QAB was performed in [45]. The LQR technique was implemented into two control loops, a power balance loop and a power distribution loop. The objective of these two loops is to balance the power and voltage at the MV side respectively. Despite the effort reported, nonlinearity and uncertainty are still a challenge in MAB such as QAB [19]. LQR is designed with linear systems, which has a limited operation range, and cannot be directly applied to a nonlinear system [46]. So, other combined techniques have been investigated to mitigate the phenomena mentioned earlier.

Several adaptive control methods were proposed for different applications [30][46]. The ALQR is a useful tool in modern optimal control design. The power balance loop mentioned in [45] monitors the change in the duty cycle of the SST LV side, D_1 . However, we also have to consider the duty cycle at the MV side, D_2 in the control design to limit its uncertainty. In this paper, an adaptive method is introduced to track the nonlinear change of the converter due to the duty cycle D_2 and the voltage at the MV side. In this work, the power balance loop is implemented using ALQR based state feedback control assuming that the system is fully controllable.

A second dc/dc converter was added to control the voltage fed into the MV ports. This control loop, referred to as the power distribution control, used LQR. However, since LQR is designed for linear systems, it is often inadequate to describe a nonlinear multivariable plant. Several control techniques could be used to overcome the limitation of LQR. This motivates the use of NMPC which has been widely proposed as a promising technique for the control of power

electronic converters [35][47][48]. NMPC is an optimization-based method for the feedback control. It shows several advantages, such as fast dynamic response and flexibility to include constraints in the control loop [48]. In our control architecture, the power distribution control is implemented using NMPC.

The objective of this chapter is to develop a control strategy to improve the regulation of the SST based QAB, maintain the output voltage, and mitigate the effects of non-linearity and uncertainty associated with reference tracking. Therefore, the ALQR control and NMPC are implemented together for the QAB.

4.1 System Description and Converter Model

The dual active bridge (DAB) and quad active bridge (QAB) have been widely used as a module of the DC/DC stage of the SST as described in [1][11]. The QAB provides the same advantages as the DAB based SST but with minimal number of transformers [11][21]. The QAB designs have four active bridges, each of them is denoted by a , b , c , and d as presented in Fig. 14. The voltage at the medium voltage (MV) side and the low voltage (LV) side is represented as V_M and V_L , respectively. Bridge a is connected to the LV side, whereas bridges b , c , and d are connected to the MV side. The duty cycle for bridge a is given by D_1 while the duty cycles for the MV bridges are given by D_{2i} , where i reflects the ports b , c , and d . The triangular current modulation (TCM) is used to modulate the QAB in the SST to guarantee the soft switching operation as shown in Fig. 15.

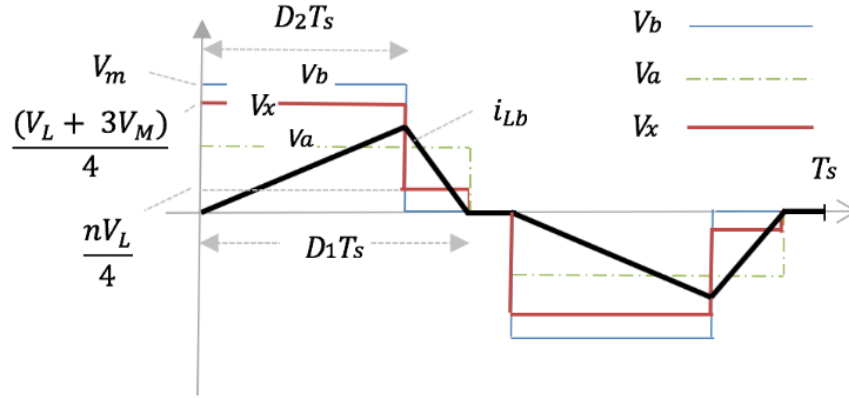


Figure 15 Modulation of the QAB

The operational principle of the TCM is described in [11]. As a result, the relation between D_1 and D_2 is presented in (4.1). The inductance value, L , can be calculated with (4.2). In this study, it is assumed that the QAB operates with unbalanced power flow through each of the SST ports, $P_b \neq P_c \neq P_d$. Thus, the duty cycle of each port of the MV side will have a nominal value, D_2 , and dynamic value, ΔD_{2i} , defined by (4.3). The transformer turns ratio and the switching frequency are represented by n and f , respectively.

$$D_2 = \frac{n V_L}{V_M} D_1 \quad ; \quad D_1 \leq 0.5 \quad (4.1)$$

$$L = \frac{3D_1^2 (V_L n)^2 (V_M - nV_L)}{4 P f_s V_M} \quad (4.2)$$

$$D_{2i} = D_2 - \Delta D_{2i} \quad (4.3)$$

where; $\Delta D_{2i} = P_{ref} - P_i$

$$P_{ref} = \frac{1}{3} P_{a1} \cdot I_i$$

$$P_i = V_i \cdot I_i$$

4.2 Controller Design for Regulating QAB Port Power and DC Output Voltage

Three control loops are implemented in this work for regulating power and voltage at the MV of SST based QAB. First, a feedback voltage regulator is used to maintain the output voltage at the LV side. Secondly, ALQR is implemented here to balance the unequal processed power at the MV side. Last loop is related to the inner DC-DC converter to regulate the voltage given to the MV ports of QAB. This will be explained in the forthcoming sections.

4.2.1 Proposed Output Voltage Control

A feedback voltage regulator $G_v(s)$ is designed to maintain a constant voltage level at the LV side. The voltage regulator $G_v(s)$ operates by comparing the actual output voltage, V_L , to the voltage reference set-value, V_{ref} . To maintain the output voltage, the transfer function, (4.4a) between the output voltage and duty cycle were obtained. Coefficients a and b for transfer function, $G_v(s)$, have been analytically developed. Note that T_s is the switching time, τ is the control delay, and C_a represents the capacitor on bridge a .

$$G_v(s) = \frac{\tilde{v}_L(s)}{\tilde{d}_1(s)} = \frac{b}{s + a} e^{-\tau s} \quad (4.4a)$$

$$a = \left(\frac{6n}{8LfC_a} - \frac{12n^2V_L}{8LfC_aV_M} \right) D_1 \quad (4.4b)$$

$$b = \left(\frac{6n}{8LfC_a} - \frac{6n^2V_L}{8LfC_aV_M} \right) V_L \quad (4.4c)$$

4.2.2 Proposed Power Balance Control

In the unbalanced condition, $P_{b1} + P_{c1} + P_{d1} = P_{a1}$ must hold. A change in any of the duty cycles in the QAB will alter peak currents and, hence, port power. Two operational scenarios of current i_i were examined analytically to quantify the relationship between ΔD_{2i} and the dynamic power change ΔP_i at the MV bridges as described in (4.5). The discrete state space model of the balanced plant, (4.6), which focuses only on bridge b and c , can be constructed using (4.5) as explained in [45]. Here, it is assumed that A is not changed, but matrix B , (4.7), will alter according to the disturbances in the voltages and duty cycles on the MV side. Note that matrix B_1 , (4.7), is expressed as B_0 when $V_b = V_c = V_d = V_M$. The plant is a nonlinear abnormal system. Therefore, the ALQR controller is implemented to achieve the power balance control goal for the nominal model as shown in Fig. 16.

$$\begin{bmatrix} \Delta P_b \\ \Delta P_c \\ \Delta P_d \end{bmatrix} = \begin{bmatrix} \frac{3V_b^2}{4Lf} D_{2b} & -\frac{V_b V_c}{4Lf} & -\frac{V_b V_d}{4Lf} \\ -\frac{V_b V_c}{4Lf} & \frac{3V_c^2}{4Lf} D_{2c} & -\frac{V_c V_d}{4Lf} \\ -\frac{V_b V_d}{4Lf} & -\frac{V_c V_d}{4Lf} & \frac{3V_d^2}{4Lf} D_{2d} \end{bmatrix} \begin{bmatrix} \Delta D_{2b} \\ \Delta D_{2c} \\ \Delta D_{2d} \end{bmatrix} \quad (4.5)$$

$$\begin{bmatrix} P_{b1}(n+1) \\ P_{c1}(n+1) \end{bmatrix} = A \begin{bmatrix} P_{b1}(n) \\ P_{c1}(n) \end{bmatrix} + B \begin{bmatrix} \Delta D_{2b} \\ \Delta D_{2c} \end{bmatrix} \quad (4.6)$$

$$B = \begin{bmatrix} D_{2b} & 0 \\ 0 & D_{2c} \end{bmatrix} \begin{bmatrix} \frac{3V_b^2}{4Lf} & -\frac{V_b V_c}{4Lf} \\ -\frac{V_b V_c}{4Lf} & \frac{3V_c^2}{4Lf} \end{bmatrix} = D_2 B_1 \quad (4.7)$$

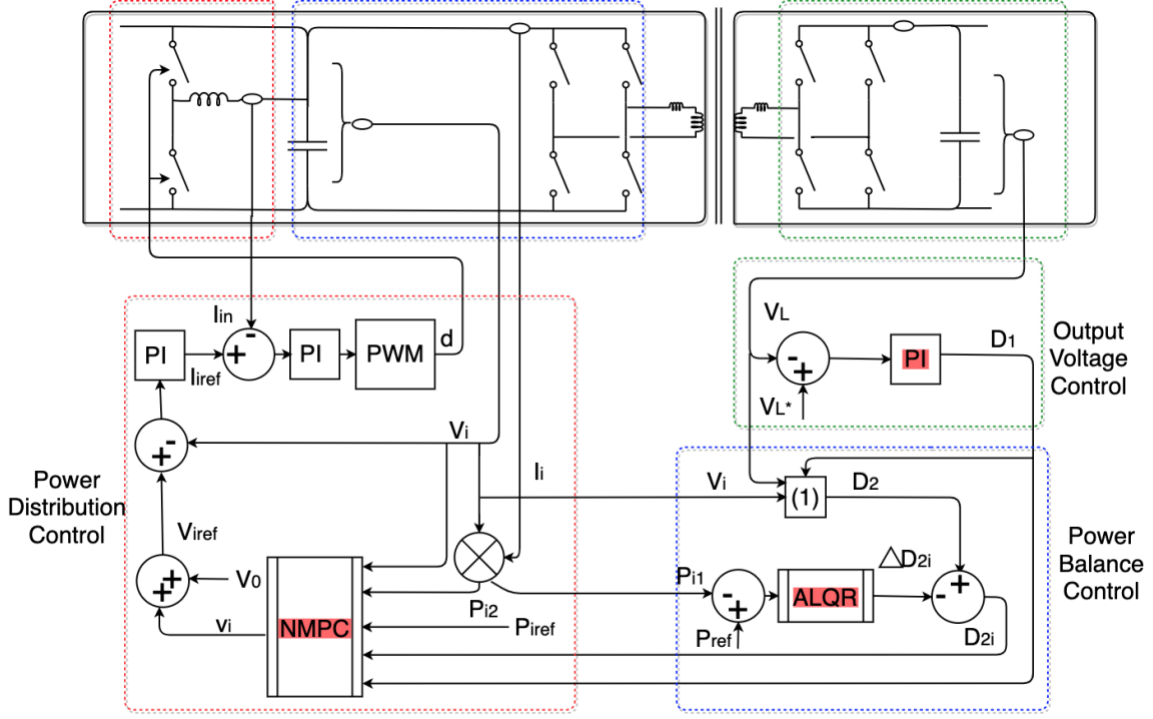


Figure 16 Control Structure for the SST based QAB

Assuming that we can measure the state $x = \begin{bmatrix} P_{b1} \\ P_{c1} \end{bmatrix}$ of the model expressed in (4.6), we can build a balanced control system with a high tracking performance by the following state-feedback system [31]. Consider $r(n) = \begin{bmatrix} \frac{1}{3} P_{a1}(n) \\ \frac{1}{3} P_{a1}(n) \end{bmatrix}$ as the setpoints of P_{b1} and P_{c1} at the current time, the control signal is defined as $u(n) = \begin{bmatrix} \Delta D_{2b} \\ \Delta D_{2c} \end{bmatrix}$, and error is $e(n) = r(n) - x(n)$.

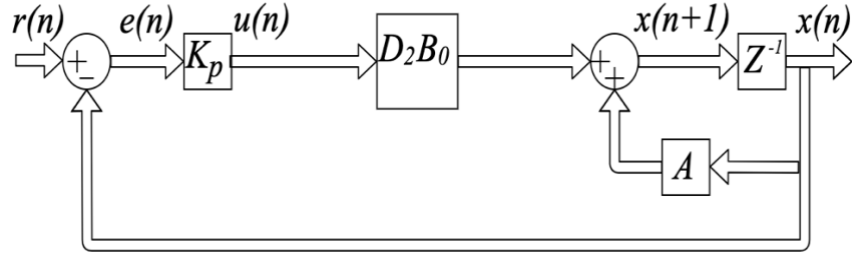


Figure 17 The design structure of the balanced control loop

The state feedback matrix, K_p , can be found by designing the control system for the nominal plant, $D_2 B_0$. The state space model of the nominal plant including the integrator in Fig. 17 is described as (4.8) where the last term, $r(n) - r(n + 1)$, represents disturbances in the conversion system. If the system is stabilized and P_{a1} converges to a specified value, the disturbance terms decline and ultimately reach zero. Thus, K_p can be obtained as a result of the minimization of quadratic cost function - observe (4.9a) or (4.10a). The state cost, Q , and the input cost, R , can be set in inverse proportion to $|e|_{max}^2$ and $|u|_{max}^2$, taking into account the maximum value that $|e|$ and $|u|$ can reach.

$$e(n + 1) = I_{2 \times 2} e(n) + D_2 B_0 u(n) + (r(n) - r(n + 1)) \quad (4.8)$$

$$J(u) = \sum_{n=1}^{\infty} (e(n)^T Q e(n) + u(n)^T R u(n)) \quad (4.9a)$$

$$K_{po} = (B B_0^T S_0 B B_0 + R)^{-1} \cdot B B_0^T S_0 A \quad (4.9b)$$

$$J(u) = \sum_{n=1}^{\infty} (e(n)^T Q e(n) + u(n)^T w^2 R u(n)) \quad (4.10a)$$

$$K_p = (w^2 B B_0^T S B B_0 + w^2 R)^{-1} \cdot (w B B_0^T) S A \quad (4.10b)$$

$$\begin{aligned}
\text{So, } K_p &= \frac{1}{w} K_{p0} \\
u(n) &= -K_p e(n) = -\frac{1}{w} K_{p0} e(n) \\
u(n) &= \frac{D_{20}}{D_2} K_{p0} [x(n) - r(n)]
\end{aligned} \tag{4.11}$$

Let's consider the state feedback matrix based LQR, K_{p0} , as the controllers obtained by using nominal set-point, (4.1), based upon parameters in Table IV; $D_{20} = 0.35$ [11]. When we assume that $A = I$, I being the identify matrix, and $BB_0 = D_{20} \cdot B_0$, K_{p0} can be determined from (4.9b), where, S_0 is a solution of the discrete-time Riccati equation. However, this controller cannot guarantee that the minimization of the evaluation cost function (4.9a) is achieved when D_2 changes. Therefore, the ALQR control is implemented which copes with the change of D_2 . Assuming that D_2 changes according to $D_2 = D_{20}w$, where w is a weight to represent the change of D_2 . Then, the ALQR problem can be set to minimize the performance cost function listed as (4.10a). The state feedback matrix based ALQR, K_p , can be determined by (4.10b). Although D_2 is changed according to $D_{20}w$, the same LQR control performance can be maintained along with the factor $\frac{D_{20}}{D_2}$ as shown in (4.11).

4.2.3 Proposed Power Distribution Control

The overall structure of a NMPC scheme is illustrated in Fig. 18. It is necessary to obtain measurements of the states of the system. The idea of the NMPC is that we optimize the predicted

future behavior of the system by minimizing a cost function over a finite time horizon using a model of the system. Then, use the optimal solution as a feedback control for the next sampling interval until new measurements of the state are available [47]-[48].

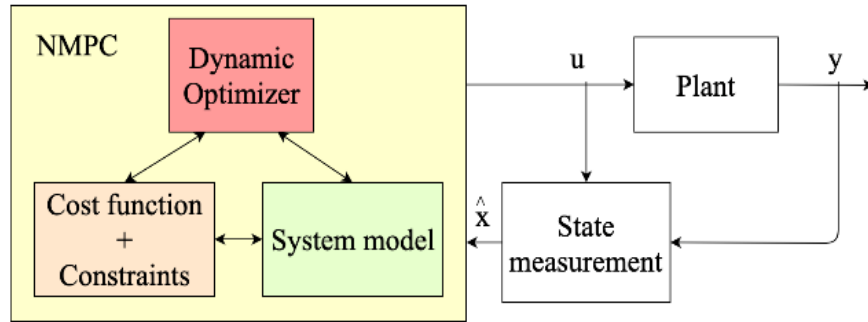


Figure 18 Basic NMPC control loop

Referring to the dashed blue region in Fig. 16 and using the predicted and locally measured parameters, the offset signals, v_i , are acquired. This signal along with the voltage set point at no load, V_0 , are used to obtain the voltage reference, V_{iref} . The current reference, I_{iref} , is generated by regulating the difference between, V_{iref} , and the output voltage, V_i . Then, the duty cycle for the inner DC-DC converter, the dashed red box in Fig. 16, is obtained to balance the voltage.

The half period starts at $t = 0$, (v_b, v_c, v_d) are constant where i_{i0} is the initial value of the current at the start of the half cycle. The mean value of the power (P_{b2} , P_{c2} and P_{d2}) in one cycle, which considers only the half period, is derived analytically (4.12). The QAB distribution plant with $P_2 = [P_{b2}, P_{c2}, P_{d2}]^T$ as control value and $v = [v_b, v_c, v_d]^T$ as control signal, is a nonlinear multivariable plant which changes according to D_{2i} .

$$P_{b2} = \frac{v_b(3v_b - v_c - v_d - nv_L)D_{2b}^2}{8Lf} + i_{b0} \cdot D_{2b} \cdot v_b \quad (4.12a)$$

$$P_{c2} = \frac{v_c[(3v_c - v_d - nv_L)D_{2c}^2 + v_bD_{2b}^2 - 2v_bD_{2b}D_{2c}]}{8Lf} + i_{c0} \cdot D_{2c} \cdot v_c \quad (4.12b)$$

$$P_{d2} = \frac{v_d[(3v_d - nv_L)D_{2d}^2 + v_bD_{2b}^2 + v_cD_{2c}^2 - 2(v_bD_{2b} + v_cD_{2c})D_{2d}]}{8Lf} + \dots \quad (4.12c)$$

$$i_{c0} \cdot D_{2d} \cdot v_d$$

$$J_P(v) = (P_{bref}(n+1) - P_{b2}(n+1))^2 + (P_{cref}(n+1) - P_{c2}(n+1))^2 \dots \quad (4.13)$$

$$+(P_{dref}(n+1) - P_{d2}(n+1))^2$$

The NMPC control process involves: the model predictive using measurement value, i_{i0} , using the mean power (4.12), minimizing the cost function, (4.13) and the online optimization using Resilient Backpropagation (RPROP), Fig. 5. The variable i_{i0} is used for prediction because it is almost constant over a certain period of time (for samples taken at n and $n+1$ as an example). This controller is designed by an algorithm that realizes a gradient descent characteristic of (4.13) under these system constraints. The cost function used for the NMPC algorithm, (4.13), will be minimized by the optimization algorithm, RPROP. Equation (4.14) is used to calculate the Jacobian of the cost function, (4.13), for v_i .

$$\begin{bmatrix} \frac{\partial J_P}{\partial v_b} \\ \frac{\partial J_P}{\partial v_c} \\ \frac{\partial J_P}{\partial v_d} \end{bmatrix} = 2 \cdot \begin{bmatrix} \frac{\partial P_{b2}}{\partial v_b} & \frac{\partial P_{c2}}{\partial v_b} & \frac{\partial P_{d2}}{\partial v_b} \\ \frac{\partial P_{b2}}{\partial v_c} & \frac{\partial P_{c2}}{\partial v_c} & \frac{\partial P_{d2}}{\partial v_c} \\ \frac{\partial P_{b2}}{\partial v_d} & \frac{\partial P_{c2}}{\partial v_d} & \frac{\partial P_{d2}}{\partial v_d} \end{bmatrix} \cdot \begin{bmatrix} P_{b2} - P_{bref} \\ P_{c2} - P_{cref} \\ P_{d2} - P_{dref} \end{bmatrix} \quad (4.14)$$

Where,

$$\frac{\partial P_{b2}}{\partial v_b} = \frac{(6v_b - v_c - v_d - nv_L) \cdot D_{2b}^2}{8 \cdot L \cdot f} + i_b D_{2b}$$

$$\frac{\partial P_{c2}}{\partial v_b} = \frac{v_c D_{2b} (D_{2b} - 2D_{2c})}{8 \cdot L \cdot f}$$

$$\frac{\partial P_{d2}}{\partial v_b} = \frac{v_d D_{2b} (D_{2b} - 2D_{2d})}{8 \cdot L \cdot f}$$

$$\frac{\partial P_{b2}}{\partial v_c} = \frac{-v_b \cdot D_{2b}^2}{8 \cdot L \cdot f}$$

$$\frac{\partial P_{c2}}{\partial v_c} = \frac{(6v_c - v_d - nv_L) \cdot D_{2c}^2 + v_b D_{2b} (D_{2b} - 2D_{2c})}{8 \cdot L \cdot f} + i_c D_{2c}$$

$$\frac{\partial P_{d2}}{\partial v_c} = \frac{v_d D_{2c} (D_{2c} - 2D_{2d})}{8 \cdot L \cdot f}$$

$$\frac{\partial P_{b2}}{\partial v_d} = \frac{\partial P_{b2}}{\partial v_c}$$

$$\frac{\partial P_{c2}}{\partial v_d} = \frac{-v_c \cdot D_{2c}^2}{8 \cdot L \cdot f}$$

$$\frac{\partial P_{d2}}{\partial v_d} = \frac{(6v_c - nv_L) D_{2d}^2 - 2(v_b D_{2b} + v_c D_{2c}) D_{2d}}{8 \cdot L \cdot f} - \frac{\partial P_{b2}}{\partial v_c} - \frac{\partial P_{c2}}{\partial v_d} + i_d D_{2d}$$

RPROP is a learning scheme that performs a direct adaptation of each weight based on local gradient information. It considers only the sign of the partial derivative to perform both learning and adaptation [49]. The RPROP algorithm can be repeated several times in one control cycle to improve the accuracy in determining the optimal solution. At this time, P_{i2} and v_i are changed according to the result of the previous execution, and P_{iref} is fixed to $P_{iref}(n + 1)$. If the cost function value at the preceding execution process is smaller than the current execution process, the repeated execution is stopped to ensure monotonicity reduction characteristics of

optimization. The voltage constraint is supplemented to the RPROP algorithm. RPROP, as seen in Table 3, introducing a time varying weight step Δ_i that determines the size of the weight update, while Δ_{vi} represents the weight update itself.

Note that, $(t - 1)$ represents the previous execution process, (t) represents current execution process, and $(t + 1)$ represents the next execution process. In the algorithm, the minimum step is $\Delta_{min} = 0.1$ and the maximum step is $\Delta_{max} = 10$. The optimizer parameters are set to $\eta^+ = 1.2$, $\eta^- = 0.5$, and $S = 1e - 6$. In order to reduce the effect of voltage saturation or D_1 saturation, a setpoint and saturation information are implemented in the control scheme. V_{max} and V_{min} are set as the more deviating values from the constraint voltage as $V_{max} = 1200 + \Delta_{max}/2$ and $V_{min} = 1010 - \Delta_{min}/2$.

Table 3 The Resilient Backpropagation (RPROP) algorithm

Algorithm 1
<p>If $\frac{\partial J_P}{\partial v_i}(t-1) \cdot \frac{\partial J_P}{\partial v_i}(t) > S$ then</p> $\Delta_i(t) = \min(\Delta_i(t-1) \times \eta^+, \Delta_{max})$ $\Delta_{v_i}(t) = -sign(\frac{\partial J_P}{\partial v_i}(t)) \times \Delta_i(t)$ <p>else if $\frac{\partial J_P}{\partial v_i}(t-1) \cdot \frac{\partial J_P}{\partial v_i}(t) < -S$ then</p> $\Delta_i(t) = \max(\Delta_i(t-1) \times \eta^-, \Delta_{min})$ $\Delta_{v_i}(t) = -\Delta_{v_i}(t-1)$ $\frac{\partial J_P}{\partial v_i}(t) = 0$ <p>else</p> $\Delta_{v_i}(t) = -sign(\frac{\partial J_P}{\partial v_i}(t)) \times \Delta_i(t-1)$ <p>End</p> $v_{temp} = v_i(t) + \Delta_{v_i}(t)$ <p>if $\Delta_{v_i}(t) > 0 \ \&\& \ v_{temp} > V_{max}$ then</p> $\Delta_{v_i}(t) = \max(0, V_{max} - v_i(t))$ $v_{temp} = V_{max}$ $\frac{\partial J_P}{\partial v_i}(t) = 0$ <p>else if $\Delta_{v_i}(t) < 0 \ \&\& \ v_{temp} < V_{min}$ then</p> $\Delta_{v_i}(t) = \min(0, V_{min} - v_i(t))$ $v_{temp} = V_{min}$ $\frac{\partial J_P}{\partial v_i}(t) = 0$ <p>End</p> $v_i(t+1) = v_{temp}$

4.3 Power and Voltage Regulation Verification

The parameters of the QAB converter are shown in Table 4. Different cases are examined here such as a step load change on the LV side, and a change in the state of power on the MV side as shown in Table 5. Note: a resistive-inductive load is connected at the output side of QAB. The proposed control scheme maintains the LV bus at 700 V and regulates the MV bus to its nominal value as shown in Fig. 19.

The QAB converter is initiated to serve $8.7 \times 10^4 \text{W}$. Then, a load step change is initiated at 0.03 seconds to $13.6 \times 10^4 \text{W}$. The transition at 0.06 and 0.085 seconds is performed by changing the injected power at ports b and c to simulate the change in the power states at the MV side of the converter. Port d responds to this change accordingly to perform the power regulation as shown in Fig. 20. The system regulation to the reference can be seen in Fig 21. The transition processes are achieved smoothly, which validates the effectiveness of the proposed control scheme. As these system alterations occur, the duty cycle D_1 is updated accordingly resulting in duty cycle updates to D_{2b} , D_{2c} , and D_{2d} , according to (1) and (3), as shown in Fig. 22.

Table 4 Parameters of the Simulation Model

Symbol	Parameters	Value
V_M	DC input voltage	1120 V
V_L	Output voltage	700 V
n	T.F turns ratio	1.2
$L_{b,c,d}$	MV Inductors	12.7 μH
L_a	LV Inductor	7.5 μH
f_s	Switching frequency	20 kHz

Table 5 Power Alterations at Each MV Port

Time (s)	P_a (W)	P_{bref} (W)	P_{cref} (W)	P_{dref} (W)
0.00 - 0.03	8.7×10^4	$P_b + P_c + P_d = P_a$		
0.03 - 0.06	13.6×10^4	9×10^4	7×10^4	-2.4×10^4
0.06 - 0.085	13.6×10^4	9×10^4	5×10^4	-0.4×10^4
0.085 - 0.12	13.6×10^4	7×10^4	5×10^4	1.6×10^4

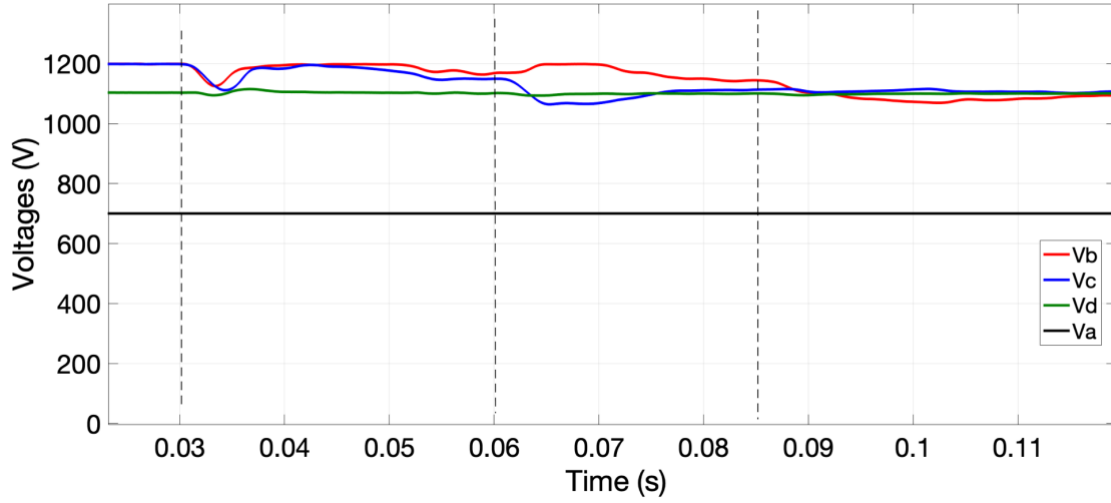


Figure 19 Measured voltages on the MV and LV side

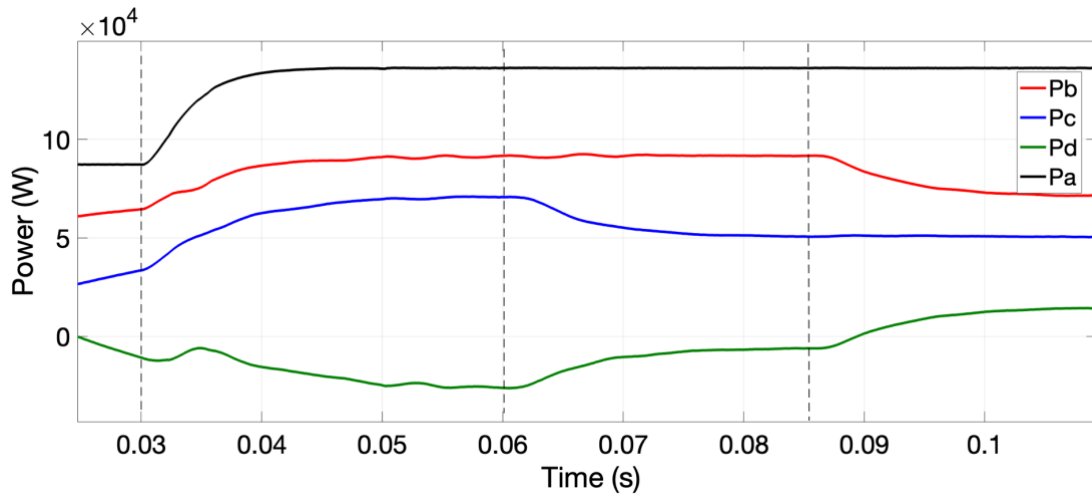


Figure 20 Power measurements throughout the QAB

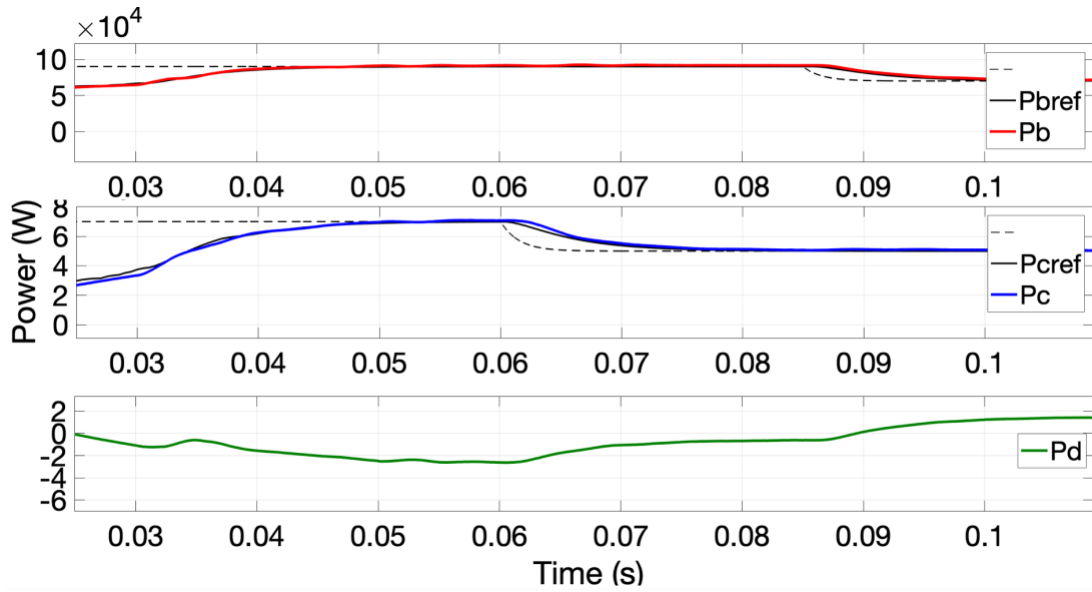


Figure 21 Power references and measurements on MV side

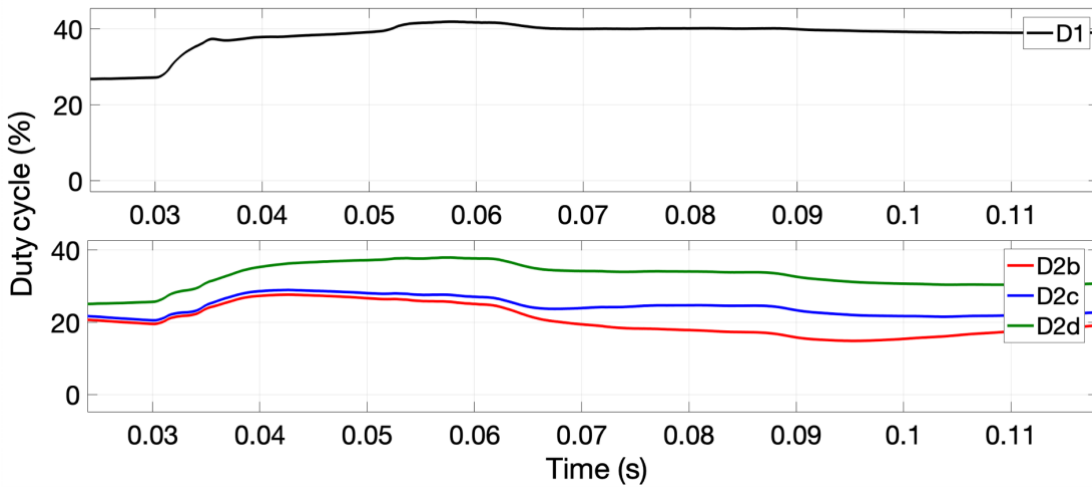


Figure 22 Duty cycles at MV side and LV side

For verification purposes, the voltage (V_a , V_b , and V_x) and current waveforms (i_{La} , i_{Lb} , i_{Lc} , and i_{Ld}) in the unbalance condition are shown in Fig.23. The current i_{Lb} , i_{Lc} and i_{Ld} have an offset due ΔD_{2b} , ΔD_{2c} , and ΔD_{2d} , respectively. Lastly, the QAB converter maintains ZCS at the LV side.

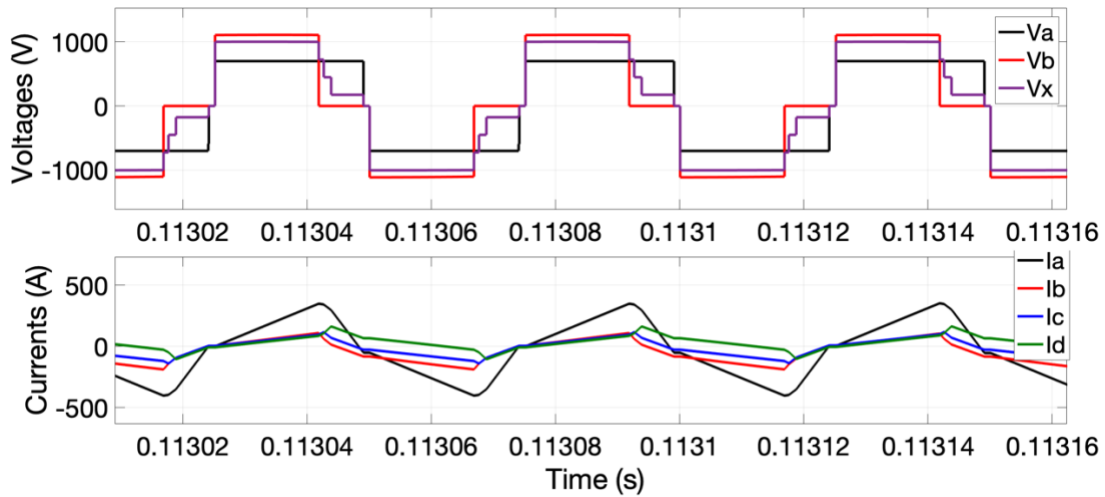


Figure 23 Voltages and currents using TCM

4.4 Conclusion

The power and voltage regulation for the SST based QAB has been performed on the MV side using the ALQR and NMPC techniques. Two operations were simulated, it has been shown that the power flow regulation in the converter can be achieved which validates the effectiveness of the proposed control scheme.

5.0 Power and Voltage Regulation of Quad Active Bridge DC-DC Converter Considering Stability

The SST has received substantial attention because of its potential in helping to achieve more intelligent grid systems. The SST is a combination of power electronic (PE) converters and a high-frequency transformer (HFT) as shown in Fig.24.

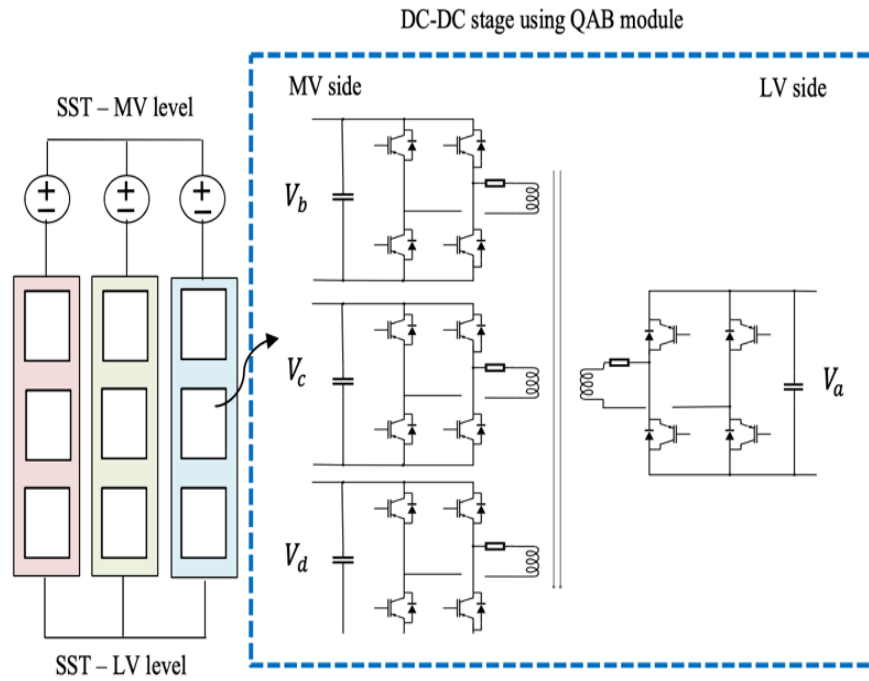


Figure 24 SST based QAB module

The voltage regulation routines must be investigated to target the voltage unbalances in order to maintain constant output voltage at the LV side of the QAB module, labeled *a* in Fig 24. A challenge identified and solved in this work is balancing the power at each of the ports on the MV side of the QAB module, labeled *b*, *c*, and *d* in Fig. 24.

Power and voltage regulation of a SST based QAB was performed in [45]. The LQR technique was implemented into two control loops, a power balance loop and a power distribution loop. The objective of these two loops is to balance the power and voltage at the MV side respectively. Despite the effort reported, nonlinearity and uncertainty are still a challenge in MAB such as QAB [19]. LQR is designed for linear systems, which has a limited operation range, it is often inadequate to describe a nonlinear multivariable plant. So, other combined techniques have been investigated to mitigate the phenomena mentioned earlier [51].

The ALQR and NMPC techniques were implemented into the power balance loop and power distribution loop, respectively [51]. The adaptive method was introduced to track the nonlinear change of the converter due to the duty cycle D_2 and the voltage at the MV side to balance the power at the MV side. The power distribution control loop is implemented using NMPC through a second dc/dc converter at the MV side. The NMPC is an optimization-based method for the feedback control. An important advantage of the NMPC is its ability to cope with hard constraints on controls and states [47][48].

Although regulation purpose was maintained in [51], stability is still a challenging point in the NMPC design. The objective of this chapter is to develop a control strategy to improve the regulation of the SST based QAB considering a practical NMPC scheme that guarantees asymptotic stability. The ALQR control and NMPC are implemented together for the DC-DC stage of the SST. This section presents the stability based suboptimal fixed horizon versions of NMPC for discrete-time systems.

5.1 Background of Model Predictive Control

The idea of the NMPC is that we optimize the predicted future behavior of the system by minimizing a cost function over a finite time horizon using a model of the system. Then, use the optimal solution as a feedback control signal for the next sampling interval until new measurements of the states are available [47][48].

NMPC has been receiving more attention in the last decade. This interest is motivated by the performance specifications. In addition, more constraints need to be satisfied such as environmental and safety considerations. These requirements can only be met when process nonlinearities and constraints are considered in the controller design. The NMPC is an extension of well-established linear model predictive control (MPC) to the nonlinear system. The industrial applications of NMPC are growing rapidly. However, none of the NMPC algorithms provided by vendors include stability constraints. Mostly, they rely upon setting the prediction horizon long enough to approximate an infinite horizon. Future developments in NMPC will hopefully contribute to making the gap between academia and industry even smaller [52].

Stability has been one of the critical issues in MPC, ever since linear MPC was criticized for its loss of stability [53]. This problem has been solved for MPC using infinite horizon predictive control and terminal constraints [36]. Stability has been intensively investigated, resulting in different strategies to impose stability: a locally stabilizing terminal feedback controller, a terminal constraint, and a terminal cost.

With regards to NMPC, the first stability result was given by Mayne and Michalska [54]. They show that NMPC can stabilize plants when a terminal equality constraint is embedded in the optimization problem. However, solving the NMPC optimization problem with equality constraints is highly computationally intensive, and is difficult to perform within a finite

computational time and early termination of the optimization could lead to stability problems. In addition, the feasible region is very small, and a global solution of an objective cannot usually be guaranteed. To avoid this, inequality constraints were used instead of equality constraints which allow the terminal state to be a region rather than a point in the state space [55]. In view of the difficulty of guaranteeing the global solution, Scokaert et al. [56] has relaxed this condition for discrete-time systems. In addition, it presents a practical implementation of NMPC, discrete-time systems, using a suboptimal solution. It shows that feasibility rather than optimality suffices for stability. Another interesting paper that establishes nominal robustness of suboptimal MPC is found in [57].

The purpose of this chapter is to establish stability of suboptimal fixed horizon versions of NMPC for discrete-time systems. To guarantee stability, a dual mode control is proposed where the control is employed outside the terminal region. When the state arrives on the boundary of the terminal region, a linear state feedback controller is employed to drive the state to an equilibrium.

5.2 System Description and Mathematical Model

5.2.1 Converter Modeling

The QAB designs have four active bridges, each of them is denoted by a , b , c , and d as presented in Fig. 24. The voltage at the medium voltage (MV) side and the low voltage (LV) side is represented as V_M and V_L , respectively. Bridge a is connected to the LV side, whereas bridges b , c , and d are connected to the MV side. The duty cycle for bridge a is given by D_1 while the duty cycles for the MV bridges are given by D_i , where i reflects the ports b , c , and d . The voltages at

the MV voltage side will be presented as v_i . The triangular current modulation (TCM) is used to modulate the QAB in the SST as shown in Fig. 25. Note that Fig.25 shows the balance operation.

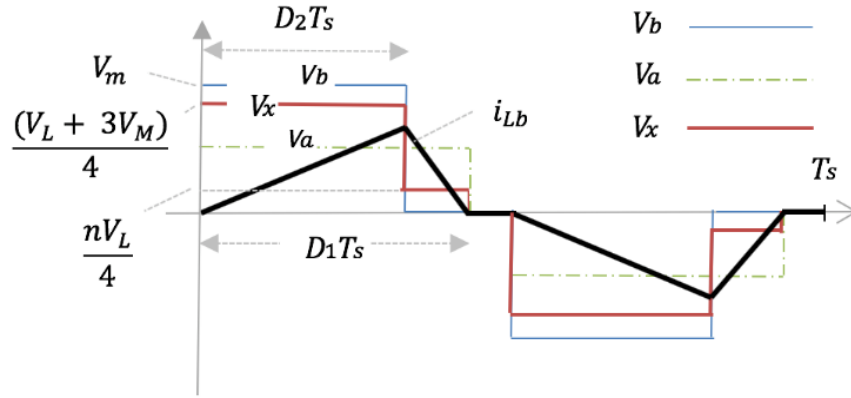


Figure 25 Modulation of the QAB

The operational principle of the TCM is described in [3]. As a result, the relation between D_1 and D_2 is presented in (5.1). The inductance value, L , can be calculated with (5.2). In this study, it is assumed that the QAB operates with unbalanced power flow through each of the SST ports, $P_b \neq P_c \neq P_d$, Fig. 26. Thus, the duty cycle of each port of the MV side is defined by (5.3). The transformer turns ratio and the switching frequency are represented by n and f , respectively.

$$D_2 = \frac{n V_L}{V_M} D_1 \quad (5.1)$$

$$L = \frac{3D_1^2 (V_L n)^2 (V_M - nV_L)}{4 P f_s V_M} \quad (5.2)$$

$$D_i = P_{ref} - P_i \quad (5.3)$$

Where,

$$D_i = D_2$$

$$P_{ref} = \frac{1}{3}P_a$$

$$P_i = V_i \cdot I_i$$

5.2.2 The Mathematical Model and Error Modeling

In this section, the mathematical model of the power at the MV side is evaluated, and the modeling error, unknown noise term, is estimated.

The unbalance power operation is presented in Fig. 26. As presented in Fig.25 and 26, the currents are increased in the first half cycle, D_2T_s , then decreased. The mean value of the power (P_{b1} , P_{c1} and P_{d1}) in one cycle, which considers only the first half period, is derived analytically (4). Note that, i_{0i1} is the initial current, (5.5), at the first half cycle which can be derived using (5.4).

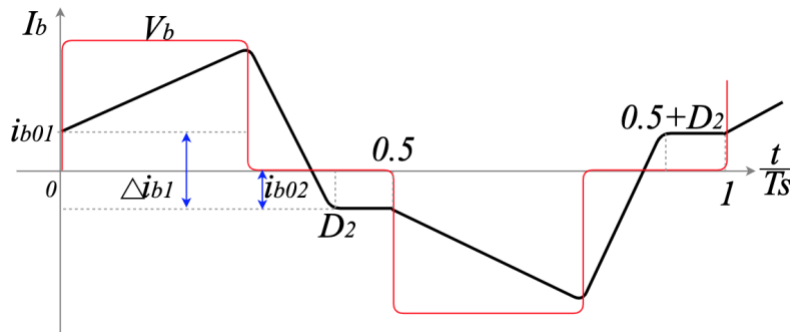


Figure 26 Unbalance power flow through the QAB

$$P_{b1} = \frac{v_b(3v_b - v_c - v_d - nv_L)D_b^2}{8Lf} + i_{0b1} \cdot D_b \cdot v_b \quad (5.4a)$$

$$P_{c1} = \frac{v_c[(3v_c - v_d - nv_L)D_c^2 + v_bD_b^2 - 2v_bD_bD_c]}{8Lf} + i_{0c1} \cdot D_c \cdot v_c \quad (5.4b)$$

$$P_{d1} = \frac{v_d[(3v_d - nv_L)D_d^2 + v_bD_b^2 + v_cD_c^2 - 2(v_bD_b + v_cD_c)D_{2d}]}{8Lf} + i_{0d1} \cdot D_d \cdot v_d \quad (5.4c)$$

$$\hat{i}_{0b1} = \frac{\left[P_{b1} - \frac{v_b(3v_b - v_c - v_d - nv_L)D_b^2}{8Lf} \right]}{D_b \cdot v_b} \quad (5.5a)$$

$$\hat{i}_{0c1} = \frac{\left[P_{c1} - \frac{v_c[(3v_c - v_d - nv_L)D_c^2 + v_bD_b^2 - 2v_bD_bD_c]}{8Lf} \right]}{D_c \cdot v_c} \quad (5.5b)$$

$$\hat{i}_{0d1} = \frac{\left[P_{d1} - \frac{v_d[(3v_d - nv_L)D_{2d}^2 + v_bD_{2b}^2 + v_cD_{2c}^2 - 2(v_bD_{2b} + v_cD_{2c})D_{2d}]}{8Lf} \right]}{D_d \cdot v_d} \quad (5.5c)$$

Meanwhile, in order to estimate the initial current in the next half cycle, the current change in the first half cycle, Δi_i , has to be calculated (5.6), see Fig. 26. Assuming that the voltage and duty cycle during one cycle do not change, the initial current in the next half cycle is given in (5.7).

$$\Delta i_b = \frac{1}{4Lf} (3v_bD_b - v_cD_c - v_dD_d - nv_LD_1) \quad (5.6a)$$

$$\Delta i_c = \frac{1}{4Lf} (3v_cD_c - v_bD_b - v_dD_d - nv_LD_1) \quad (5.6b)$$

$$\Delta i_d = \frac{1}{4Lf} (3v_dD_d - v_bD_b - v_cD_c - nv_LD_1) \quad (5.6c)$$

$$\hat{i}_{0b2} = \hat{i}_{0b1} + \Delta i_b = i_{b0} + \frac{1}{4Lf} (3v_bD_b - v_cD_c - v_dD_d - nv_LD_1) \quad (5.7a)$$

$$\hat{i}_{0c2} = \hat{i}_{0c1} + \Delta i_c = i_{c0} + \frac{1}{4Lf} (3v_cD_c - v_bD_b - v_dD_d - nv_LD_1) \quad (5.7b)$$

$$\hat{i}_{0d2} = \hat{i}_{0d1} + \Delta i_d = i_{d0} + \frac{1}{4Lf} (3v_d D_d - v_b D_b - v_c D_c - nv_L D_1) \quad (5.7c)$$

The mean value of the power, P_{b2} , P_{c2} and P_{d2} , in one cycle, (5.8) which considers only the second half cycle, is derived similarly to (5.4); considering that the output voltages at the MV side are inverted.

$$P_{b2} = \frac{v_b(3v_b - v_c - v_d - nv_L)D_b^2}{8Lf} - i_{0b2} \cdot D_b \cdot v_b \quad (5.8a)$$

$$P_{c2} = \frac{v_c[(3v_c - v_d - nv_L)D_c^2 + v_b D_b^2 - 2v_b D_b D_c]}{8Lf} - i_{0c2} \cdot D_c \cdot v_c \quad (5.8b)$$

$$P_{d2} = \frac{v_d[(3v_d - nv_L)D_d^2 + v_b D_b^2 + v_c D_c^2 - 2(v_b D_b + v_c D_c)D_d]}{8Lf} - i_{0d2} \cdot D_d \cdot v_d \quad (5.8c)$$

If equations (5.4) and (5.8) are used directly in the power distribution control, the model will be switched every cycle according to D_2 . Therefore, an approximation model is introduced to obtain a model that is suitable for the control design (5.9), where, j and i represent b , c and d . This approximation model should come along with an error as shown in (5.10). Note that P_{ir1} and P_{ir2} are the values obtained by calculation (5.9), whereas P_{i1} and P_{i2} are measured values, and d_{i1} and d_{i2} are modeling errors.

$$P_{jr1} = \frac{v_{sj}(3v_j - \sum_{i \neq j} v_i - nv_L)D_j^2}{8Lf} + i_{0j1} \cdot D_j \cdot v_j \quad (5.9a)$$

$$P_{jr2} = \frac{v_{sj}(3v_j - \sum_{i \neq j} v_i - nv_L)D_j^2}{8Lf} - i_{0j2} \cdot D_j \cdot v_j \quad (5.9b)$$

$$P_{i1} = P_{ir1} + d_{i1} \quad (5.10a)$$

$$P_{i2} = P_{ir2} + d_{i2} \quad (5.10b)$$

The modeling errors, noise terms, from Eq. (5.10) can be one of the values expressed in (5.11) depending on the duty cycle value. This error is constant when the voltage and duty cycle at the MV side are constant.

$$d_{i1} = \begin{cases} (i_{0b1} - \hat{i}_{0b1}) \cdot D_b \cdot v_b \\ (i_{0c1} - \hat{i}_{0c1}) \cdot D_c \cdot v_c + \frac{v_b \cdot D_c(D_c - D_b) + v_b \cdot D_b(D_b - D_c)}{8Lf} \\ (i_{0d1} - \hat{i}_{0d1}) \cdot D_d \cdot v_d + \frac{2[v_b \cdot D_b(D_b - D_d) + v_c \cdot D_c(D_c - D_d)]}{8Lf} \end{cases} \quad (5.11a)$$

$$d_{i2} = \begin{cases} (\hat{i}_{0b2} - i_{0b2}) \cdot D_b \cdot v_b \\ (\hat{i}_{0c2} - i_{0c2}) \cdot D_c \cdot v_c + \frac{v_b \cdot D_c(D_c - D_b) + v_b \cdot D_b(D_b - D_c)}{8Lf} \\ (\hat{i}_{0d2} - i_{0d2}) \cdot D_d \cdot v_d + \frac{2[v_b \cdot D_b(D_b - D_d) + v_c \cdot D_c(D_c - D_d)]}{8Lf} \end{cases} \quad (5.11b)$$

While considering the noise measurement, the estimated values of d_{i1} and d_{i2} can be used for future predictive control at k time using the following first order filter (5.12). Note, f_1 is the coefficient parameter of discrete filter $(\frac{1-f_1}{1-f_1z^{-1}})$, and $0 < f_1 < 1$. In our case f_1 was set to 0.5.

$$\hat{d}_{i1}(k) = f_1 \hat{d}_{i1}(k-1) + (1-f_1)d_{i1}(k) \quad (5.12a)$$

$$\hat{d}_{i2}(k) = f_1 \hat{d}_{i2}(k-1) + (1-f_1)d_{i2}(k) \quad (5.12b)$$

Assuming the modeling error does not change over each control step, the predictive control implements the following model to realize the power distribution control as will be presented later,

section 5.4. This Consider the effect of the output voltage control, D_1 , and the power balance control, D_b and D_c , on the power distribution control according to equation (5.9). Note that, in the power balance control loop, the duty rates are used as control signals, whereas the MV set voltage is only used as a control signal in the power distribution control.

$$\hat{P}_{b1} = \frac{v_b(3v_b - v_c - v_d - nv_L)D_b^2}{8Lf} + \hat{I}_{b1} \cdot D_b \cdot v_b + \hat{d}_{b1} \quad (5.13a)$$

$$\hat{P}_{c1} = \frac{v_c(3v_c - v_b - v_d - nv_L)D_c^2}{8Lf} + \hat{I}_{c1} \cdot D_c \cdot v_c + \hat{d}_{c1} \quad (5.13b)$$

$$\hat{P}_{d1} = \frac{v_d(3v_d - v_b - v_c - nv_L)D_d^2}{8Lf} + \hat{I}_{d1} \cdot D_d \cdot v_d + \hat{d}_{d1} \quad (5.13c)$$

$$\hat{P}_{b2} = \frac{v_b(3v_b - v_c - v_d - nv_L)D_b^2}{8Lf} - \hat{I}_{b2} \cdot D_b \cdot v_b + \hat{d}_{b2} \quad (5.13d)$$

$$\hat{P}_{c2} = \frac{v_c(3v_c - v_b - v_d - nv_L)D_c^2}{8Lf} - \hat{I}_{c2} \cdot D_c \cdot v_c + \hat{d}_{c2} \quad (5.13e)$$

$$\hat{P}_{d2} = \frac{v_d(3v_d - v_b - v_c - nv_L)D_d^2}{8Lf} - \hat{I}_{d2} \cdot D_d \cdot v_d + \hat{d}_{d2} \quad (5.13f)$$

5.3 Controller Design for Regulating QAB Port Power and Dc Output Voltage

Three control loops are implemented in this work for regulating the power and voltage at the MV side of the QAB, Fig. 27. First, a feedback voltage regulator is used to maintain the output voltage at the LV side. Second, ALQR is implemented to balance the unequal processed power at the MV side. The third control loop, related to the inner DC-DC converter, is used to regulate the voltage given to the MV side of the QAB.

5.3.1 Proposed Output Voltage Control

A feedback voltage regulator $G_v(s)$ is designed to maintain a constant voltage level at the LV side. The voltage regulator $G_v(s)$ operates by comparing the actual output voltage, V_L , to the voltage reference set-value, V_{ref} . To maintain the output voltage, the transfer function, (5.14a) between the output voltage and duty cycle were obtained. Coefficients a and b for transfer function, $G_v(s)$, have been analytically developed in [45]. First, the averaged, state-space relationships were obtained for the time period between $0 < t < \frac{1}{2}T_s$. Then, we applied a small signal approximation to linearize. Note that T_s is the switching time, τ is the control delay, and C_a represents the capacitor on bridge a .

$$G_v(s) = \frac{\tilde{v}_L(s)}{\tilde{d}_1(s)} = \frac{b}{s + a} e^{-\tau s} \quad (5.14a)$$

$$a = \left(\frac{6n}{8LfC_a} - \frac{12n^2V_L}{8LfC_aV_M} \right) D_1 \quad (5.14b)$$

$$b = \left(\frac{6n}{8LfC_a} - \frac{6n^2V_L}{8LfC_aV_M} \right) V_L \quad (5.14c)$$

In order to consider the effect of the output voltage control loop, in the predictive control that will be explained later, it is assumed that the current change on the LV-side, ΔI_L , is fully compensated by C_a in one PWM cycle, T_s . It is assumed that the current, I_L , is started at the beginning of T_s , and then linearly decrease to zero at the end of the PWM period, T_s . The capacitor voltage, the voltage at the LV-side, is expressed by v_{L0} , and the power delivered to the LV side is expressed by P_a . The current change, ΔI_L , in the PWM period can be expressed as (5.15). Considering the relationship between voltage and current in the capacitor, equation (5.16) can be

written where v_L is the final voltage value in one PWM period (5.17). When the voltage at the LV side is changed from v_{L0} to v_L , D_1 is also changed using the voltage controller (5.18). Where, K_{pv} and K_{iv} are the PI controller parameters, and v_{Lref} is the voltage reference at the LV side. Equations (5.15) - (5.18) can be used to calculate the changes of D_1 , v_L and then D_2 .

$$\Delta I_L = P_a/v_{L0} - I_L \quad (5.15)$$

$$C_a \frac{v_L - v_{L0}}{T_s} = \frac{1}{2} \Delta I_L \quad (5.16)$$

$$v_L = \Delta I_L \frac{T_s}{2C_a} + v_{L0} \quad (5.17)$$

$$D_1(k + 1) = D_1(k) + K_{pv}(v_{L0} - v_L) + K_{iv}(v_{Lref} - v_L) \cdot T_s \quad (5.18)$$

5.3.2 Proposed Power Balance Control

In the unbalanced condition, $P_{b1} + P_{c1} + P_{d1} = P_{a1}$ must hold. A change in any of the duty cycles in the QAB will alter peak currents and, hence, port power. The discrete state space model of the balanced plant, (5.19), which focuses only on bridge b and c , can be constructed as explained in [15]. Here, it is assumed that A is not changed, but matrix B , (5.20), will alter according to the disturbances in the voltages and duty cycles on the MV side. The plant is a nonlinear abnormal system. Therefore, the ALQR controller is implemented to achieve the power balance control goal for the nominal model as shown in Fig. 27.

$$\begin{bmatrix} P_{b1}(n + 1) \\ P_{c1}(n + 1) \end{bmatrix} = A \begin{bmatrix} P_{b1}(n) \\ P_{c1}(n) \end{bmatrix} + B \begin{bmatrix} \Delta D_b \\ \Delta D_c \end{bmatrix} \quad (5.19)$$

$$B = \begin{bmatrix} D_b & 0 \\ 0 & D_c \end{bmatrix} \begin{bmatrix} \frac{3V_b^2}{4Lf} & -\frac{V_b V_c}{4Lf} \\ -\frac{V_b V_c}{4Lf} & \frac{3V_c^2}{4Lf} \end{bmatrix} = D_2 B_1 \quad (5.20)$$

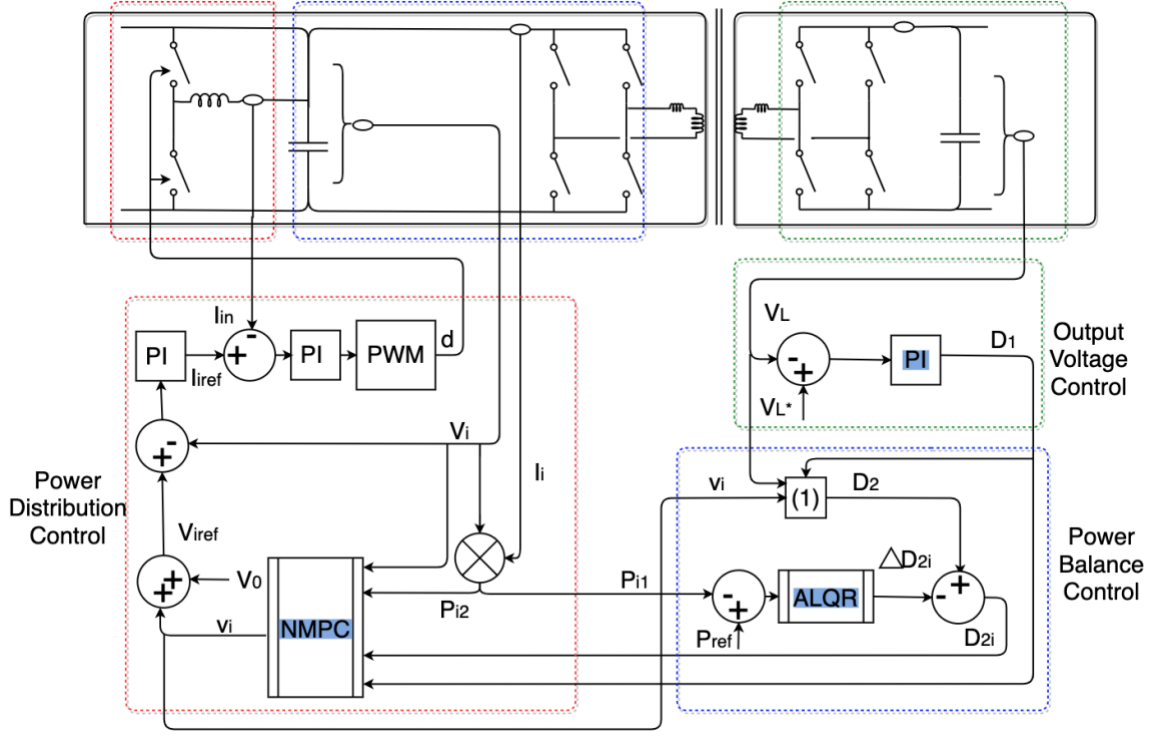


Figure 27 Control Structure for the SST based QAB

Assuming that we can measure the state $x(n) = [P_{b1}(n) P_{c1}(n)]^T$ of the model expressed in (5.19), we can build a balanced control system with a high tracking performance by the following state-feedback system [45]. Consider $r(n) = [\frac{1}{3}P_{a1}(n) \frac{1}{3}P_{a1}(n)]^T$ as the setpoints of P_{b1} and P_{c1} at the current time, the control signal is defined as $u(n) = \begin{bmatrix} \Delta D_{2b} \\ \Delta D_{2c} \end{bmatrix}$, and error is $e(n) = r(n) - x(n)$.

The state feedback matrix, K_{p0} , can be found by designing the control system as a result of the minimization of quadratic cost function, Fig. 28. The ALQR control is implemented which copes with the change of D_2 as presented in detail in the previous work [51], (5.21). The relationship between duty cycles in the neighboring PWM periods can be expressed as in (5.22). Using the nominal set-point, (5.1), based upon parameters in Table 6; $D_{20} = 0.35$ [11], and $\frac{D_{20}}{D_a(k)} K_{p0}$ is a coefficient matrix.

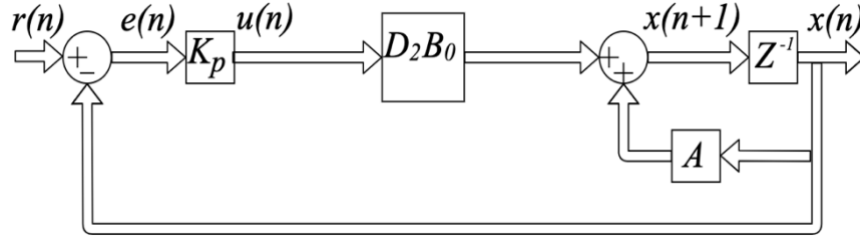


Figure 28 The design structure of the balanced control loop

$$u(n) = \frac{D_{20}}{D_2} K_{ai} [x(n) - r(n)] \quad (5.21)$$

$$\begin{bmatrix} D_b(k+1) \\ D_c(k+1) \end{bmatrix} = \begin{bmatrix} D_b(k) \\ D_c(k) \end{bmatrix} - \frac{D_{20}}{D_a(k)} K_{p0} \begin{bmatrix} \frac{P_{b1}(k) + P_{c1}(k) + P_{d1}(k)}{3} - P_{b1}(k) \\ \frac{P_{b1}(k) + P_{r1}(k) + P_{r1}(k)}{3} - P_{c1}(k) \end{bmatrix} \quad (5.22a)$$

$$D_a(k+1) = D_1(k) \cdot \frac{nv_L(k)}{v_d(k)} \quad (5.22b)$$

5.3.3 Proposed Power Distribution Control

The power distribution control is implemented using the NMPC control with the duty cycle changes and power at the MV-side as a state which consider various constraints such as the power balance loop and voltage control loop. However, it is very difficult to realize a real time stabilizing control based on a global and accurate solution considering these various limitations. Therefore, we turned to the suboptimal NMPC control method that guarantees a certain level of control performance and stability within a limited period of time [18]. It is important to properly determine the control period here.

Referring to the dashed red region in Fig. 27 and using the predicted and locally measured parameters, the offset signals, v_i , are acquired. This signal along with the voltage set point at no load, V_0 , are used to obtain the voltage reference, V_{iref} . The current reference, I_{iref} , is generated by regulating the difference between, V_{iref} , and the output voltage, V_i . Then, the duty cycle for the inner DC-DC converter is obtained to balance the voltage.

5.4 Principle of Operation in NMPC Controller for Power Distribution Control

The goal of the NMPC is to regulate the state of the system to the origin while satisfying control and state constraints of the form for all k (5.23). At each state-time pair (x, k) , the Dual-mode fixed- horizon NMPC minimizes the objective function (5.24) considering the control and state constraints, (5.23), and the inequality stability constraint, (5.25). Where, W is a compact subset of \mathbb{X} , contains an open neighborhood of the origin. Eq. (5.26) represent the state equation.

$$u_k \in \mathbb{U} \quad (5.23)$$

$$x_k \in \mathbb{X}$$

$$\phi(x, \pi) = \sum_{j=k}^{k+N-1} L(x_j, v_j) \quad (5.24)$$

$$x_{k+N} \in W \quad (5.25)$$

$$x_{j+1} = f(x_j, v_j), x_k = x \quad (5.26)$$

The voltage variation at the MV side, through the control signal of power distribution control v_j , could have a significant impact on the stability of the overall system. Therefore, it is definite to realize the control signal, v_j , once every five PWM periods, (5.27). Thus, the control period of the power distribution control, T_c , is set to 5 times the PWM period, T_s , where, $\pi = (v_k, \dots, v_{N-1})$ is the decision variable. In order to reduce the amount of computation time, the state change step for prediction was set as one PWM cycle, T_s , whereas the prediction time was set as the control period, T_c [56].

$$v_{k-5} \ v_k, v_{k+1}(= v_k), v_{k+2}(= v_k), v_{k+3}(= v_k), v_{k+4}(= v_k), v_{k+5}, \dots \quad (5.27)$$

$$v_{k+6}(= v_{k+5}), v_{k+7}(= v_{k+5}), v_{k+8}(= v_{k+5}), v_{k+9}(= v_{k+5}), v_{k+10} \dots$$

$$\text{So, } v_k = v_{k+1} = v_{k+2} = v_{k+3} = v_{k+4},$$

$$\pi = (v_k, v_k, v_k, v_k, v_k)$$

The suboptimal version of fixed-horizon dual-mode NMPC requires a locally control law $u = h(x_k)$ such that $h: W \rightarrow \mathbb{U}$, Where, W is a compact subset of \mathbb{X} , contains an open neighborhood of the origin. The suboptimal version of dual mode NMPC is defined by Algorithm 2 and displayed in Fig 29.

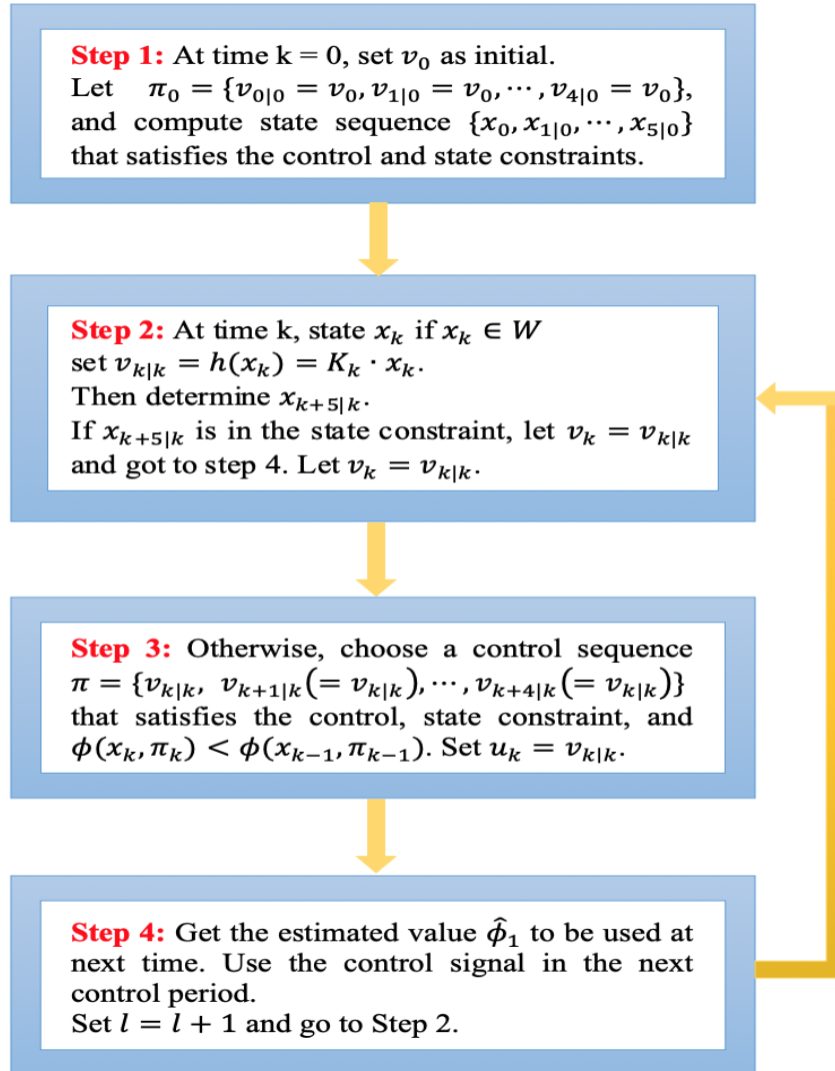


Figure 29 The suboptimal dual mode NMPC algorithm

Table 6 Suboptimal verison of Dual mode NMPC

Algorithm 2

Step 1: Set $v_0(= [1130; 1130; 1130])$ at $k = 0$ and let $\pi_0 = \{v_{0|0} = v_0, v_{1|0} = v_0, \dots, v_{4|0} = v_0\}$, and compute the corresponding state sequence $\{x_0, x_{1|0}, \dots, x_{5|0}\}$ satisfying the state constraints and Eq. (5.21). Let $l = 0$.

Step 2: For the state x_k at $k = 5 \cdot l$, get $v_{k|k} = h(x_k) = K_k \cdot x_k$, the solution of finite time LQ control problem in fixed horizon ($Nl = 5 \times 4$) for. (5.24) and (5.26), and then determine $x_{k+5|k}$. If $x_{k+5|k}$ is in the state constraint and $\sum_{j=k}^{k+4} L(x_j, v_{k|k}) < obj0$, let $v_k = v_{k|k}$ and got to step 4.

Step 3: Choose a control sequence π_k that satisfies $\phi(x_k, \pi_k) < \phi(x_{k-1}, \pi_{k-1})$, the state and control signal constraint using $\pi = \{v_{k|k}, v_{k+1|k}(= v_{k|k}), \dots, v_{k+4|k}(= v_{k|k})\}$ as an initial guess, where $\pi_{k-1} = \{v_{k-5|k-5}(= v_{k-5}), v_{k-4|k-5}(= v_{k-5}), \dots, v_{k-1|k-1}(= v_{k-5})\}$. and $\phi(x_{k-1}, \pi_{k-1})$ is expressed as (5.28).

$$\phi(x_{k-1}, \pi_{k-1}) = L(x_{k-1}, v_{k-5}) + \sum_{j=k}^{k+3} L(x_j, v_{k-5})$$

The first term is expressed as $\phi_1(k - 5)$ which is related to the past state, and the second term is expressed as $\phi_2(k)$ which is a predictable amount from the current state. Eq. (28) can be written as (29). The estimated value $\hat{\phi}_1(k - 5)$ calculated at the previous control step is used instead of $\phi_1(k - 5)$.

$$\phi(x_{k-1}, \pi_{k-1}) = \phi_1(k - 5) + \phi_2(k)$$

Step 4: Get the estimated value $\hat{\phi}_1$ to be used at next time, and then filter the control signal to be used at the next control period. Let $l = l + 1$ and go to Step 2. where l denotes the current control period and increases by 1 after 5 PWM periods (one control period).

The suboptimal dual-mode NMPC law drives the system state to W in finite time in the presence of model inaccuracies and disturbances, $\mu > 0$. If the local control law $v_{k|k} = h(x_k)$ is robust such as it maintains trajectories that originate in W in W , then the stability guarantee for dual-mode NMPC holds in the presence of inaccuracies and disturbances provided a feasible solution (5.23), where (5.26) and (5.28) can be found. Neither the global nor local minimization of the objective is required. The design of the finite time LQ control, step 2, and the suboptimal solution, steps 3 and 4, will be described in the next subsections. To do so, the state space will be driven to find the state equation that could be used in the design stage, Appendix C.

5.4.1 The Design of Finite Time LQ Control System

The states $x(k)$ and control $u(k)$ are defined, (5.30a) and (5.30b), for the finite time LQ control considering the change in the control signal of the power balance control ΔD_i . The state equation can be expressed by (5.30c). When $x(k) \rightarrow 0$, the purpose of power distribution control can be realized.

$$x(k) = \begin{bmatrix} D_b(k) - D_b(k-1) \\ D_c(k) - D_c(k-1) \\ D_d(k) - D_d(k-1) \\ P_b(k) - P_{bref} \\ P_c(k) - P_{cref} \\ [P_{bref} - P_b(k) + P_{cref} - P_c(k)] \end{bmatrix} \quad (5.30a)$$

$$u(k) = \Delta v_{bcd}(k) \quad (5.30b)$$

$$x(k+1) = Ax(k) + Bu(k) \quad (5.30c)$$

Where,

$$A = \begin{bmatrix} A_{bcd} & O_{3 \times 3} \\ C_P & I_{3 \times 3} \end{bmatrix}, \quad B = \begin{bmatrix} B_{bcd} \\ D_P \end{bmatrix}$$

Eq. (5.30c) is a nonlinear state space model since the matrices A and B of the state space model are related to the voltages, initial current and duty cycles at the MV side which change nonlinearly.

Assuming that for some finite time, the voltages and duty cycles at the MV side are invariant and ΔD_{bcd} and Δv_{bcd} are relatively small, Eq. (5.30c) can be seen as the state-space model of time-variant system whose parameters A and B do not change for some time. These state-space model matrices of the system can be updated at every control period based on the measured data. Under these assumptions, let's express the state change in one control period with the following state space model, (5.31).

$$x(l + 1) = AAx(l) + BBu(l) \quad (5.31)$$

As mentioned, l denotes the current control period and increases by 1 after 5 PWM periods (one control period). That is, $x(l) = x(l \cdot T_c) = x(k \cdot T_{pwm})$ and $x(l + 1) = x((l + 1) \cdot T_c) = x((k + 5) \cdot T_{pwm})$ where $k = 5l$ and T_c is control period and T_{pwm} is PWM period.

$$x(k + 1) = Ax(k) + Bu(k)$$

$$x(k + 2) = Ax(k + 1) + Bu(k) = A[Ax(k) + Bu(k)] + Bu(k)$$

$$= A^2x(k) + ABu(k) + Bu(k)$$

$$x(k + 3) = A^3x(k) + A^2Bu(k) + ABu(k) + Bu(k)$$

$$x(k + 4) = A^4x(k) + A^3Bu(k) + A^2Bu(k) + ABu(k) + Bu(k)$$

$$x(k + 5) = A^5x(k) + [(A^4 + A^3 + A^2 + A)B + B]u(k) = AAx(k) + BBu(k)$$

Therefore,

$$AA = A^5, \quad BB = (A^4 + A^3 + A^2 + A)B + B$$

For the time-variant system, (5.31), we solve the finite time LQ control problem of step 2 in the Algorithm 2. The finite time horizon for LQ control should be defined as the horizon in which the voltages, initial currents, and duty cycles change slightly. Here, we determine it as the size of four control periods. Therefore, the cost function of finite time LQ control at l th period is set as (5.32). The weight matrix, Q and R , are defined considering that the voltages and duty cycles on port d change less than the other ports b and c .

$$J = \frac{1}{2} \sum_{m=l}^{l+3} [x^T(m)Qx(m) + u^T(m)Ru(m)] \quad (5.32)$$

Where,

$$Q = \begin{bmatrix} 10^4 & 0 & 0 & 0 & 0 & 0 \\ 0 & 10^4 & 0 & 0 & 0 & 0 \\ 0 & 0 & 10^6 & 0 & 0 & 0 \\ 0 & 0 & 0 & 50 & 0 & 0 \\ 0 & 0 & 0 & 0 & 50 & 0 \\ 0 & 0 & 0 & 0 & 0 & 50 \end{bmatrix}, \quad R = \begin{bmatrix} 10^3 & 0 & 0 \\ 0 & 10^3 & 0 \\ 0 & 0 & 10^4 \end{bmatrix}$$

$$u(l) = K_k x(l) \quad (5.33)$$

For (5.31) and (5.32), the state feedback matrix K_k can be obtained at every l th period by the general finite time LQ control system design method. The control signal (candidate control variable for power distribution control) is determined by (5.33).

5.4.2 Suboptimal Control When Out of Equilibrium State

Considering that the control period in finite time LQ control is five times of the computational period in sub-optimization, $u(l)$, the candidate control variable obtained above, is notated as $u(k)$ where $k = 5l$. Then, the initial value v_k^0 of MV side voltage for sub-optimization can be obtained (5.34). The objective function for sub-optimization (5.24), is specified as (5.35), taking into account the purpose in this paper and the cost function in finite time LQ control discussed above. Note that $L(x_j, v_k)$, (5.35), cannot be specifically expressed as a function, but we can take it as the average value (5.36). Appendix C is used to calculate the values of (5.35) to reflect the effects of both output voltage control and MV power balance control.

$$v_k^0 = v_{k-5} + u(k) \quad (5.34)$$

$$\phi(x_k, \pi_k) = \phi(x_k, v_k) = \frac{[\sum_{j=k}^{k+4} x^T(k) Q x(k)]}{5} + (v_k - v_{k-5})^T R (v_k - v_{k-5}) \quad (5.35)$$

$$= \sum_{j=k}^{k+4} L(x_j, v_k)$$

$$L(x_j, v_k) = \frac{1}{5} \phi(x_k, \pi_k) \quad (5.36)$$

where $j = k, k + 1, \dots, k + 4$.

5.5 Power and Voltage Regulation Verification

The parameters of the QAB converter are shown in Table 7. Different cases are examined here such as a step load change on the LV side, and a change in the state of power on the MV side as shown in Table 8.

Note: a resistive-inductive load is connected at the output side of QAB. The proposed control scheme maintains the LV bus at 700 V and regulates the MV bus to its nominal value as shown in Fig. 30.

The QAB converter is initiated to serve $8.7 \times 10^4 \text{W}$. Then, a load step change is initiated at 0.03 seconds to $13.6 \times 10^4 \text{W}$. The transition at 0.06 and 0.085 seconds is performed by changing the injected power at ports *b* and *c* to simulate the change in the power states at the MV side of the converter. Port *d* responds to this change accordingly to perform the power regulation as shown in Fig. 31.

Table 7 Parameters of the Simulation Model

Symbol	Parameters	Value
V_M	DC input voltage	1120 V
V_L	Output voltage	700 V
n	T.F turns ratio	1.2
$L_{b,c,d}$	MV Inductors	$12.7 \mu\text{H}$
L_a	LV Inductor	$7.5 \mu\text{H}$
f_s	Switching frequency	20 kHz

Table 8 Power Alterations at Each MV Port

Time (s)	P_a (W)	P_{bref} (W)	P_{cref} (W)	P_{dref} (W)
0.00 - 0.03	8.7×10^4	$P_b + P_c + P_d = P_a$		
0.03 - 0.06	13.6×10^4	9×10^4	7×10^4	-2.4×10^4
0.06 - 0.085	13.6×10^4	9×10^4	5×10^4	-0.4×10^4
0.085 - 0.12	13.6×10^4	7×10^4	5×10^4	1.6×10^4

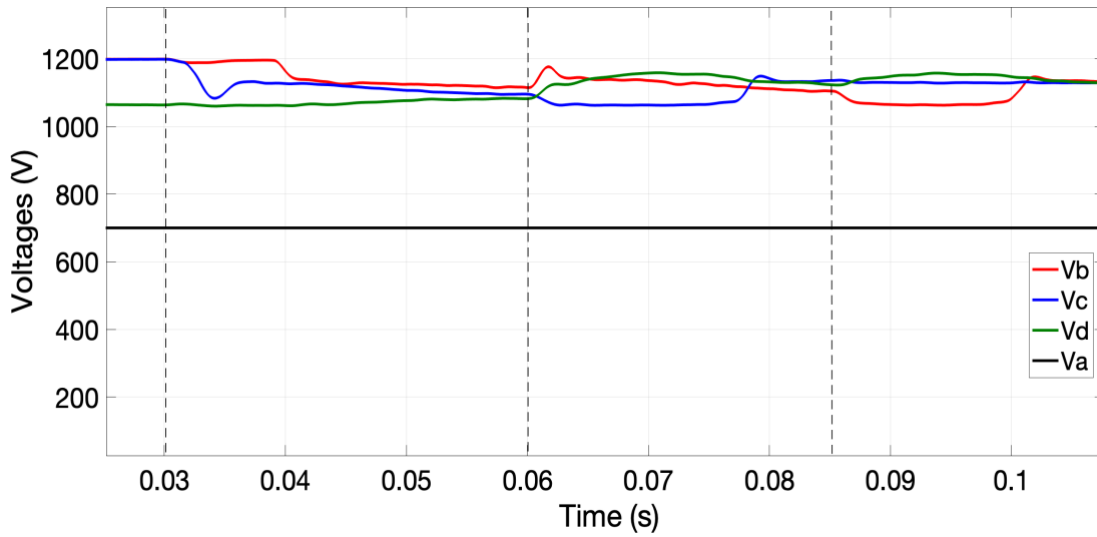


Figure 30 Measured voltages on the MV and LV side

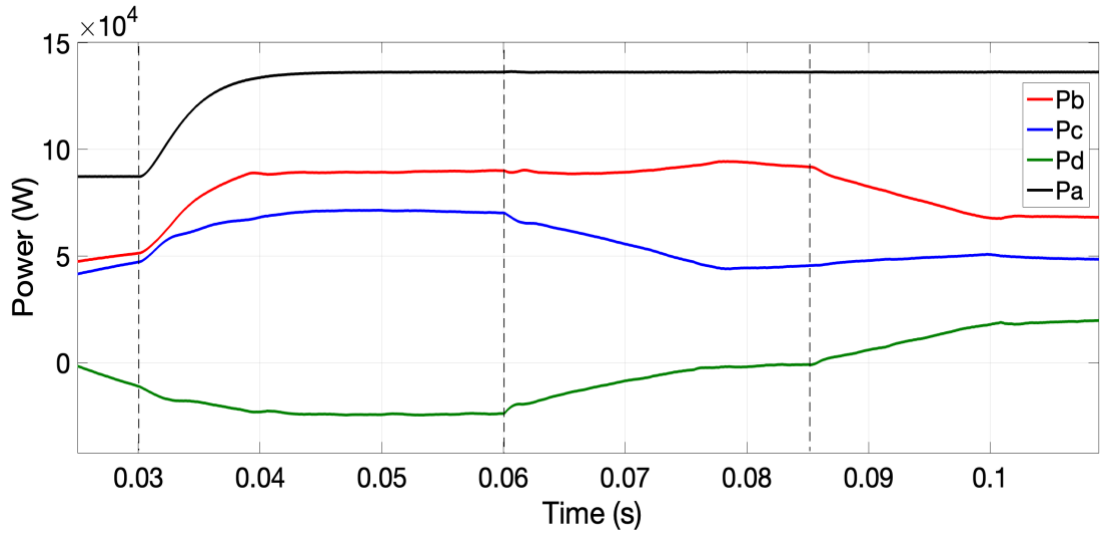


Figure 31 Power measurements throughout the QAB

In all scenarios, the transition processes are achieved smoothly, which validates the effectiveness of the proposed control scheme. As the system variations occur, the duty cycle D_1 is updated which results in duty cycle updates to D_b , D_c , and D_d , according to (1) and (3), as shown in Fig. 32.

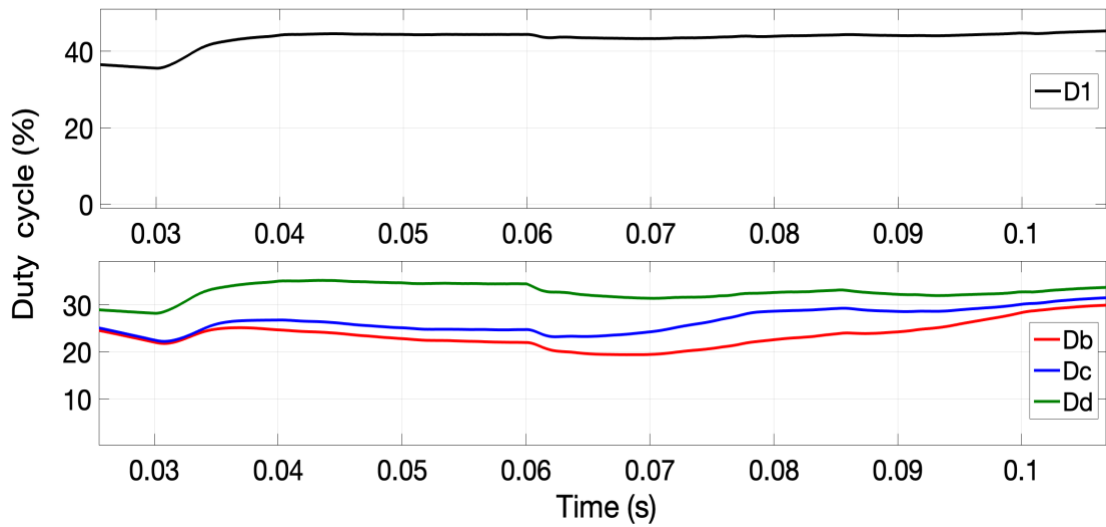


Figure 32 Duty cycles at MV side and LV side

As we can see the system response is managed well on time and maintained the stability. As this is discrete time system, eigenvalue tool is used to validate the stability results as shown in Fig. 33.

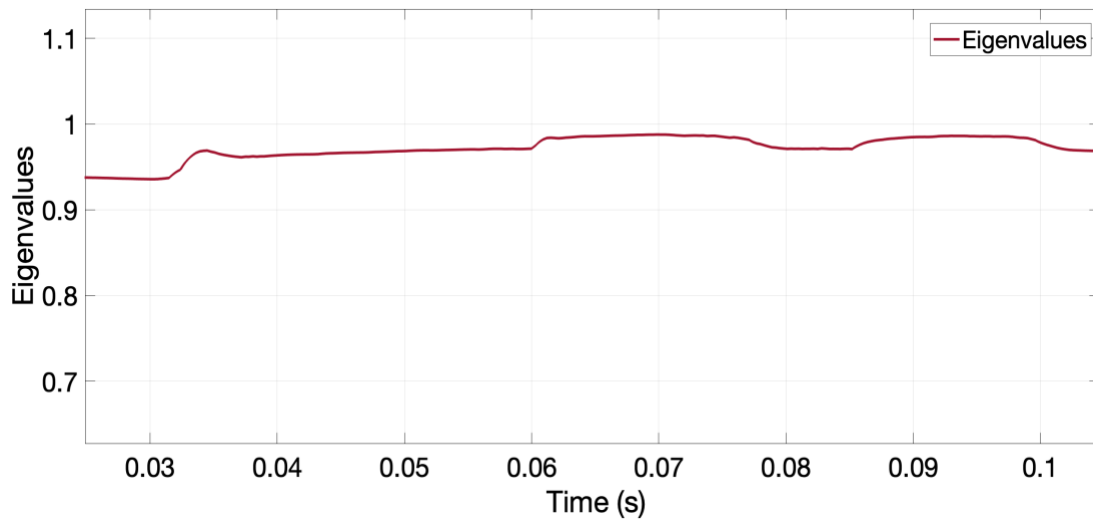


Figure 33 Eigenvalue of the control system

5.6 Conclusion

The power and voltage regulation for the SST based QAB has been performed on the MV side using the ALQR and NMPC techniques. In this work, we consider optimization problem that arise with the practical implementation of NMPC discrete-time system and show that feasibility rather than optimality suffices for stability. We illustrate this result by establishing stability for suboptimal version of dual mode NMPC. The previous work used Resilient Backpropagation (RPROP), causes computational difficulties. This difficulty is avoided in the suboptimal NMPC strategies presented here.

6.0 Summary of Research

This objective of this thesis is to propose control strategies for dc-dc conversion in order to regulate the power and voltage. Although this work is done with the specified values, the equations are kept flexible enough for applications at any value.

In this chapter, a brief summary of this thesis is presented. The contributions in the area of the control of power electronics are also presented.

The QAB converter has the same features of the DAB converter. Furthermore, the number of the HF transformer is reduced since more active bridges are connected to a single transformer. The TCM is used for converter modulation. This modulation has the advantage to operate with ZCS for a wide range of voltage, reducing the switching losses. A multi-terminal QAB converter was developed for the purpose of integration of multiple renewable energy sources.

The QAB converters have some specific characteristics, which require new control schemes. The objective of this dissertation is to apply different control strategies to regulate the QAB converters for SST applications. Two control approaches have been followed to design the controls for the QAB which are SISO and MIMO:

- A control technique that complements the SISO controller has been introduced through the PI controller.
- A full-state-feedback MIMO controller as the LQR has been designed. In addition, the MPC has been designed through two alternative methods as optimal control and suboptimal control.

In the present thesis, three control strategies were developed for the QAB converter for the voltage and power regulation taking into account the cross-coupling characteristics of the QAB converters. The main results obtained in the thesis are summarized as follows:

- Power and voltage regulation of the QAB has been performed. The linear–quadratic regulator (LQR) has been implemented into two control loops, a power balance loop and a power distribution loop. The objective of these two loops is to balance the power and voltage at the MV side respectively.
- Despite the effort reported, nonlinearity and duty cycle uncertainty are still a challenge in power conversion applications. Thus, other combined techniques have been investigated to mitigate the phenomena mentioned earlier. This motivates the use of adaptive linear–quadratic regulator (ALQR) and nonlinear model predictive control (NMPC) to track the nonlinear change of the QAB converter. The ALQR and NMPC techniques have been implemented into the power balance loop and power distribution loop respectively.
- Although regulation is desired, converter stability is absolutely required and, still, a challenging task in the NMPC design. Thus, a NMPC control strategy is proposed to improve the regulation of the QAB and guarantees system stability. This part has presented the stability based suboptimal fixed horizon versions of NMPC for discrete-time systems.

The dynamic performance of the designed QAB control loops based on the proposed SISO as well as the MIMO are verified through extensive simulation of the QAB.

Appendix A Supplementary materials used in Chapter 3

Appendix A.1 Output voltage loop

PI control code for output voltage loop

```
n=1.2;L=12.7e-6;C=68000e-6;Vm=1130;Vl=700;D1=0.48;r=4.5;
fsw=20e3;
wc1=2*pi*fsw/10;
alp1=(2/3-1/5)*pi;

k1=(3*n/(8*L*fsw)-1/r)/C;
% k1=(3*n/(8*L*fsw))/C;

k2=3*n^2/(8*L*Vm*fsw*C);
k3=3*n/(8*L*C*fsw);

a=-2*((k3-2*k2*Vl)*D1-0.5/C/r);
% a=-2*((k3-2*k2*Vl)*D1);
b=2*(k3-k2*Vl)*Vl;

ta=tan(pi/4);

Gv=b/(j*wc1+a)*exp(-j*wc1/fsw);
Re=real(Gv);
Im=imag(Gv);
tt=inv([Re Im/wc1;Im -Re/wc1])*[-1/sqrt(ta^2+1);-ta/sqrt(ta^2+1)];
Pv=tt(1)
Iv=tt(2)
```

Appendix A.2 Power balance loop

LQR code for power balance loop

```
A=eye(2);
Q=1e-4*eye(2);R=4e1*eye(2);N=zeros(2,2);

L=12.7e-
6;f=2e4;D2b=0.35;D2c=0.35;D2d=0.32;Vb=1113;Vc=1129;Vd=1130;Vl=700;n=1.2;Vm=11
30;
```

```

kk=3.3e4/3;

B=0.5*kk*[2/Vm -1/Vm ; -1/ Vm 2/Vm];

[Kpi, S, e] = dlqr(A, B, Q, R, N)

e=eig(A-B*Kpi)

```

Appendix A.3 Power distribution loop

LQR code for power distribution loop.

```

A=eye(3); Q=1*eye(3); R=10*eye(3); N=zeros(3,3);
L=12.7e-6; f=2e4; D2b=0.35; D2c=0.35; D2d=0.32;
Vb=1130; Vc=1130; Vd=1130; V1=700; n=1.2;
kb=D2b*D2b/4/L/f;
kc=D2c*D2c/4/L/f;
kd=D2d*D2d/4/L/f;

B=0.5*kb*[6*Vb-Vc-Vd-n*V1 -Vb -Vb; -Vc 6*Vc-Vb-Vd-n*V1 -Vc; -Vd -Vd 6*Vd-Vb-Vc-
n*V1];
[Kp, S, e] = dlqr(A, B, Q, R, N);
eig(A-B*Kp)
Kp

```

Appendix B Supplementary materials used in Chapter 4

Appendix B.1 Power distribution loop (NMPC)

The variables are defined as:

```
function y = NMPC_control(V,D, P2, Pr, L, f, n, D0, alp, delMax, delMin,
etaP, etaM)
persistent del0 delB0 delC0 delD0 dpdvB0 dpdvC0 dpdvD0 delVB0 delVC0 delVD0
Vmax Vmin Vmax1 Vmin1 Imax s state0 q
if isempty(delB0),
    del0=(delMax+delMin)/2;
    delB0=del0;
    delC0=del0;
    delD0=del0;
    dpdvB0=0;
    dpdvC0=0;
    dpdvD0=0;
    delVB0=0;
    delVC0=0;
    delVD0=0;
    Vmax=1200;
    Vmin=1010;
    Vmax1=Vmax+delMin/2;
    Vmin1=Vmin-delMin/2;
    s=1e-6;
    state0=0;
    Imax=450;
    q=1;
end
```

```
Vb=V(1);Vc=V(2);Vd=V(3);Vl=V(4);
Db=0.01*D(1);Dc=0.01*D(2);Dd=0.01*D(3);
Pob=P2(1);Poc=P2(2);Pod=P2(3);
Pbref2=Pr(1);Pcref2=Pr(2);
Pdref2=Pod;
Pr1=Pbref2;Pr2=Pcref2;Pr3=Pdref2;
Vbr0=Vb; Vcr0=Vc;Vdr0=Vd;
state=0;
```

The plant model can be classified into six categories, eq. (4.14).

```
if Db<=Dc && Dc<=Dd,
    Ds1=Db;Ds2=Dc;Ds3=Dd;
    Vs1=Vb;Vs2=Vc;Vs3=Vd;
    Ps1=Pob;Ps2=Poc;Ps3=Pod;
    Pr1=Pbref2;Pr2=Pcref2;Pr3=Pdref2;
    q1=q;q2=q;q3=1;
```

```

state=1;
elseif Db<=Dd && Dd<=Dc,
    Ds1=Db;Ds2=Dd;Ds3=Dc;
    Vs1=Vb;Vs2=Vd;Vs3=Vc;
    Ps1=Pob;Ps2=Pod;Ps3=Poc;
    Pr1=Pbref2;Pr2=Pdref2;Pr3=Pcref2;
    q1=q;q2=1;q3=q;
    state=2;
elseif Dc<=Db && Db<=Dd,
    Ds1=Dc;Ds2=Db;Ds3=Dd;
    Vs1=Vc;Vs2=Vb;Vs3=Vd;
    Ps1=Poc;Ps2=Pob;Ps3=Pod;
    Pr1=Pcref2;Pr2=Pbref2;Pr3=Pdref2;
    q1=q;q2=q;q3=1;
    state=3;
elseif Dc<=Dd && Dd<=Db,
    Ds1=Dc;Ds2=Dd;Ds3=Db;
    Vs1=Vc;Vs2=Vd;Vs3=Vb;
    Ps1=Poc;Ps2=Pod;Ps3=Pob;
    Pr1=Pcref2;Pr2=Pdref2;Pr3=Pbref2;
    q1=q;q2=1;q3=q;
    state=4;
elseif Dd<=Db && Db<=Dc,
    Ds1=Dd;Ds2=Db;Ds3=Dc;
    Vs1=Vd;Vs2=Vb;Vs3=Vc;
    Ps1=Pod;Ps2=Pob;Ps3=Poc;
    Pr1=Pdref2;Pr2=Pbref2;Pr3=Pcref2;
    q1=1;q2=q;q3=q;
    state=5;
else
    Ds1=Dd;Ds2=Dc;Ds3=Db;
    Vs1=Vd;Vs2=Vc;Vs3=Vb;
    Ps1=Pod;Ps2=Poc;Ps3=Pob;
    Pr1=Pdref2;Pr2=Pcref2;Pr3=Pbref2;
    q1=1;q2=q;q3=q;
    state=6;
end
% if state0~=state,
%     delB0=del0;
%     delC0=del0;
%     delD0=del0;
%
% end
% state0=state;

L8f=L*8*f;nV1=n*V1;

```

This presents the initial currents, eq. (4.12).

```

Is1=(Ps1-Vs1*((3*Vs1-Vs2-Vs3)*Ds1^2-nV1*Ds1^2)/L8f)/Vs1/Ds1;
Is2=(Ps2-Vs2*((3*Vs2-Vs3)*Ds2^2-nV1*Ds2^2+Vs1*Ds1^2-
2*Vs1*Ds1*Ds2)/L8f)/Vs2/Ds2;
Is3=(Ps3-Vs3*((3*Vs3*Ds3^2-nV1*Ds3^2+Vs1*Ds1^2+Vs2*Ds2^2-
2*(Vs1*Ds1+Vs2*Ds2)*Ds3)/L8f)/Vs3/Ds3;

```

$$\text{ErrP0} = q_1 * (\text{Pr1} - \text{Ps1})^2 + q_2 * (\text{Pr2} - \text{Ps2})^2 + q_3 * (\text{Pr3} - \text{Ps3})^2;$$

The RPROP algorithm is used to execute an algorithm that realizes the gradient descent of cost function value expressed by eq. (4-13).

```

for R=1:5
    Pv11=(6*Vs1-Vs2-Vs3-nV1)*Ds1^2/L8f+Is1*Ds1;
    Pv21=Vs2*Ds1*(Ds1-2*Ds2)/L8f;
    Pv31=Vs3*Ds1*(Ds1-2*Ds3)/L8f;
    Pv12=-Vs1*Ds1^2/L8f;
    Pv22=((6*Vs2-Vs3-nV1)*Ds2^2+Vs1*Ds1*(Ds1-2*Ds2))/L8f+Is2*Ds2;
    Pv32=Vs3*Ds2*(Ds2-2*Ds3)/L8f;
    Pv13=Pv12;
    Pv23=-Vs2*Ds2^2/L8f;
    Pv33=((6*Vs3-nV1)*Ds3^2-2*(Vs1*Ds1+Vs2*Ds2)*Ds3)/L8f-Pv12-Pv23+Is3*Ds3;

    F=[Pv11 Pv21 Pv31;Pv12 Pv22 Pv32;Pv13 Pv23 Pv33];

    dpdv=inv(F*diag([q1;q2;q3])*F'+1e6*eye(3))*F*[q1*(Ps1-Pr1);q2*(Ps2-Pr2);q3*(Ps3-Pr3)];

    dpdv1=dpdv(1);
    dpdv2=dpdv(2);
    dpdv3=dpdv(3);

    if abs(dpdv1)>1,
        dpdv1=sign(dpdv1);
    end
    if abs(dpdv2)>1,
        dpdv2=sign(dpdv2);
    end
    if abs(dpdv3)>1,
        dpdv3=sign(dpdv3);
    end

if state==1,%b,c,d

    dpdvB=dpdv1;
    dpdvC=dpdv2;
    dpdvD=dpdv3;

    if dpdvB0*dpdvB>s,
        delB=min(delB0*etaP,delMax);
        delVB=-(dpdvB)*delB;
        delB0=delB;
    elseif dpdvB0*dpdvB<-s
        delB=max(delB0*etaM,delMin);
        dpdvB=0;
        delB0=delB;
        delVB=-delVB0;

else,

```

```

    delVB=-(dpdvB)*delB0;
end
dpdvB0=dpdvB;
Vtemp=Vs1+delVB;
if delVB>0 && Vtemp>Vmax1,
    delVB=max(0,Vmax1-Vs1);
    Vtemp=Vmax1;
    dpdvB0=0;
elseif delVB<0 && Vtemp<Vmin1,
    delVB=min(0,Vmin1-Vs1);
    Vtemp=Vmin1;
    dpdvB0=0;
end
delVB0=delVB;
Vs1=Vtemp;

if dpdvC0*dpdvC>s,
    delC=min(delC0*etaP,delMax);
    delVC=-(dpdvC)*delC;
    delC0=delC;

elseif dpdvC0*dpdvC<-s
    delC=max(delC0*etaM,delMin);
    dpdvC=0;
    delC0=delC;
    delVC=-delVC0;

else,
    delVC=-(dpdvC)*delC0;

end
dpdvC0=dpdvC;
Vtemp=Vs2+delVC;
if delVC>0 && Vtemp>Vmax1,
    delVC=max(0,Vmax1-Vs2);
    Vtemp=Vmax1;
    dpdvC0=0;
elseif delVC<0 && Vtemp<Vmin1,
    delVC=min(0,Vmin1-Vs2);
    Vtemp=Vmin1;
    dpdvC0=0;
end
delVC0=delVC;
Vs2=Vtemp;

if dpdvD0*dpdvD>s,
    delD=min(delD0*etaP,delMax);
    delVD=-(dpdvD)*delD;

    delD0=delD;
elseif dpdvD0*dpdvD<-s,
    delD=max(delD0*etaM,delMin);

    dpdvD=0;
    delD0=delD;

```

```

        delVD=-delVD0;

    else
        delVD=-(dpdvD)*delD0;
    end
    dpdvD0=dpdvD;
    Vtemp=Vs3+delVD;
    if delVD>0 && Vtemp>Vmax1,
        delVD=max(0,Vmax1-Vs3);
        Vtemp=Vmax1;
        dpdvD0=0;
    elseif delVD<0 && Vtemp<Vmin1,
        delVD=min(0,Vmin1-Vs3);
        Vtemp=Vmin1;
        dpdvD0=0;
    end
    delVD0=delVD;
    Vs3=Vtemp;

    Ps1=Is1*Vs1*Ds1+Vs1*((3*Vs1-Vs2-Vs3)*Ds12-nV1*Ds12)/L8f;
    Ps2=Is2*Vs2*Ds2+Vs2*((3*Vs2-Vs3)*Ds22-nV1*Ds22+Vs1*Ds12-
2*Vs1*Ds1*Ds2)/L8f;
    Ps3=Is3*Vs3*Ds3+Vs3*(3*Vs3*Ds32-nV1*Ds32+Vs1*Ds12+Vs2*Ds22-
2*(Vs1*Ds1+Vs2*Ds2)*Ds3)/L8f;

% Pr3=Psum-Ps1-Ps2;
Vbr=Vs1; Vcr=Vs2;Vdr=Vs3;
elseif state==2,%b,d,c
    dpdvB=dpdv1;
    dpdvD=dpdv2;
    dpdvC=dpdv3;

    if dpdvB0*dpdvB>s,
        delB=min(delB0*etaP,delMax);
        delVB=-(dpdvB)*delB;

        delB0=delB;

    elseif dpdvB0*dpdvB<-s,
        delB=max(delB0*etaM,delMin);

        dpdvB=0;
        delB0=delB;
        delVB=-delVB0;

    else,
        delVB=-(dpdvB)*delB0;
    end
    dpdvB0=dpdvB;
    Vtemp=Vs1+delVB;
    if delVB>0 && Vtemp>Vmax1,
        delVB=max(0,Vmax1-Vs1);
        Vtemp=Vmax1;
        dpdvB0=0;
    elseif delVB<0 && Vtemp<Vmin1,

```



```

        delVB=min(0,Vmin1-Vs1);
        Vtemp=Vmin1;
        dpdvB0=0;
    end
delVB0=delVB;
Vs1=Vtemp;

    if dpdvC0*dpdvC>s,
        delC=min(delC0*etaP,delMax);
        delVC=-(dpdvC)*delC;

        delC0=delC;

    elseif dpdvC0*dpdvC<-s ,
        delC=max(delC0*etaM,delMin);
        dpdvC=0;
        delC0=delC;
        delVC=-delVC0;

    else,
        delVC=-(dpdvC)*delC0;

    end
dpdvC0=dpdvC;
Vtemp=Vs3+delVC;
    if delVC>0 && Vtemp>Vmax1,
        delVC=max(0,Vmax1-Vs3);
        Vtemp=Vmax1;
        dpdvC0=0;
    elseif delVC<0 && Vtemp<Vmin1,
        delVC=min(0,Vmin1-Vs3);
        Vtemp=Vmin1;
        dpdvC0=0;
    end
delVC0=delVC;
Vs3=Vtemp;

    if dpdvD0*dpdvD>s,
        delD=min(delD0*etaP,delMax);
        delVD=-(dpdvD)*delD;

        delD0=delD;

    elseif dpdvD0*dpdvD<-s,
        delD=max(delD0*etaM,delMin);

        dpdvD=0;
        delD0=delD;
        delVD=-delVD0;

    else,
        delVD=-(dpdvD)*delD0;

    end
dpdvD0=dpdvD;

```

```

Vtemp=Vs2+delVD;
if delVD>0 && Vtemp>Vmax1,
    delVD=max(0,Vmax1-Vs2);
    Vtemp=Vmax1;
    dpdvD0=0;
elseif delVD<0 && Vtemp<Vmin1,
    delVD=min(0,Vmin1-Vs2);
    Vtemp=Vmin1;
    dpdvD0=0;
end
delVD0=delVD;
Vs2=Vtemp;

Ps1=Is1*Vs1*Ds1+Vs1*((3*Vs1-Vs2-Vs3)*Ds1^2-nV1*Ds1^2)/L8f;
Ps3=Is3*Vs3*Ds3+Vs3*(3*Vs3*Ds3^2-nV1*Ds3^2+Vs1*Ds1^2+Vs2*Ds2^2-
2*(Vs1*Ds1+Vs2*Ds2)*Ds3)/L8f;
Ps2=Is2*Vs2*Ds2+Vs2*((3*Vs2-Vs3)*Ds2^2-nV1*Ds2^2+Vs1*Ds1^2-
2*Vs1*Ds1*Ds2)/L8f;

% Pr2=Psum-Ps1-Ps3;
Vbr=Vs1; Vcr=Vs3;Vdr=Vs2;
elseif state==3,%c,b,d

dpdvC=dpdv1;
dpdvB=dpdv2;
dpdvD=dpdv3;

if dpdvB0*dpdvB>s,
    delB=min(delB0*etaP,delMax);
    delVB=-(dpdvB)*delB;

    delB0=delB;
elseif dpdvB0*dpdvB<-s ,
    delB=max(delB0*etaM,delMin);

    dpdvB=0;
    delB0=delB;
    delVB=-delVB0;

else,
    delVB=-(dpdvB)*delB0;

end
dpdvB0=dpdvB;
Vtemp=Vs2+delVB;
if delVB>0 && Vtemp>Vmax1,
    delVB=max(0,Vmax1-Vs2);
    Vtemp=Vmax1;
    dpdvB0=0;
elseif delVB<0 && Vtemp<Vmin1,
    delVB=min(0,Vmin1-Vs2);
    Vtemp=Vmin1;
    dpdvB0=0;
end
delVB0=delVB;

```

```

Vs2=Vtemp;

    if dpdvC0*dpdvC>s,
        delC=min(delC0*etaP,delMax);
        delVC=-(dpdvC)*delC;

        delC0=delC;

    elseif dpdvC0*dpdvC<-s,
        delC=max(delC0*etaM,delMin);

        dpdvC=0;
        delC0=delC;
        delVC=-delVC0;
    else,
        delVC=-(dpdvC)*delC0;

    end
dpdvC0=dpdvC;
Vtemp=Vs1+delVC;
    if delVC>0 && Vtemp>Vmax1,
        delVC=max(0,Vmax1-Vs1);
        Vtemp=Vmax1;
        dpdvC0=0;
    elseif delVC<0 && Vtemp<Vmin1,
        delVC=min(0,Vmin1-Vs1);
        Vtemp=Vmin1;
        dpdvC0=0;
    end
delVC0=delVC;
Vs1=Vtemp;

    if dpdvD0*dpdvD>s,
        delD=min(delD0*etaP,delMax);
        delVD=-(dpdvD)*delD;
        delD0=delD;

    elseif dpdvD0*dpdvD<-s,
        delD=max(delD0*etaM,delMin);

        dpdvD=0;
        delD0=delD;
        delVD=-delVD0;

    else,
        delVD=-(dpdvD)*delD0;

    end
dpdvD0=dpdvD;
Vtemp=Vs3+delVD;
    if delVD>0 && Vtemp>Vmax1,
        delVD=max(0,Vmax1-Vs3);
        Vtemp=Vmax1;
        dpdvD0=0;
    elseif delVD<0 && Vtemp<Vmin1,

```

```

        delVD=min(0,Vmin1-Vs3);
        Vtemp=Vmin1;
        dpdvD0=0;
    end
delVD0=delVD;
Vs3=Vtemp;

    Ps1=Is1*Vs1*Ds1+Vs1*((3*Vs1-Vs2-Vs3)*Ds1^2-nV1*Ds1^2)/L8f;
    Ps2=Is2*Vs2*Ds2+Vs2*((3*Vs2-Vs3)*Ds2^2-nV1*Ds2^2+Vs1*Ds1^2-
2*Vs1*Ds1*Ds2)/L8f;
    Ps3=Is3*Vs3*Ds3+Vs3*(3*Vs3*Ds3^2-nV1*Ds3^2+Vs1*Ds1^2+Vs2*Ds2^2-
2*(Vs1*Ds1+Vs2*Ds2)*Ds3)/L8f;

%     Pr3=Psum-Ps1-Ps2;
    Vcr=Vs1; Vbr=Vs2;Vdr=Vs3;
elseif state==4,%c,d,b

    dpdvC=dpdv1;
    dpdvD=dpdv2;
    dpdvB=dpdv3;

    if dpdvB0*dpdvB>s,
        delB=min(delB0*etaP,delMax);
        delVB=-(dpdvB)*delB;

        delB0=delB;

    elseif dpdvB0*dpdvB<-s,
        delB=max(delB0*etaM,delMin);

        dpdvB=0;
        delB0=delB;
        delVB=-delVB0;
    else,
        delVB=-(dpdvB)*delB0;
    end
dpdvB0=dpdvB;
Vtemp=Vs3+delVB;
if delVB>0 && Vtemp>Vmax1,
    delVB=max(0,Vmax1-Vs3);
    Vtemp=Vmax1;
    dpdvB0=0;
elseif delVB<0 && Vtemp<Vmin1,
    delVB=min(0,Vmin1-Vs3);
    Vtemp=Vmin1;
    dpdvB0=0;
end
delVB0=delVB;
Vs3=Vtemp;

    if dpdvC0*dpdvC>s,
        delC=min(delC0*etaP,delMax);

```

```

    delVC=- (dpdvC) *delC;

    delC0=delC;

elseif dpdvC0*dpdvC<-s,
    delC=max (delC0*etaM, delMin);

    dpdvC=0;
    delC0=delC;
    delVC=-delVC0;
else,
    delVC=- (dpdvC) *delC0;

end
dpdvC0=dpdvC;
Vtemp=Vs1+delVC;
if delVC>0 && Vtemp>Vmax1,
    delVC=max (0, Vmax1-Vs1);
    Vtemp=Vmax1;
    dpdvC0=0;
elseif delVC<0 && Vtemp<Vmin1,
    delVC=min (0, Vmin1-Vs1);
    Vtemp=Vmin1;
    dpdvC0=0;
end
delVC0=delVC;
Vs1=Vtemp;

if dpdvD0*dpdvD>s,
    delD=min (delD0*etaP, delMax);
    delVD=- (dpdvD) *delD;

    delD0=delD;

elseif dpdvD0*dpdvD<-s,
    delD=max (delD0*etaM, delMin);

    dpdvD=0;
    delD0=delD;
    delVD=-delVD0;
else,
    delVD=- (dpdvD) *delD0;

end
dpdvD0=dpdvD;
Vtemp=Vs2+delVD;
if delVD>0 && Vtemp>Vmax1,
    delVD=max (0, Vmax1-Vs2);
    Vtemp=Vmax1;
    dpdvD0=0;
elseif delVD<0 && Vtemp<Vmin1,
    delVD=min (0, Vmin1-Vs2);
    Vtemp=Vmin1;
    dpdvD0=0;
end

```

```

delVD0=delVD;
Vs2=Vtemp;

Ps1=Is1*Vs1*Ds1+Vs1*( (3*Vs1-Vs2-Vs3)*Ds1^2-nV1*Ds1^2)/L8f;
Ps3=Is3*Vs3*Ds3+Vs3*(3*Vs3*Ds3^2-nV1*Ds3^2+Vs1*Ds1^2+Vs2*Ds2^2-
2*(Vs1*Ds1+Vs2*Ds2)*Ds3)/L8f;
Ps2=Is2*Vs2*Ds2+Vs2*( (3*Vs2-Vs3)*Ds2^2-nV1*Ds2^2+Vs1*Ds1^2-
2*Vs1*Ds1*Ds2)/L8f;

% Pr2=Psum-Ps1-Ps3;
Vcr=Vs1; Vbr=Vs3;Vdr=Vs2;
elseif state==5,%d,b,c

dpdvD=dpdv1;
dpdvB=dpdv2;
dpdvC=dpdv3;

if dpdvB0*dpdvB>s,
delB=min(delB0*etaP,delMax);
delVB=-(dpdvB)*delB;

delB0=delB;

elseif dpdvB0*dpdvB<-s,
delB=max(delB0*etaM,delMin);

dpdvB=0;
delB0=delB;
delVB=-delVB0;
else,
delVB=-(dpdvB)*delB0;

end
dpdvB0=dpdvB;
Vtemp=Vs2+delVB;
if delVB>0 && Vtemp>Vmax1,
delVB=max(0,Vmax1-Vs2);
Vtemp=Vmax1;
dpdvB0=0;
elseif delVB<0 && Vtemp<Vmin1,
delVB=min(0,Vmin1-Vs2);
Vtemp=Vmin1;
dpdvB0=0;
end
delVB0=delVB;
Vs2=Vtemp;

if dpdvC0*dpdvC>s,
delC=min(delC0*etaP,delMax);
delVC=-(dpdvC)*delC;

delC0=delC;

elseif dpdvC0*dpdvC<-s,
delC=max(delC0*etaM,delMin);

```

```

        dpdvC=0;
        delC0=delC;
        delVC=-delVC0;
    else,
        delVC=-(dpdvC)*delC0;

    end
    dpdvC0=dpdvC;
    Vtemp=Vs3+delVC;
    if delVC>0 && Vtemp>Vmax1,
        delVC=max(0,Vmax1-Vs3);
        Vtemp=Vmax1;
        dpdvC0=0;
    elseif delVC<0 && Vtemp<Vmin1,
        delVC=min(0,Vmin1-Vs3);
        Vtemp=Vmin1;
        dpdvC0=0;
    end
    delVC0=delVC;
    Vs3=Vtemp;

    if dpdvD0*dpdvD>s,
        delD=min(delD0*etaP,delMax);
        delVD=-(dpdvD)*delD;

        delD0=delD;

    elseif dpdvD0*dpdvD<-s,
        delD=max(delD0*etaM,delMin);

        dpdvD=0;
        delD0=delD;
        delVD=-delVD0;
    else,
        delVD=-(dpdvD)*delD0;

    end
    dpdvD0=dpdvD;
    Vtemp=Vs1+delVD;
    if delVD>0 && Vtemp>Vmax1,
        delVD=max(0,Vmax1-Vs1);
        Vtemp=Vmax1;
        dpdvD0=0;
    elseif delVD<0 && Vtemp<Vmin1,
        delVD=min(0,Vmin1-Vs1);
        Vtemp=Vmin1;
        dpdvD0=0;
    end
    delVD0=delVD;
    Vs1=Vtemp;

    Ps2=Is2*Vs2*Ds2+Vs2*((3*Vs2-Vs3)*Ds2^2-nV1*Ds2^2+Vs1*Ds1^2-
    2*Vs1*Ds1*Ds2)/L8f;

```

```

    Ps3=Is3*Vs3*Ds3+Vs3*(3*Vs3*Ds3^2-nV1*Ds3^2+Vs1*Ds1^2+Vs2*Ds2^2-
2*(Vs1*Ds1+Vs2*Ds2)*Ds3)/L8f;
    Ps1=Is1*Vs1*Ds1+Vs1*((3*Vs1-Vs2-Vs3)*Ds1^2-nV1*Ds1^2)/L8f;

%    Pr1=Psum-Ps2-Ps3;
    Vbr=Vs2; Vcr=Vs3;Vdr=Vs1;
else %d,c,b

    dpdvD=dpdv1;
    dpdvC=dpdv2;
    dpdvB=dpdv3;

    if dpdvB0*dpdvB>s,
        delB=min(delB0*etaP,delMax);
        delVB=-(dpdvB)*delB;

        delB0=delB;

    elseif dpdvB0*dpdvB<-s ,
        delB=max(delB0*etaM,delMin);

        dpdvB=0;
        delB0=delB;
        delVB=-delVB0;
    else,
        delVB=-(dpdvB)*delB0;

    end
    dpdvB0=dpdvB;
    Vtemp=Vs3+delVB;
    if delVB>0 && Vtemp>Vmax1,
        delVB=max(0,Vmax1-Vs3);
        Vtemp=Vmax1;
        dpdvB0=0;
    elseif delVB<0 && Vtemp<Vmin1,
        delVB=min(0,Vmin1-Vs3);
        Vtemp=Vmin1;
        dpdvB0=0;
    end
    delVB0=delVB;
    Vs3=Vtemp;

    if dpdvC0*dpdvC>s,
        delC=min(delC0*etaP,delMax);
        delVC=-(dpdvC)*delC;

        delC0=delC;

    elseif dpdvC0*dpdvC<-s ,
        delC=max(delC0*etaM,delMin);

        dpdvC=0;
        delC0=delC;
        delVC=-delVC0;
    else,

```



```

delVC=- (dpdvC) *delC0;

end
dpdvC0=dpdvC;
Vtemp=Vs2+delVC;
if delVC>0 && Vtemp>Vmax1,
    delVC=max(0,Vmax1-Vs2);
    Vtemp=Vmax1;
    dpdvC0=0;
elseif delVC<0 && Vtemp<Vmin1,
    delVC=min(0,Vmin1-Vs2);
    Vtemp=Vmin1;
    dpdvC0=0;
end
delVC0=delVC;
Vs2=Vtemp;

if dpdvD0*dpdvD>s,
    delD=min(delD0*etaP,delMax);
    delVD=- (dpdvD) *delD;

    delD0=delD;

elseif dpdvD0*dpdvD<-s ,
    delD=max(delD0*etaM,delMin);

    dpdvD=0;
    delD0=delD;
    delVD=-delVD0;
else,
    delVD=- (dpdvD) *delD0;

end
dpdvD0=dpdvD;
Vtemp=Vs1+delVD;
if delVD>0 && Vtemp>Vmax1,
    delVD=max(0,Vmax1-Vs1);
    Vtemp=Vmax1;
    dpdvD0=0;
elseif delVD<0 && Vtemp<Vmin1,
    delVD=min(0,Vmin1-Vs1);
    Vtemp=Vmin1;
    dpdvD0=0;
end
delVD0=delVD;
Vs1=Vtemp;

Ps2=Is2*Vs2*Ds2+Vs2*( (3*Vs2-Vs3) *Ds2^2-nV1*Ds2^2+Vs1*Ds1^2-
2*Vs1*Ds1*Ds2)/L8f;
Ps3=Is3*Vs3*Ds3+Vs3*(3*Vs3*Ds3^2-nV1*Ds3^2+Vs1*Ds1^2+Vs2*Ds2^2-
2*(Vs1*Ds1+Vs2*Ds2)*Ds3)/L8f;
Ps1=Is1*Vs1*Ds1+Vs1*( (3*Vs1-Vs2-Vs3) *Ds1^2-nV1*Ds1^2)/L8f;

% Pr1=Psum-Ps2-Ps3;
Vcr=Vs2; Vbr=Vs3;Vdr=Vs1;

```

```

end

    ErrP=q1*(Pr1-Ps1)^2+q2*(Pr2-Ps2)^2+q3*(Pr3-Ps3)^2;
if ErrP0<ErrP,
    break;
else
    Vbr0=Vbr; Vcr0=Vcr;Vdr0=Vdr;
end
ErrP0=ErrP;
end
Vbr0=max(Vmin1,min(Vmax1,Vbr0));
Vcr0=max(Vmin1,min(Vmax1,Vcr0));
Vdr0=max(Vmin1,min(Vmax1,Vdr0));

y =[Vbr0-1130;Vcr0-1130;Vdr0-1130];

```

Appendix C Supplementary materials used in chapter 5

Appendix C.1 Power distribution loop (NMPC: Stability)

```
function [y,Eiga] = MPC_control(V,D, P2, Pr, L, f, n)
persistent Vmax Vmin
persistent Kdi count EigMax
persistent Is1e Is2e Is3e delPs1 delPs2 delPs3 delPr1 delPr2 delPr3
persistent Vstates delVB1 delVC1 delVD1 delVB2 delVC2 delVD2 Vd0 Db0 Dc0 Dd0
Rk1 Qk1 Kpv Kiv Dlmin Dlmax CaT
if isempty(count),
    Kdi=-1e-6*[0.2578    0.0175
    0.0175    0.2578];
    count=0;
    EigMax=0;
%     Pa0=0;
    Rk1=diag([1e3 1e3 1e4]);
    Qk1=[diag([1e4 1e4 1e6]) zeros(3,3);zeros(3,3) eye(3)*5e1];
    Db0=0;
    Dc0=0;
    Dd0=0;

    Kpv=1.3256;
    Kiv=2.6596e3/20e3;
    Dlmin=0.25;
    Dlmax=0.4999;
    CaT=2*68000e-6*20e3;

    Is1e=0;
    Is2e=0;
    Is3e=0;

    Vd0=1130;

    Vstates = [-1 -1 -1;-1 -1 0;-1 -1 1;-1 0 -1;-1 0 0;-1 0 1;-1 1 -1;-1 1
0;-1 -1 1;0 -1 -1;0 -1 0;0 -1 1;0 0 -1;0 0 0;0 0 1;0 1 -1;0 1 0;0 -1 1;1 -1 -
1;1 -1 0;1 -1 1;1 0 -1;1 0 0;1 0 1;1 1 -1;1 1 0;1 -1 1];

    delPr1=0;
    delPr2=0;
    delPr3=0;

    delPs1=0;
    delPs2=0;
    delPs3=0;
```

```

delVB1=0;
delVC1=0;
delVD1=0;

delVB2=0;
delVC2=0;
delVD2=0;

Vmax=1200;
Vmin=1010;

```

end

```

Vb=V(1);Vc=V(2);Vd=V(3);Vl=V(4);D1=0.01*D(4);
L8f=L*8*f;nVl=n*Vl;L4f=L*4*f;

```

```

Db=0.01*D(1);Dc=0.01*D(2);Dd=0.01*D(3);

```

```

Pob=P2(1);Poc=P2(2);Pod=P2(3);
Pbref2=Pr(1);Pcref2=Pr(2);Pdref2=Pr(3);
Pbref0=Pr(4);Pcref0=Pr(5);Pa=Pr(6);

```

```

Pr1=Pbref2;Pr2=Pcref2;Pr3=Pdref2;

```

```

state=0;
if Db<=Dc && Dc<=Dd,
    Ds1=Db;Ds2=Dc;Ds3=Dd;
    Vs1=Vb;Vs2=Vc;Vs3=Vd;
    Ps1=Pob;Ps2=Poc;Ps3=Pod;
    Pr1=Pbref2;Pr2=Pcref2;Pr3=Pdref2;

```

```

    state=1;
elseif Db<=Dd && Dd<=Dc,
    Ds1=Db;Ds2=Dd;Ds3=Dc;
    Vs1=Vb;Vs2=Vd;Vs3=Vc;
    Ps1=Pob;Ps2=Pod;Ps3=Poc;
    Pr1=Pbref2;Pr2=Pdref2;Pr3=Pcref2;

```

```

    state=2;
elseif Dc<=Db && Db<=Dd,
    Ds1=Dc;Ds2=Db;Ds3=Dd;
    Vs1=Vc;Vs2=Vb;Vs3=Vd;
    Ps1=Poc;Ps2=Pob;Ps3=Pod;
    Pr1=Pcref2;Pr2=Pbref2;Pr3=Pdref2;

```

```

    state=3;
elseif Dc<=Dd && Dd<=Db,
    Ds1=Dc;Ds2=Dd;Ds3=Db;
    Vs1=Vc;Vs2=Vd;Vs3=Vb;
    Ps1=Poc;Ps2=Pod;Ps3=Pob;
    Pr1=Pcref2;Pr2=Pdref2;Pr3=Pbref2;

```

```

        state=4;
elseif Dd<=Db && Db<=Dc,
    Ds1=Dd;Ds2=Db;Ds3=Dc;
    Vs1=Vd;Vs2=Vb;Vs3=Vc;
    Ps1=Pod;Ps2=Pob;Ps3=Poc;
    Pr1=Pdref2;Pr2=Pbref2;Pr3=Pcref2;

    state=5;
else
    Ds1=Dd;Ds2=Dc;Ds3=Db;
    Vs1=Vd;Vs2=Vc;Vs3=Vb;
    Ps1=Pod;Ps2=Poc;Ps3=Pob;
    Pr1=Pdref2;Pr2=Pcref2;Pr3=Pbref2;

    state=6;
end

dP1=Vs1*((3*Vs1-Vs2-Vs3)*Ds1^2-nV1*Ds1^2)/L8f;
dP2=Vs2*((3*Vs2-Vs3)*Ds2^2-nV1*Ds2^2+Vs1*Ds1^2-2*Vs1*Ds1*Ds2)/L8f;
dP3=Vs3*(3*Vs3*Ds3^2-nV1*Ds3^2+Vs1*Ds1^2+Vs2*Ds2^2-
2*(Vs1*Ds1+Vs2*Ds2)*Ds3)/L8f;

Is1o=(Pr1-dP1)/Vs1/Ds1;
Is2o=(Pr2-dP2)/Vs2/Ds2;
Is3o=(Pr3-dP3)/Vs3/Ds3;

if isfinite(Is1o) && isfinite(Is2o) && isfinite(Is3o)
    Is1e=Is1o;
    Is2e=Is2o;
    Is3e=Is3o;
end

Is1=Is1e+(3*Vs1*Ds1-Vs2*Ds2-Vs3*Ds3-nV1*D1)/L4f;
Is2=Is2e+(3*Vs2*Ds2-Vs1*Ds1-Vs3*Ds3-nV1*D1)/L4f;
Is3=Is3e+(3*Vs3*Ds3-Vs2*Ds2-Vs1*Ds1-nV1*D1)/L4f;

dP1=Vs1*((3*Vs1-Vs2-Vs3)*Ds1^2-nV1*Ds1^2)/L8f;
dP2=Vs2*((3*Vs2-Vs1-Vs3)*Ds2^2-nV1*Ds2^2)/L8f;
dP3=Vs3*((3*Vs3-Vs1-Vs2)*Ds3^2-nV1*Ds3^2)/L8f;

Pre1=Is1e*Vs1*Ds1+dP1;
Pre2=Is2e*Vs2*Ds2+dP2;
Pre3=Is3e*Vs3*Ds3+dP3;

delPr1=0.5*delPr1+0.5*(Pr1-Pre1);
delPr2=0.5*delPr2+0.5*(Pr2-Pre2);
delPr3=0.5*delPr3+0.5*(Pr3-Pre3);

Pse1=-Is1*Vs1*Ds1+dP1;
Pse2=-Is2*Vs2*Ds2+dP2;
Pse3=-Is3*Vs3*Ds3+dP3;

delPs1=0.5*delPs1+0.5*(Ps1-Pse1);

```

```

delPs2=0.5*delPs2+0.5*(Ps2-Pse2);
delPs3=0.5*delPs3+0.5*(Ps3-Pse3);

Ib1=Is1e;
Ic1=Is2e;
Id1=Is3e;
Ib2=Is1e;
Ic2=Is2e;
Id2=Is3e;
if state==1
    Ib1=Is1e;
    Ic1=Is2e;
    Id1=Is3e;
    Ib2=Is1;
    Ic2=Is2;
    Id2=Is3;

    dbr=delPr1;dcr=delPr2;ddr=delPr3;
    dbs=delPs1;dcs=delPs2;dds=delPs3;

elseif state==2
    Ib1=Is1e;
    Id1=Is2e;
    Ic1=Is3e;
    Ib2=Is1;
    Id2=Is2;
    Ic2=Is3;

    dbr=delPr1;ddr=delPr2;dcr=delPr3;
    dbs=delPs1;dds=delPs2;dcs=delPs3;

elseif state==3
    Ic1=Is1e;
    Ib1=Is2e;
    Id1=Is3e;
    Ic2=Is1;
    Ib2=Is2;
    Id2=Is3;

    dcr=delPr1;dbr=delPr2;ddr=delPr3;
    dcs=delPs1;dbs=delPs2;dds=delPs3;

elseif state==4
    Ic1=Is1e;
    Id1=Is2e;
    Ib1=Is3e;
    Ic2=Is1;
    Id2=Is2;
    Ib2=Is3;
    dcr=delPr1;ddr=delPr2;dbr=delPr3;
    dcs=delPs1;dds=delPs2;dbs=delPs3;

elseif state==5
    Id1=Is1e;

```

```

Ib1=Is2e;
Ic1=Is3e;
Id2=Is1;
Ib2=Is2;
Ic2=Is3;

ddr=delPr1;dbr=delPr2;dcr=delPr3;
dds=delPs1;dbs=delPs2;dcs=delPs3;

else
    Id1=Is1e;
    Ic1=Is2e;
    Ib1=Is3e;
    Id2=Is1;
    Ic2=Is2;
    Ib2=Is3;

    ddr=delPr1;dcr=delPr2;dbr=delPr3;
    dds=delPs1;dcs=delPs2;dbs=delPs3;

end

Pars=Pa;

count=count+1;
if count>5
    count=0;
end

if count==1 ,

    Vb=Vd0+delVB2;
    Vc=Vd0+delVC2;
    Vd=Vd0+delVD2;
    Vbi=Vd0+delVB1;
    Vci=Vd0+delVC1;
    Vdi=Vd0+delVD1;
    Dd=D1*nV1/Vd;

    ePb=Pdref2+Pob-Pbref0;
    ePc=Pcref2+Poc-Pcref0;

    Dbr=Db;Dcr=Dc;Ddr=D1*nV1/Vd;

    K12=Kdi*[-2 1 1;1 -2 1]*0.35/Ddr/3;
    Apr=[(Ib1+(3*Vb-Vc-Vd-nV1)/L4f)*Vb 0 0;0 (Ic1+(3*Vc-Vb-Vd-nV1)/L4f)*Vc
0;0 0 (Id1+(3*Vd-Vb-Vc-nV1)/L4f)*Vd];
    Bpr=[Dbr*(Ib1+3*Vb*Dbr)/L4f -Vb*Dbr^2/L8f -Vb*Dbr^2/L8f;-Vc*Dcr^2/L8f
Dcr*(Ic1+3*Vc*Dcr)/L4f -Vc*Dcr^2/L8f;-Vd*Ddr^2/L8f -Vd*Ddr^2/L8f
Ddr*(Id1+3*Vd*Ddr)/L4f];

    Abc=eye(2,3)-K12*Apr;Bbc=-K12*Bpr;
    Abcd=[Abc;zeros(1,3)];Bbcd=[Bbc;0 0 -Dbr/Vd];

```

```

Dp11=(Vc*(Dcr-Dbr)+Vd*(Ddr-Dbr)+nVl*(D1-Dbr))*Dbr;
Dp12=(Dcr-Dbr)*Vb*Dbr;
Dp13=(Ddr-Dbr)*Vb*Dbr;

Dp21=(Dbr-Dcr)*Vc*Dcr;
Dp22=(Vb*(Dbr-Dcr)+Vd*(Ddr-Dcr)+nVl*(D1-Dcr))*Dcr;
Dp23=(Ddr-Dcr)*Vc*Dcr;

Dp31=(Dbr-Ddr)*Vd*Ddr;
Dp32=(Dcr-Ddr)*Vd*Ddr;
Dp33=(Vb*(Dbr-Ddr)+Vc*(Dcr-Ddr)+nVl*(D1-Ddr))*Ddr;

Dp=[Dp11 Dp12 Dp13;Dp21 Dp22 Dp23;Dp31 Dp32 Dp33]/L4f;

Cp11=Vb*(Vc*(Dcr-2*Dbr)+Vd*(Ddr-2*Dbr)+nVl*(D1-2*Dbr));
Cp12=Vb*Vc*Dbr;
Cp13=Vb*Vd*Ddr;
Cp21=Vb*Vc*Dcr;
Cp22=Vc*(Vb*(Dbr-2*Dcr)+Vd*(Ddr-2*Dcr)+nVl*(D1-2*Dcr));
Cp23=Vc*Vd*Ddr;
Cp31=Vb*Vd*Ddr;
Cp32=Vc*Vd*Ddr;
Cp33=Vd*(Vb*(Dbr-2*Ddr)+Vc*(Dcr-2*Ddr)+nVl*(D1-2*Ddr));
Cp=[Cp11 Cp12 Cp13;Cp21 Cp22 Cp23;Cp31 Cp32 Cp33]/L4f;

AA=[Abcd zeros(3,3);Cp eye(3)]; BB=[Bbcd;Dp];

A2=AA^2;A3=A2*AA;A4=A3*AA;
BB=(A4+A3+A2+AA)*BB+BB;
AA=AA*A4;

Pk1=Qk1;

for repeat=1:4
    Kk=-inv(BB'*Pk1*BB+Rk1)*(BB'*Pk1)*AA;
    Pk1=(AA+BB*Kk)'*Pk1*(AA+BB*Kk)+Kk'*Rk1*Kk+Qk1;
end
%
u=Kk*[Dbr-Db0;Dcr-Dc0;Ddr-Dd0;ePb;ePc;-ePb-ePc];

Vb=Vb+u(1);
Vc=Vc+u(2);
Vd=Vd+u(3);
if V1>0
    IL=Pars/V1;
else
    IL=0.01;
end
IL0=IL;
Vl1=Vl;Dl0=Dl;
Gopt=0;

if norm(u)<1 && Vmin<Vb && Vmax>Vb && Vmin<Vc && Vmax>Vc && Vmin<Vd &&
Vmax>Vd

```



```

Vbb=Vb;Vcc=Vc;Vdd=Vd;

Vl=Vl1;nVl=n*Vl;D1=D10;IL=IL0;
Dbr=Db;Dcr=Dc;Ddr=D1*nVl/Vd;
for repeat=1:5
    K12=Kdi*[-2 1 1;1 -2 1]*0.35/Ddr/3;
    Ddr0=Ddr;

    Ib2=Ib1+(3*Vb*Dbr-Vc*Dcr-Vd*Ddr-nVl*D1)/L4f;
    Ic2=Ic1+(3*Vc*Dcr-Vb*Dbr-Vd*Ddr-nVl*D1)/L4f;
    Id2=Id1+(3*Vd*Ddr-Vb*Dbr-Vc*Dcr-nVl*D1)/L4f;
    dPb=Vb*( (3*Vb-Vc-Vd)*Dbr^2-nVl*Dbr^2)/L8f;
    dPc=Vc*( (3*Vc-Vb-Vd)*Dcr^2-nVl*Dcr^2)/L8f;
    dPd=Vd*( (3*Vd-Vb-Vc)*Ddr^2-nVl*Ddr^2)/L8f;

    Prb=Ib1*Vb*Dbr+dPb+dbr;
    Prc=Ic1*Vc*Dcr+dPc+dcr;
    Prd=Id1*Vd*Ddr+dPd+ddr;

    Psb=-Ib2*Vb*Dbr+dPb+dbs;
    Psc=-Ic2*Vc*Dcr+dPc+dcs;
    Psd=-Id2*Vd*Ddr+dPd+dds;

    Pars=Prb+Prc+Prd+Psb+Psc+Psd;

    Pr0=(Prb+Prc+Prd)/3;

    if Ddr>0 && isfinite(Ddr)
        delDbc=Kdi*[Pr0-Prb;Pr0-Prc]*0.35/Ddr;
    else
        delDbc=[0;0];
    end
    Dbr1=Dbr-delDbc(1);
    Dcr1=Dcr-delDbc(2);

    V10=Vl;

    IL1=Pars/V10;
    Vl=(IL1-IL)/CaT+V10;
    IL=Pars/Vl;

    D1=min(D1max,max(D1min,D1+Kpv*(V10-Vl)+Kiv*(700-Vl));

    if Dbr1>D1 || Dcr1>D1
        Gopt=Gopt+1e12;
        break;
    end

    Dbr=Dbr1;Dcr=Dcr1;
    nVl=n*Vl;
    Ddr=D1*nVl/Vd;

```

```

    Gopt=Gopt+50*((Pbref0-Prb-Psb)^2+(Pcref0-Prc-Psc)^2+(Pa-
    Pars)^2)+1e4*(delDbc(1)^2+delDbc(2)^2)+1e6*(Ddr-Ddr0)^2;

```

```

end

```

```

    Gopt=Gopt/5+1e3*((Vb-Vbi)^2+(Vc-Vci)^2)+1e4*(Vd-Vdi)^2;

```

```

else

```

```

delVB=Vb+u(1)-Vd0;
delVC=Vc+u(2)-Vd0;
delVD=Vd+u(3)-Vd0;

```

```

delVB=min(70,abs(delVB));
delVC=min(70,abs(delVC));
delVD=min(70,abs(delVD));

```

```

g = zeros(1,27);%Vdd=Vd;
dV=zeros(3,27);

```

```

for mode=1:27,
    Vb=Vd0+delVB*Vstates(mode,1);
    Vc=Vd0+delVC*Vstates(mode,2);
    Vd=Vd0+delVD*Vstates(mode,3);
    %    Vd=Vdd+delVD*Vstates(mode,3);

```

```

Vb=min(Vmax,max(Vmin,Vb));
Vc=min(Vmax,max(Vmin,Vc));
Vd=min(Vmax,max(Vmin,Vd));

```

```

dV(:,mode)=[Vb-Vbi;Vc-Vci;Vd-Vdi];

```

```

Vl=Vl1;nVl=n*Vl;D1=D10;IL=IL0;
Dbr=Db;Dcr=Dc;Ddr=D1*nVl/Vd;

```

```

for repeat=1:5
    K12=Kdi*[-2 1 1;1 -2 1]*0.35/Ddr/3;
    Ddr0=Ddr;

```

```

    Ib2=Ib1+(3*Vb*Dbr-Vc*Dcr-Vd*Ddr-nVl*D1)/L4f;
    Ic2=Ic1+(3*Vc*Dcr-Vb*Dbr-Vd*Ddr-nVl*D1)/L4f;
    Id2=Id1+(3*Vd*Ddr-Vb*Dbr-Vc*Dcr-nVl*D1)/L4f;
    dPb=Vb*((3*Vb-Vc-Vd)*Dbr^2-nVl*Dbr^2)/L8f;
    dPc=Vc*((3*Vc-Vb-Vd)*Dcr^2-nVl*Dcr^2)/L8f;
    dPd=Vd*((3*Vd-Vb-Vc)*Ddr^2-nVl*Ddr^2)/L8f;

```

```

    Prb=Ib1*Vb*Dbr+dPb+dbr;
    Prc=Ic1*Vc*Dcr+dPc+dcr;
    Prd=Id1*Vd*Ddr+dPd+drr;

```

```

Psb=-Ib2*Vb*Dbr+dPb+dbs;
Psc=-Ic2*Vc*Dcr+dPc+dcs;
Psd=-Id2*Vd*Ddr+dPd+dds;

Pars=Prb+PrC+Prd+Psb+Psc+Psd;

Pr0=(Prb+PrC+Prd)/3;

if Ddr>0 && isfinite(Ddr)
    delDbc=Kdi*[Pr0-Prb;Pr0-PrC]*0.35/Ddr;
else
    delDbc=[0;0];
end
Dbr1=Dbr-delDbc(1);
Dcr1=Dcr-delDbc(2);

Vl0=Vl;

IL1=Pars/Vl0;
Vl=(IL1-IL)/CaT+Vl0;
IL=Pars/Vl;

Dl=min(Dlmax,max(Dlmin,Dl+Kpv*(Vl0-Vl)+Kiv*(700-Vl)));
if Dbr1>Dl || Dcr1>Dl
    g(mode)=g(mode)+1e12;
    break;
end

Dbr=Dbr1;Dcr=Dcr1;
nVl=n*Vl;
Ddr=Dl*nVl/Vd;

g(mode)=g(mode)+50*((Pbref0-Prb-Psb)^2+(Pcref0-PrC-Psc)^2+(Pa-
Pars)^2)+1e4*(delDbc(1)^2+delDbc(2)^2)+1e6*(Ddr-Ddr0)^2;

end

g(mode)=g(mode)/5+1e3*(dV(1,mode)^2+dV(2,mode)^2)+1e4*dV(3,mode)^2;
end

[~, x_opt] = min(g);
Vb=Vd0+delVB*Vstates(x_opt,1);
Vc=Vd0+delVC*Vstates(x_opt,2);
Vd=Vd0+delVD*Vstates(x_opt,3);

Vbb=min(Vmax,max(Vmin,Vb));
Vcc=min(Vmax,max(Vmin,Vc));
Vdd=min(Vmax,max(Vmin,Vd));
Gopt=g(x_opt);
end

Vb=Vd0+delVB2;
Vc=Vd0+delVC2;

```

```

Vd=Vd0+delVD2;

Vl=Vl1;nVl=n*Vl;D1=D10;IL=IL0;

Dbr=Db;Dcr=Dc;Ddr=D1*nVl/Vd;
g_prev=0;
for repeat=1:5
    K12=Kdi*[-2 1 1;1 -2 1]*0.35/Ddr/3;
    Ddr0=Ddr;
    Pars0=Pars;
    Ib2=Ib1+(3*Vb*Dbr-Vc*Dcr-Vd*Ddr-nVl*D1)/L4f;
    Ic2=Ic1+(3*Vc*Dcr-Vb*Dbr-Vd*Ddr-nVl*D1)/L4f;
    Id2=Id1+(3*Vd*Ddr-Vb*Dbr-Vc*Dcr-nVl*D1)/L4f;
    dPb=Vb*( (3*Vb-Vc-Vd)*Dbr^2-nVl*Dbr^2)/L8f;
    dPc=Vc*( (3*Vc-Vb-Vd)*Dcr^2-nVl*Dcr^2)/L8f;
    dPd=Vd*( (3*Vd-Vb-Vc)*Ddr^2-nVl*Ddr^2)/L8f;

    Prb=Ib1*Vb*Dbr+dPb+dbr;
    Prc=Ic1*Vc*Dcr+dPc+dcr;
    Prd=Id1*Vd*Ddr+dPd+ddr;

    Psb=-Ib2*Vb*Dbr+dPb+dbs;
    Psc=-Ic2*Vc*Dcr+dPc+dcs;
    Psd=-Id2*Vd*Ddr+dPd+dds;

    Pars=Prb+Prc+Prd+Psb+Psc+Psd;

    Pr0=(Prb+Prc+Prd)/3;

    if Ddr>0 && isfinite(Ddr)
        delDbc=Kdi*[Pr0-Prb;Pr0-Prc]*0.35/Ddr;
    else
        delDbc=[0;0];
    end
    Dbr1=Dbr-delDbc(1);
    Dcr1=Dcr-delDbc(2);

    Vl0=Vl;
    IL1=Pars/Vl0;
    Vl=(IL1-IL)/CaT+Vl0;
    IL=Pars/Vl;

    D1=min(D1max,max(D1min,D1+Kpv*(Vl0-Vl)+Kiv*(700-Vl));

    if Dbr1>D1 || Dcr1>D1
        g_prev=g_prev+1e12;
        break;
    end

    Dbr=Dbr1;Dcr=Dcr1;
    nVl=n*Vl;
    Ddr=D1*nVl/Vd;

```

```

    g_prev=g_prev+50*((Pbref0-Prb-Psb)^2+(Pcref0-PrC-Psc)^2+(Pa-
Pars)^2)+1e4*(delDbc(1)^2+delDbc(2)^2)+1e6*(Ddr-Ddr0)^2;
    end
    g_prev=g_prev/5+1e3*((delVB1-delVB2)^2+(delVC1-
delVC2)^2)+1e4*(delVD1-delVD2)^2;

    if g_prev>Gopt
        Vb=Vbb;
        Vc=Vcc;
        Vd=Vdd;

    end

    Dbr=Db;Dcr=Dc;Ddr=D1*nVl/Vd;

    K12=Kdi*[-2 1 1;1 -2 1]*0.35/Ddr/3;
    Apr=[(Ib1+(3*Vb-Vc-Vd-nVl)/L4f)*Vb 0;0 (Ic1+(3*Vc-Vb-Vd-nVl)/L4f)*Vc;0
0];
    Abc=eye(2)-K12*Apr;

    Eig_Abc=eig(Abc);
    EigMax=max(abs(Eig_Abc(1)),abs(Eig_Abc(2)));

    delVB2=0.9*delVB2+0.1*delVB1;
    delVC2=0.9*delVC2+0.1*delVC1;
    delVD2=0.9*delVD2+0.1*delVD1;

    delVB1=Vb-Vd0;
    delVC1=Vc-Vd0;
    delVD1=Vd-Vd0;

    end

    Db0=Db;Dc0=Dc;Dd0=Dd;
    y =[delVB1;delVC1;delVD1];
    Eiga=EigMax;

```

Appendix C.2 The State space representation of the system

Here, the state space will be derived. First, the state equation base on duty variable at power balance control, (3c), then state equation based on the power distribution control- set point and the power, (8c).

First, let's make up a state equation, (1c), that has the MV side duty rate differences as the state using

$$\begin{aligned}\Delta D_{bcd}(k) &= \begin{bmatrix} D_b(k) - D_b(k-1) \\ D_c(k) - D_c(k-1) \\ D_d(k) - D_d(k-1) \end{bmatrix} \\ \Delta v_{bcd}(k) &= \begin{bmatrix} v_b(k) - v_b(k-1) \\ v_c(k) - v_c(k-1) \\ v_d(k) - v_d(k-1) \end{bmatrix} \\ \Delta D_{bcd}(k+1) &= \Delta D_{bcd}(k) - \begin{bmatrix} K_{12}(P_{b1}(k) - P_{b1}(k-1)) \\ K_{12}(P_{c1}(k) - P_{c1}(k-1)) \\ D_d(k) - D_d(k-1) \end{bmatrix} \dots \\ &+ \begin{bmatrix} 0 \\ 0 \\ D_1(k) \cdot \frac{nv_L(k)}{v_d(k)} - D_1(k-1) \cdot \frac{nv_L(k-1)}{v_d(k-1)} \end{bmatrix}\end{aligned}\quad (1c)$$

Ignoring the effect of the output voltage control, assuming that D_1 and v_L are invariant, the following approximation equation, (2c), can be written using (5.9). Where $P_1(k) = [P_{b1}(k), P_{c1}(k), P_{d1}(k)]^T$.

$$P_1(k) \approx P_1(k-1) + A_{pr} \cdot \Delta D_{bcd}(k) + B_{pr} \cdot \Delta v_{bcd}(k) \quad (2c)$$

Where, $A_{pr} = \left. \frac{\partial P_r}{\partial D_{bcd}} \right|_k =$

$$\begin{bmatrix} \left(\hat{I}_{b1} + \frac{(3v_b - v_c - v_d - nv_L)D_b}{4Lf} \right) v_b & 0 & 0 \\ 0 & \left(\hat{I}_{c1} + \frac{(3v_c - v_b - v_d - nv_L)D_c}{4Lf} \right) v_c & 0 \\ 0 & 0 & \left(\hat{I}_{d1} + \frac{(3v_d - v_b - v_c - nv_L)D_d}{4Lf} \right) v_d \end{bmatrix}$$

and

$$B_{pr} = \left. \frac{\partial P_r}{\partial v_{bcd}} \right|_k = \begin{bmatrix} \frac{D_b \cdot (\hat{I}_{b1} + 3v_b \cdot D_b)}{4Lf} & -\frac{v_b \cdot D_b^2}{8Lf} & -\frac{v_b \cdot D_b^2}{8Lf} \\ -\frac{v_c \cdot D_c^2}{8Lf} & \frac{D_c \cdot (\hat{I}_{c1} + 3v_c \cdot D_c)}{4Lf} & -\frac{v_c \cdot D_c^2}{8Lf} \\ -\frac{v_d \cdot D_d^2}{8Lf} & -\frac{v_d \cdot D_d^2}{8Lf} & \frac{D_d \cdot (\hat{I}_{d1} + 3v_d \cdot D_d)}{4Lf} \end{bmatrix}$$

Eq. (2c) can be used to rewrite (1c) as shown in (3c) as a result of the state equation with the difference in duty rates in the MV side.

$$\Delta D_{bcd}(k+1) = A_{bcd} \cdot \Delta D_{bcd}(k) + B_{bcd} \cdot \Delta v_{bcd}(k) \quad (3c)$$

Where,

$$A_{bcd} = \begin{bmatrix} 1 & 0 & 0 \\ 0 & 1 & 0 \\ 0 & 0 & 0 \end{bmatrix} - \begin{bmatrix} K_{12} \cdot A_{pr} \\ 0 & 0 & 0 \end{bmatrix}$$

$$B_{bcd} = \begin{bmatrix} -K_{12} \cdot B_{pr} \\ 0 & 0 & -\frac{D_d}{v_d} \end{bmatrix}$$

Next, let's make up a state equation for evaluating the state of error between the power distribution setpoint and the MV side power. Using (5.5) and (5.9), the equation for MV power can be written as (4c). Note that the notation of current PWM time k is abbreviated.

$$P_b(k) = P_{b1}(k) + P_{b2}(k) \quad (4c)$$

$$\begin{aligned}
&= \frac{v_b \cdot (3v_b - v_c - v_d - nv_L) \cdot D_b^2}{8Lf} + \hat{I}_{b1} \cdot D_b \cdot v_b + d_{b1} \dots \\
&\quad + \frac{v_b \cdot (3v_b - v_c - v_d - nv_L) \cdot D_b^2}{8Lf} \dots \\
&\quad - \left(\hat{I}_{bb} + \frac{3v_b D_b - v_c D_c - v_d D_d - nv_L D_1}{4Lf} \right) \cdot D_b \cdot v_b + d_{b2} \\
P_b(k) &= \left(\frac{3v_b D_b - v_c D_c - v_d D_d - nv_L D_1}{4Lf} - \frac{3v_b D_b - v_c D_c - v_d D_d - nv_L D_1}{4Lf} \right) \dots \\
&\quad \cdot D_b \cdot v_b + d_{b1} + d_{b2}
\end{aligned}$$

$$\text{So,} \quad (5c)$$

$$P_b(k) = v_b \cdot D_b \cdot \frac{v_c \cdot (D_c - D_b) + v_d \cdot (D_d - D_b) + nv_L \cdot (D_1 - D_b)}{4Lf} + d_{b1} + d_{b2}$$

$$P_c(k) = v_c \cdot D_c \cdot \frac{v_b \cdot (D_b - D_c) + v_d \cdot (D_d - D_c) + nv_L \cdot (D_1 - D_c)}{4Lf} + d_{c1} + d_{c2}$$

$$P_d(k) = v_d \cdot D_d \cdot \frac{v_b \cdot (D_b - D_d) + v_c \cdot (D_c - D_d) + nv_L \cdot (D_1 - D_d)}{4Lf} + d_{d1} + d_{d2}$$

Define $P(k) = [P_b(k), P_c(k), P_d(k)]^T$. The approximation deviation equation between the MV side power in the neighboring PWM periods can be written as (6c) which can be found by taking partial derivative of (5c).

$$P(k + 1) \approx P(k) + C_P \Delta D_{bcd}(k) + D_P \Delta v_{bcd}(k) \quad (6c)$$

Where,

$$C_P = \left. \frac{\partial P}{\partial D_{bcd}} \right|_k = \begin{bmatrix} C_{P11} & C_{P12} & C_{P13} \\ C_{P21} & C_{P22} & C_{P23} \\ C_{P31} & C_{P32} & C_{P33} \end{bmatrix}$$

$$D_P = \left. \frac{\partial P}{\partial v_{bcd}} \right|_k = \begin{bmatrix} D_{P11} & D_{P12} & D_{P13} \\ D_{P21} & D_{P22} & D_{P23} \\ D_{P31} & D_{P32} & D_{P33} \end{bmatrix}$$

Where,

$$C_{P11} = \frac{\partial P_b}{\partial D_b} = v_b \frac{v_c \cdot (D_c - D_b) + v_d \cdot (D_d - D_b) + nv_L \cdot (D_1 - D_b) + D_b(-v_c - v_d - nv_L)}{4Lf}$$

$$C_{P11} = v_b \frac{v_c \cdot (D_c - 2D_b) + v_d \cdot (D_d - 2D_b) + nv_L \cdot (D_1 - 2D_b)}{4Lf}$$

$$C_{P12} = \frac{\partial P_b}{\partial D_c} = \frac{v_b \cdot v_c \cdot D_b}{4Lf}$$

$$C_{P13} = \frac{\partial P_b}{\partial D_d} = \frac{v_b \cdot v_d \cdot D_b}{4Lf}$$

$$C_{P21} = \frac{\partial P_c}{\partial D_b} = \frac{v_b \cdot v_c \cdot D_c}{4Lf}$$

$$C_{P22} = \frac{\partial P_c}{\partial D_c} = v_c \frac{v_b \cdot (D_b - 2D_c) + v_d \cdot (D_d - 2D_c) + nv_L \cdot (D_1 - 2D_c)}{4Lf}$$

$$C_{P23} = \frac{\partial P_c}{\partial D_d} = \frac{v_c \cdot v_d \cdot D_c}{4Lf}$$

$$C_{P31} = \frac{\partial P_d}{\partial D_b} = \frac{v_b \cdot v_d \cdot D_d}{4Lf}$$

$$C_{P32} = \frac{\partial P_d}{\partial D_c} = \frac{v_c \cdot v_d \cdot D_d}{4Lf}$$

$$C_{P33} = \frac{\partial P_d}{\partial D_d} = v_d \frac{v_b \cdot (D_b - 2D_d) + v_c \cdot (D_c - 2D_d) + nv_L \cdot (D_1 - 2D_d)}{4Lf}$$

$$D_{P11} = \frac{\partial P_b}{\partial v_b} = \frac{v_c \cdot (D_c - D_b) + v_d \cdot (D_d - D_b) + nv_L \cdot (D_1 - D_b)}{4Lf} \cdot D_b$$

$$D_{P12} = \frac{v_b \cdot (D_c - D_b)}{4Lf} \cdot D_b$$

$$D_{P13} = \frac{v_b \cdot (D_d - D_b)}{4Lf} \cdot D_b$$

$$D_{P21} = \frac{v_c \cdot (D_b - D_c)}{4Lf} \cdot D_c$$

$$D_{P22} = \frac{v_b \cdot (D_b - D_c) + v_d \cdot (D_d - D_c) + nv_L \cdot (D_1 - D_c)}{4Lf} \cdot D_c$$

$$D_{P23} = \frac{v_c \cdot (D_d - D_c)}{4Lf} \cdot D_c$$

$$D_{P31} = \frac{v_d \cdot (D_b - D_d)}{4Lf} \cdot D_d$$

$$D_{P32} = \frac{v_d \cdot (D_c - D_d)}{4Lf} \cdot D_d$$

$$D_{P33} = \frac{v_b \cdot (D_b - D_d) + v_c \cdot (D_c - D_d) + nv_L \cdot (D_1 - D_d)}{4Lf} \cdot D_d$$

Ignore the approximation error and let Eq. (6.c) be expressed respectively for MV_b , MV_c and MV_d .

$$P_b(k+1) = P_b(k) + [C_{P11}, C_{P12}, C_{P13}] \Delta D_{bcd}(k) + [D_{P11}, D_{P12}, D_{P13}] \Delta v_{bcd}(k) \quad (7c.a)$$

$$P_c(k+1) = P_c(k) + [C_{P21}, C_{P22}, C_{P23}] \Delta D_{bcd}(k) + [D_{P21}, D_{P22}, D_{P23}] \Delta v_{bcd}(k) \quad (7c.b)$$

$$P_d(k+1) = P_d(k) + [C_{P31}, C_{P32}, C_{P33}] \Delta D_{bcd}(k) + [D_{P31}, D_{P32}, D_{P33}] \Delta v_{bcd}(k) \quad (7c.c)$$

By subtracting the power setpoints P_{bref} and P_{cref} on MV_b and MV_c from both sides. (7c.a) and (7c.b), respectively, the following equation (8c) is obtained. It can be assumed that the power setpoint P_{bref} and P_{cref} on MV_b and MV_c are invariant for enough time. Let $P_a - P_{bref} - P_{cref} = P_{dref}$. Also, by subtracting $P_a - P_{bref} - P_{cref}$ from both sides of Eq. (8c.c), the following equation is obtained. Finally, (8c) is the state equation relating to the error state between the power distribution setpoint and the power in the MV side.

$$P_b(k+1) - P_{bref} =$$

$$P_b(k) - P_{bref} + [C_{P11}, C_{P12}, C_{P13}] \Delta D_{bcd}(k) + [D_{P11}, D_{P12}, D_{P13}] \Delta v_{bcd}(k) \quad (8c.a)$$

$$P_c(k+1) - P_{cref} =$$

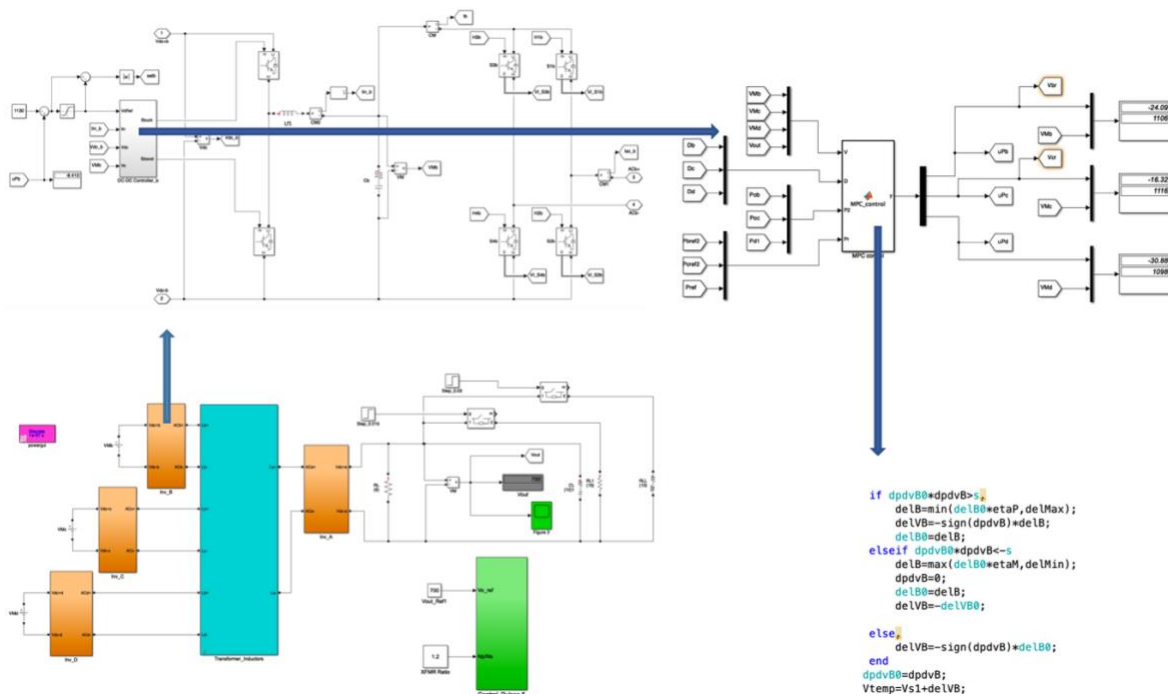
$$P_c(k) - P_{cref} + [C_{P21}, C_{P22}, C_{P23}] \Delta D_{bcd}(k) + [D_{P21}, D_{P22}, D_{P23}] \Delta v_{bcd}(k) \quad (8c.b)$$

$$P_{bref} - P_b(k+1) + P_{cref} - P_c(k+1) =$$

$$(8c.c)$$

$$P_{bref} - P_b(k) + P_{cref} - P_c(k) + [C_{P31}, C_{P32}, C_{P33}] \Delta D_{bcd}(k) + [D_{P31}, D_{P32}, D_{P33}] \Delta v_{bcd}(k)$$

Appendix C.3 Simulink file



Appendix Figure 1 Simulink file, QAB

Bibliography

- [1] J. W. Kolar, G. Ortiz, "Solid-State-Transformers: Key Components of Future Traction and Smart Grid Systems," Proceedings of the International Power Electronics Conference - ECCE Asia (IPEC 2014), Hiroshima, Japan, May 18-21, 2014.
- [2] Drazen Dujic, "Presentation on Power Electronic Transformer for rail-way on-board applications - an overview," ABB Corporate Research, Baden-Dattwil, Switzerland, 2013.
- [3] M. Liserre, G. Buticchi, M. Andresen, G. De Carne, L. F. Costa, and Z. X. Zou, "The smart transformer: impact on the electric grid and technology challenges," IEEE Ind. Electron. Mag., vol. 10, no. 2, pp. 46–58, June 2016.
- [4] J. W. Kolar, J. Huber, T. Guillod, D. Rothmund, F. Krismer, "Research Challenges and Future Perspectives of Solid-State Transformer Technology," presented at the 5th Int. Conf. Power Engineering Energy Electrical Drives, Riga, Latvia, 2015.
- [5] G. Brando, A. Dannier and R. Rizzo, "Power Electronic Transformer application to grid connected photovoltaic systems," in *International Conference on Clean Electrical Power*, Capri, 2009, pp. 685-690, 2009.
- [6] X. She, F. Wang, R. Burgos and A. Q. Huang, "Solid state transformer interfaced wind energy system with integrated active power transfer, reactive power compensation and voltage conversion functions," IEEE Energy Conversion Congress and Exposition (ECCE), Raleigh, NC, 2012, pp. 3140-3147, 2012.
- [7] M. Rashidi, A. Nasiri and R. Cuzner, "Application of multi-port solid-state transformers for microgrid-based distribution systems," in IEEE International Conference on Renewable Energy Research and Applications (ICRERA), Birmingham, 2016.
- [8] G. Ortiz, D. Bortis, J. W. Kolar and O. Apeldoorn, "Soft-switching techniques for medium-voltage isolated bidirectional DC/DC converters in solid state transformers," in 38th Annual Conference on IEEE Industrial Electronics Society (IECON), pp. 5233-5240, Montreal, QC, 2012.
- [9] G. Buticchi, L. F. Costa, D. Barater, M. Liserre and E. D. Amarillo, "A Quadruple Active Bridge Converter for the Storage Integration on the More Electric Aircraft," in IEEE Transactions on Power Electronics, vol. 33, no. 9, pp. 8174-8186, Sept. 2018.
- [10] Zengin S, Boztepe M, "Trapezoid current modulated DCM AC/DC DAB converter for two-stage solid state transformer," in IEEE 9th International Conference on Electrical and Electronics Engineering (ELECO), pp. 634–638, 2015.

- [11] Costa, Levy Ferreira, Giampaolo Buticchi, and Marco Liserre. "Quad-active-bridge dc-dc converter as cross-link for medium-voltage modular inverters." *IEEE Transactions on Industry Applications* 53, no. 2, pp. 1243-1253, 2017.
- [12] S. Cui, N. Soltau and R. W. De Doncker, "Dynamic performance and fault-tolerant capability of a TLC-MMC hybrid DC-DC converter for interconnection of MVDC and HVDC grids," *IEEE Energy Conversion Congress and Exposition (ECCE)*, pp. 1622-1628, Cincinnati, OH, 2017.
- [13] L. Costa, G. Buticchi and M. Liserre, "Bidirectional series-resonant DC-DC converter with fault-tolerance capability for smart transformer," *IEEE Energy Conversion Congress and Exposition (ECCE)*, pp. 1-7 Milwaukee, WI, 2016.
- [14] Wang L, Zhang D, Wang Y, et al. "Power and voltage balance control of a novel three-phase solid-state transformer using multilevel cascaded H-bridge inverters for microgrid applications." *IEEE Trans. Power Electr.* 31, pp. 3289-3301, 2016.
- [15] T. Zhao, G. Wang, S. Bhattacharya and A. Q. Huang, "Voltage and Power Balance Control for a Cascaded H-Bridge Converter-Based Solid-State Transformer," in *IEEE Transactions on Power Electronics*, vol. 28, no. 4, pp. 1523-1532, April 2013.
- [16] She X, Huang AQ, Ni X, "Current sensorless power balance strategy for DC/DC converters in a cascaded multilevel converter based solid state transformer," *IEEE Trans. Power Electron* 29, pp. 17-22, 2014.
- [17] Wang X, Liu J, Xu T, et al., "Control of a three-stage three-phase cascaded modular power electronic transformer," *28th Annual IEEE Applied Power Electronics Conference and Exposition (APEC)*. IEEE, pp.1309-1315, 2013.
- [18] L. Wang, D. Zhang, Y. Wang, B. Wu and H. S. Athab, "Power and Voltage Balance Control of a Novel Three-Phase Solid-State Transformer Using Multilevel Cascaded H-Bridge Inverters for Microgrid Applications," in *IEEE Transactions on Power Electronics*, vol. 31, no. 4, pp. 3289-3301, April 2016.
- [19] Falcones, S.; Ayyanar, R., "Simple control design for a three-port DC-DC converter based PV system with energy storage," *Applied Power Electronics Conference and Exposition (APEC)*, 2010 Twenty-Fifth Annual IEEE, vol., no., pp.2149-2153, Feb. 2010.
- [20] Qiang Mei; Xu Zhen-lin; Wei-yang Wu, "A novel multi-port DC-DC converter for hybrid renewable energy distributed generation systems connected to power grid," *IEEE International Conference on Industrial Technology ICIT*, pp. 1-5, April 2008.
- [21] S. Falcones, R. Ayyanar, and X. Mao, "A dc-dc multiport-converter-based solid-state transformer integrating distributed generation and storage," *IEEE Trans. Power Electron.*, vol. 28, no. 5, pp. 2192-2203, May 2013.
- [22] D. Maksimovic, A. Stankovic, V. Thottuvelil, and G. Verghese, "Modeling and simulation of power electronic converters," *Proceedings of the IEEE*, vol. 89, pp. 898-912, Jun. 2001.

- [23] R. W. Erickson and D. Maksimovic, *Fundamentals of Power Electronics: Second Edition*. Springer, 2001.
- [24] B. Lehman and R. Bass, "Switching frequency dependent averaged models for PWM dc-dc converters," *IEEE Transactions on Power Electronics*, vol. 11, pp. 89-98, Jan 1996.
- [25] G. C. Verghese, M. E. Elbuluk, and J. G. Kassakian, "A general approach to sampled-data modeling for power electronic circuits," *IEEE Transactions on Power Electronics*, vol. 1, pp. 76-89, Apr. 1986.
- [26] J. Hwang, P. Lehn, and M. Winkelkemper, "A generalized class of stationary frame-current controllers for grid-connected ac-dc converters," *IEEE Transactions on Power Delivery*, vol. 25, pp. 2742-2751, Oct. 2010.
- [27] Liu, H.; Mao, C.; Lu, J.; Wang, D., "Optimal regulator-based control of electronic power transformer for distribution systems," *Electr. Power Syst. Res.*, vol.79, pp.863-870, 2009.
- [28] A. Prodic and D. Maksimovic, "Design of a digital PID regulator based on look-up tables for control of high-frequency dc-dc converters," in *IEEE Workshop on Computers in Power Electronics*, pp. 18-22, Jun. 2002.
- [29] K. J. Astrom and B. Wittenmark, *Adaptive Control: Second Edition*. Dover Publications, 2008.
- [30] J. M. Kanieski, R. V. Tambara, H. Pinheiro, R. Cardoso and H. A. Gründling, "Robust Adaptive Controller Combined With a Linear Quadratic Regulator Based on Kalman Filtering," in *IEEE Transactions on Automatic Control*, vol. 61, no. 5, pp. 1373-1378, 2016.
- [31] H. Zhou, A. Khambadkone, and X. Kong, "Passivity-based control for an interleaved current-fed full-bridge converter with a wide operating range using the brayton-moser form," *IEEE Transactions on Power Electronics*, vol. 24, pp. 2047-2056, Sept. 2009.
- [32] S.-C. Tan, Y. Lai, C. Tse, and L. Martinez-Salamero, "Special family of PWM-based sliding-mode voltage controllers for basic dc-dc converters in discontinuous conduction mode," *IET Electric Power Applications*, vol. 1, pp. 64-74, Jan. 2007.
- [33] B. Liu, Y. Zha and T. Zhang, "D-Q frame predictive current control methods for inverter stage of solid state transformer," in *IET Power Electronics*, vol. 10, no. 6, pp. 687-696, 2017.
- [34] G. Brando, A. Dannier and A. Del Pizzo, "A simple predictive control technique of power electronic transformers with high dynamic features," *5th IET International Conference on Power Electronics, Machines and Drives (PEMD)*, pp. 1-6, Brighton, UK, 2010.

- [35] Y. Liu, Y. Liu, B. Ge and H. Abu-Rub, "Interactive Grid Interfacing System by Matrix-Converter Based Solid State Transformer with Model Predictive Control," in *IEEE Transactions on Industrial Informatics*, 2017.
- [36] Mayne, David Q., James B. Rawlings, Christopher V. Rao, and Pierre OM Sokaert. "Constrained model predictive control: Stability and optimality." *Automatica* 36, no. 6, p.p 789-814, 2000.
- [37] X. She, A. Q. Huang, and R. Burgos, "Review of solid-state transformer technologies and their application in power distribution systems," *IEEE J. Emerg. Sel. Topics Power Electron.*, vol. 1, no. 3, pp. 186–198, Sep. 2013.
- [38] X. She, X. Yu, F. Wang, and A. Q. Huang, "Design and demonstration of a 3.6-kV 120-V/10-kVA solid-state transformer for smart grid application," *IEEE Trans. Power Electron.*, vol. 29, no. 8, pp. 3982–3996, Aug. 2014.
- [39] H. Tao, J. Duarte, and M. Hendrix, "Three-port triple-half-bridge bidirectional converter with zero-voltage switching," *IEEE Trans. Power Electron.*, vol. 23, no. 2, pp. 782–792, Mar. 2008.
- [40] Costa, Levy Ferreira, Felix Hoffmann, Giampaolo Buticchi, and Marco Liserre. "Comparative analysis of multiple active bridge converters configurations in modular smart transformer." *IEEE Transactions on Industrial Electronics* 66, no. 1 (2018): 191-202.
- [41] Liu, Guangyuan, Tommaso Caldognetto, and Paolo Mattavelli. "Power- based droop control in dc microgrids enabling seamless disconnection from ac grids." In *2017 IEEE Second International Conference on DC Microgrids (ICDCM)*, pp. 523-528. IEEE, 2017.
- [42] Pugliese, Sante, Markus Andresen, Rosa Mastromauro, Giampaolo Buticchi, et. al. "Voltage balancing of modular smart transformers based on dual active bridges." In *2017 IEEE Energy Conversion Congress and Exposition (ECCE)*, pp. 1270-1275. IEEE, 2017.
- [43] D. Wang, C.X. Mao, J.M. Lu, "Coordinated control of EPT and generator excitation system for multi double-circuit transmission-lines system," *IEEE Trans. Power Deliv.* 23 (1), pp. 371-379, 2008.
- [44] Kim, Kwansu, Hyun-Gyu Kim, Yuan Song, and Insu Paek. "Design and simulation of an LQR-PI control algorithm for medium wind turbine." *Energies* 12, no. 12 (2019): 2248.
- [45] M. Hatatah and B. M. Grainger, "LQR Approach for Regulating Voltage and Power Flow through the Ports of a Medium Voltage Quad Active Bridge Solid State Transformer," *20th Workshop on Control and Modeling for Power Electronics (COMPEL)*, pp. 1-7, Toronto, ON, Canada, 2019.

- [46] Li, Qiao, Tianqi Gao, David Wenzhong Gao, and Xiao Wang. “Adaptive LQR control with Kalman filter for the variable-speed wind turbine in Region II.” In 2017 North American Power Symposium (NAPS), pp. 1-6, 2017.
- [47] Rodriguez, Jose, Marian P. Kazmierkowski, Jose R. Espinoza, Pericle Zanchetta, Haitham Abu-Rub, Hector A. Young, and Christian A. Rojas. “State of the art of finite control set model predictive control in power electronics.” *IEEE Transactions on Industrial Informatics* 9, no. 2, 2012.
- [48] Shadmand, Mohammad B., Robert S. Balog, and Haitham Abu-Rub. “Model predictive control of PV sources in a smart DC distribution system: maximum power point tracking and droop control.” *IEEE Transactions on Energy Conversion* 29, no. 4, pp. 913-921, 2014.
- [49] Nascimento, Tiago P., Carlos Eduardo Trabuco Dórea, and Luiz Marcos G. Gonçalves. “Nonlinear model predictive control for trajectory tracking of nonholonomic mobile robots: A modified approach.” *International Journal of Advanced Robotic Systems* 15, no. 1, 2018.
- [50] Wang G, She X, Wang F, et al., “Comparisons of different control strategies for 20kVA solid state transformer,” *IEEE Energy Conversion Congress and Exposition (ECCE)*. IEEE, 3173–3178, 2011.
- [51] M. Hatatah and B. M. Grainger, “Power and Voltage regulation of a Solid-State Transformer based Quad-Active Bridge DC–DC Converter using Adaptive Linear Quadratic Regulator and Nonlinear Model Predictive Control,” *IEEE Energy Conversion Congress and Exposition (ECCE)*. IEEE, 2020.
- [52] Mayne, David Q. “Model predictive control: Recent developments and future promise.” *Automatica* 50, no. 12, p.p 2967-2986, 2014.
- [53] Venkat, Aswin N., James B. Rawlings, and Stephen J. Wright. “Stability and optimality of distributed model predictive control.” In *Proceedings of the 44th IEEE Conference on Decision and Control*, pp. 6680-6685. IEEE, 2005.
- [54] Mayne, David Q., and Hannah Michalska. “Receding horizon control of nonlinear systems.” In *Proceedings of the 27th IEEE Conference on Decision and Control*, pp. 464-465, 1988.
- [55] Michalska, Hanna, and David Q. Mayne. “Robust receding horizon control of constrained nonlinear systems.” *IEEE transactions on automatic control* 38, no. 11, p.p 1623-1633, 1993.
- [56] Scokaert, Pierre OM, David Q. Mayne, and James B. Rawlings. “Suboptimal model predictive control (feasibility implies stability).” *IEEE Transactions on Automatic Control* 44, no. 3, 648-654, 1999.
- [57] Pannocchia, Gabriele, James B. Rawlings, and Stephen J. Wright. “Conditions under which suboptimal nonlinear MPC is inherently robust.” *Systems & Control Letters* 60, no. 9, p.p 747-755, 2011.